Commercial Near-Earth Launcher: Propulsion Choices

4

As presented in Chap. 2, airbreathing propulsion advocates have been fighting a losing battle to change the space launcher paradigm from expendable rockets, that are launched for the first, last, and only time, to sustained-use launchers that are more like military airlift transports with long and frequent usage (Anon 1967). Chapter 3 has details of the debate that took place in the USA, where even a sustained-use rocket launcher proposed to support the military Manned Orbiting Laboratory (MOL) was discarded, as was MOL, as not having relevance in a purposely designated "civilian" space fleet. As a result, most if not all, of the military high-performance hypersonic glider design and performance data was forever lost, together with the benefits of these high-performance systems to the civilian space organization.

It must be admitted that airbreathing propulsion proposals, based on what were indeed rational assumptions when applied to rockets, resulted (and to many is still the case today) in large, ponderous, and too costly vehicles. Even though that was challenged, as shown in Figs. 2.16 and 2.17, lasting impressions were that airbreathers were too large and too expensive, and that they required too long a development period when compared to rocket-launching systems. This is factually contrary to the actual rocket record, an example being the total lack of a US man-rated space launch system during the 12-year period when the National Space Transportation System (STS or Space Shuttle) was being developed. Most interestingly, we again do experience this US manned launch vehicle void today. Despite a range of rocket-based space launch vehicles being under development for years, the US has no operational man-rated space launch system since the last flight of the Space Shuttle on July 21, 2011.

Chapter 3 also shows that, when propulsion systems are placed on a common vehicle platform like the lifting-body configurations, there are indeed differences in weights between rocket and airbreathing propulsion, but no significant size or industrial capability index differences. Then, the fact remains that, if we are to transition from the status quo today, as illustrated in Fig. 2.23, to the commercial space scenario in Fig. 2.24, something has to change to support the flight rate such a busy commercial infrastructure would require. However, it must be said that this particular status quo has been comfortable and profitable for the telecommunications and launcher industry so far.

In order to achieve a transportation system to space analogous to the transcontinental railroad, i.e., one that can support a commercial space infrastructure, this change must include an airbreathing launcher to meet the high flight rate requirements. The MOL was designed for 20–27 persons. The support spacecraft would carry 9–12 people or materials to resupply the station. For that goal, the payload planned was a 7 t payload (15,435 lb). An airbreathing launcher would be at least 1/2 the weight of the rocket vehicle in Fig. 2.16, requiring 1/2 the resources. The MOL study identified that each crewmember replacement would need to be accompanied by a 994 lb (450 kg) resource supply payload. For a 12-person crew replacement mission, that makes the crew replacement payload 15,228 lb, well within the 7 t payload capacity. The operating parameters of the MOL station were for a nominal 21-person crew. The same study determined that 47,000 lb (21,315 kg) of resources were required per crewmember per year. For one year, with a 21-person complement, that means 448 t (987,000 lb) of supplies needed to be lifted to the station for crew support, not counting propellants to maintain the station orbit. With 21 crewmembers, there are 4 flights per year required to meet the 6-month assignment requirement. To lift the crew supplies to the station would require 64 flights per year, not counting propellant and hardware replacement missions that may require another 5–6 flights per year. The number of flights to a large station is then at least 74 flights per year. From a military mission analysis, that would require a fleet

P.A. Czysz et al., *Future Spacecraft Propulsion Systems and Integration*,
Springer Praxis Books, DOI 10.1007/978-3-662-54744-1_4

of 10 aircraft (14, counting in operational spares) flying 7 times a year for 15 years, and a 100-flight operational life (Czysz 1999; Zagainov and Plokhikh 1991). When using instead the present rocket launchers, that becomes a total of 1050 launches by 1050 rockets. To the MOL designers of 1964, it was instead a fleet of 10–14 sustained-use vehicles operated over a 15-year period, plus repair and maintenance. That vast difference in outlook between the aircraft manufacturers and the ballistic missile manufacturers remains today. Sustained use remains a poor competitor to the expendable rocket rather than being adopted as a necessity for the future of commercial space.

Just as ground transportation has railroad trains, over-the-road tractor trailers, cargo trucks, busses, and automobiles, so space must have a variety of transportation vehicles with different payload capacities and fly rates. The USA is still lacking a heavy-lift capability as we once had with the Saturn V. The first flight of the dedicated US space exploration launch system (the SLS Block 1, capable of 70 t payload to LEO) is scheduled in 2018 (Anon 2015). We need the capability of sending heavy payload to the gas giants such as Jupiter and Saturn, moderate payloads to the outer planets, and modest payloads to the boundaries of our solar system (Anfimov 1997), all in comparable travel times. Airbreathing propulsion will not help us in space, but it can enable lighter, sustained-use launchers that increase the frequency to orbit and reduce the cost to a practical value that will enable more space infrastructure and space exploration.

4.1 Propulsion System Alternatives

Incorporation of airbreathing in launchers provides many propulsion options. However, vehicle design choices are not arbitrary as requirements and propulsion performance define practical solution spaces, as discussed in detail in Chap. 3. A priori decisions, such as horizontal takeoff versus vertical takeoff, can doom to failure an otherwise workable project. From the governing equations, the keys to succeed appear to be (a) offloading at least some of the carried oxidizer and (b) designing for sustained operations over a long operational life with maintenance, not continuous overhaul and rebuilding. As illustrated in Fig. 3.54, it is possible to readily identify the design space accessible with current industrial capability and materials.

New discoveries and industrial capabilities are always important, but, as was clearly demonstrated in the 1960s, neither discovery of new technologies nor the identification of technology availability dates (TADs and TRL as well) are necessary to fabricate an operational space flight system with more capability than the current hardware. Even a cursory review of the North American X-15 and the Lockheed SR-71 shows that the presence of bureaucratic roadblocks such as TAD and TRL would have meant neither aircraft would have ever been built or flown, but rather be replaced by paper studies. It was curiosity, resourcefulness, skill, and knowledge that enabled the North American and Lockheed teams to succeed. Governmental planning had little to do with their success. The teams adapted what was available and created what was not, and only if and when necessary. The latter is Theodore von Kármán's definition of an engineer (Vandenkerckhove 1986), as obtained as a personal note to Jean, one of von Kármán's last graduate students: "*Scientists discover what is, engineers create that which never was!*"

There is an excellent documented example of what is just written above in a book published by the Society of Automotive Engineers (SAE) entitled *Advanced Engine Development at Pratt & Whitney* by Dick Mulready. The subtitle is *The Inside Story of Eight Special Projects 1946–1971* (Mulready 2001). In Sect. 6, *Boost Glide and the XLR-129—Mach 20 at 200,000 Feet*, two McDonnell Aircraft Company persons are named, Robert (Bob) Belt and Harold Altus (sic) [The spelling should be Altis.]. The former was known to lead the "belt driven machine." Figure 4.1 comes from page 114 (Fig. 6.7) in that book. It compares the development testing of the XLR-129 turbopump to its design value of 6705 psia, with that of the NASA 350K turbopump that later became the main space shuttle main engine (SSME) component (Jenkins 2001). In the last paragraph of the section, the sentence reads: "*... The liquid oxygen turbopump was the next component in line. However, before it was funded, NASA had started the Space Shuttle campaign, and the Air Force gave the XLR-129 program to NASA, granting free use of the existing hardware to Pratt & Whitney. NASA promptly canceled the liquid oxygen turbopump because it would be unfair to our competitors to fund it. I bet there were times when NASA wished it had continued the program. ...*" And this is how a rocket engine disappeared with a run record of 42 simulated flights in the test chamber without any overhaul or repair.

With the following, we are applying the sustained-use viewpoint to the relevant cross section of propulsion system options based on available and demonstrated hardware and materials. A first introduction has been provided in Sect. 3.7.3 for developing the concept of the multi-disciplinary sizing methodology in Sect. 3.7.4. This chapter provides additional propulsion and airframe integration details as applied to commercial near-Earth launchers. Since airbreathing propulsion is most valuable over the atmospheric part of the ascent flight trajectory, the following three broad categories of airbreathing propulsion are further considered:

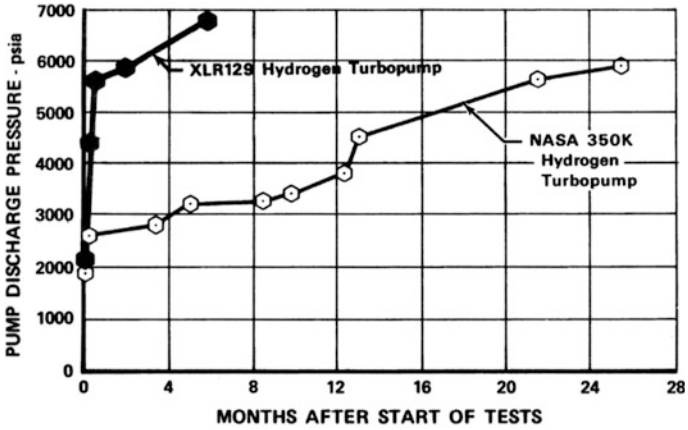

Fig. 4.1 Comparison of XLR-129 turbopump qualification history (circa 1965 for a 1960s program called ISINGLASS) with that of the space shuttle main engine (SSME) turbopump (NASA 350K), circa 1972 (Mulready 2001)

(a) Combination of individual engines operating separately (Anon 1985);
(b) Individual engine (usually a rocket engine) operating in conjunction with another engine capable of more than one cycle mode (Tanatsugu et al. 1987; Nouse et al. 1988; Balepin et al. 1996);
(c) Single combined-cycle engine capable of all cycle modes required over the entire flight trajectory (Maita et al. 1990; Yugov et al. 1989).

4.2 Propulsion System Characteristics

Assuming a combination of individual engines, the transition from one engine to another requires shutting down the first engine followed by transitioning to the second engine type which has already started, while maintaining or increasing flight speed. If the engine is airbreathing, then the flow path has also to be changed. In the past, switching the flow path from one engine to another has always been the system downfall. For a rocket engine operating in conjunction with another engine system, the operation is relatively straightforward. The key challenge is to control the fuel path to the engines. For the single combined-cycle concept, the engineering challenge is the smooth transition from one cycle to the next within a single engine. The transition from one engine cycle operation to another must be made *efficient* (on First Law basis that means the total energy losses must be minimized) and *effective* (on Second Law basis that means when energy is available for recovery as useful work, that conversion must be accomplished then or be lost).

An engine of category (c) is designed for the minimum entropy rise across the cycle. The scope and limitations of these engines are discussed in detail in references (Escher 1994; Czysz 1993a, b), and there are several advantages identified in such scheme. In the case of most airbreathing propulsion systems, the transition from one cycle to another is not a showstopper. In airbreathing propulsion, the two most important considerations to effectiveness and efficiency are as follows: (a) The airflow energy compared to the energy the fuel combustion can add to the flow, and (b) the internal airflow energy losses due to internal drag of strut injectors and cavities and to skin friction and fuel/air mixing.

4.3 Airflow Energy Entering the Engine

With a rocket propulsion system, all of the fuel and oxidizer are carried onboard the vehicle. As a consequence, other than atmospheric vehicle drag and the nozzle exit pressure compared to atmospheric pressure, the vehicle's speed relative to the atmosphere does not determine the propulsion system performance. The specific impulse, I_{sp}, is the thrust per unit propellant mass flowrate. Then, if more thrust is required more engine mass flow is required, i.e., a larger engine or increased chamber pressure to increase the mass flow.

With an airbreathing propulsion system, just the opposite is true. Because the air is entering the airbreathing engine via the vehicle inlet, see Fig. 4.2, the ability of the inlet to preserve energy, as the flow is slowed down in the inlet (for instance, by passing through a series of shock waves), is absolutely critical. The magnitude of the airflow kinetic energy recovered at the end of the inlet determines how much of the fuel–air combustion energy can be converted into thrust. Because the oxidizer is the oxygen in the air, there is a maximum energy that can be added per unit mass flow of air. Then, it is the capture area of the inlet and the airflow speed relative to the vehicle that rules how much *total* energy the burned fuel can add to the air stream. Ultimately, it is the difference between the energy lost in the inlet and the combustion energy that determines the thrust.

The energy of the air is a function of two quantities, (a) the energy of the air in the atmosphere (static enthalpy, in kJ/kg) and (b) the kinetic energy of the air stream (kinetic

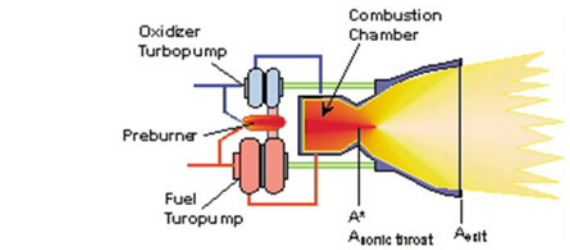

Liquid Propellant Topping Cycle Rocket Engine

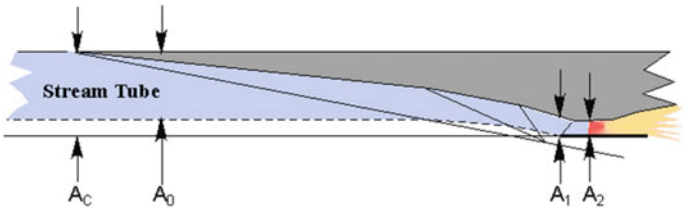

Air Breathing Engine Air Capture Inlet

Fig. 4.2 Liquid rocket engine carries its fuel and oxidizer onboard. By contrast, an airbreathing engine carries only fuel onboard, and the oxidizer is atmospheric air captured by the inlet. A_C = geometric capture area; A_0 = cowl stream tube area, which can be greater or less than A_C; A_1 = engine module cowl area; A_2 = engine module minimum area

energy, in kJ/kg), see also Eq. (2.1a). The *total* energy, or *stagnation* energy, is given as follows:

$$\underbrace{h_t}_{\text{Total energy}} = \underbrace{h_0}_{\text{Static enthalpy}} + \underbrace{\frac{V_0^2}{2}}_{\text{Kinetic energy}} \left(\frac{\text{J}}{\text{kg}};\ V_0 \text{ in m/s}\right) \tag{4.1a}$$

$$\underbrace{h_t}_{\text{Total energy}} = \underbrace{232.6}_{\text{Static enthalpy}} + \underbrace{\frac{V_0^2}{2000}}_{\text{Kinetic energy}} \left(\frac{\text{kJ}}{\text{kg}};\ V_0 \text{ in m/s}\right) \tag{4.1b}$$

The static enthalpy h_0 of air is assumed almost a constant over the altitude range over which the airbreathing propulsion system operates and is much smaller than the kinetic energy in flight: Total energy is essentially a function of the kinetic energy of the air stream. However, the energy Q added to the air by fuel combustion is approximately constant for each fuel. Thus,

$$Q = \left(\frac{\text{Fuel}}{\text{Air}}\right) \cdot Q_c \tag{4.2}$$

Q $\left(\frac{\text{kJ}}{\text{kg}}\right)_{\text{Air}}$ (Brayton cycle heat addition)

Q_c $\left(\frac{\text{kJ}}{\text{kg}}\right)_{\text{Fuel}}$ (Heat of combustion)

In an actual combustion, 100% of the fuel energy is not available to increase the energy of the air stream. (1) The first non-availability results because the atmospheric air is not at absolute zero. That loss of available energy is called the Carnot loss. Typically, the Carnot loss is about 21% of the input energy; then, around 79% is available. (2) The second non-availability in the combustor results from the temperature gradient in the combustor from the center of the combustor to the cooler wall. Typically, for metal walls in gas turbine engines and other airbreathing engines, that loss is about 4%. Then, 75% of the available combustor energy is available to produce thrust. (3) The third non-availability results from the energy required to mix the fuel and air at high combustor flow speeds (Swithenbank and Chigier 1969). This latter energy loss is a function of the kinetic energy of the fuel entering the combustor compared to the kinetic energy of the air stream.

These three non-availabilities are due to basic thermodynamics and gas dynamics. Nothing at this point has been included to account for friction and shock wave losses in the engine module. The ratio of the kinetic air stream energy to the hydrogen/air combustion heat addition is presented in Fig. 4.3 for the three energy non-availabilities.

These losses increase the entropy S of the airflow, and in fact the thermodynamic "free energy" available to do work is

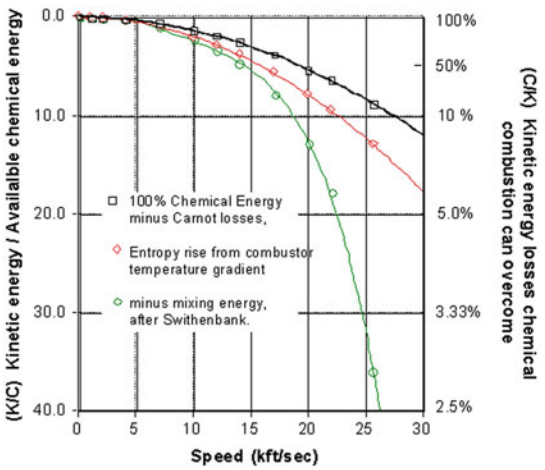

Fig. 4.3 Airflow energy compared to available chemical energy

the difference $E - T{\cdot}S$, not E (Fermi 1956). Anything producing entropy reduces free energy with a multiplier T. Remember 25,573 ft/s is the orbital speed at 100 nautical miles (Mach 23.52, 7.795 km/s, 25,573 mph). At orbital speed and with Carnot losses, the ratio of kinetic energy to energy added by burning hydrogen is about 9:1. That means, the kinetic energy of the air stream is 9 times the fuel combustion heat addition, an astonishing number. Therefore, if the air stream was to lose 11% of its energy (for instance, through friction), combustion of hydrogen fuel could not make up the deficit and there would be no net positive thrust. Adding losses caused by non-uniform combustion, that 9:1 ratio becomes about 12:1. At this point, the loss limit for the air kinetic energy is now more stringent, about 8%. Adding energy required to mix the fuel with the high-energy air, the ratio is about 38:1. The loss limit for the air kinetic energy is now 2.6%. That means that all of the internal inlet combustor-nozzle losses must be less than 2.6%, in order to just maintain thrust equal to drag, with no acceleration. That is very challenging.

The qualitative conclusion is that for a hypersonic airbreathing propulsion system the task is *not so much maximizing combustion efficiency*, but *minimizing air stream energy losses*. Clearly, hypersonic airbreathing propulsion becomes an energy conservation problem and that encompasses the entire vehicle. In fact, the entire vehicle must be conceived a thermal engine, with the energy and heat fluxes entering and exiting the vehicle "box" determining the work available, that is, $(Thrust - Drag) \times V_{flight}$. This is not necessary in a subsonic airplane, since those fluxes are very small compared to the fuel combustion power. For instance, the heat energy that enters the airframe is normally discarded, and that process is called cooling. If instead a portion of that heat energy could be recovered as useful work and converted to thrust, that could add heat corresponding roughly to 30% of the hydrogen fuel heat of combustion (Novichkov 1990a, b). Considering the loss limits discussed above, that is a very large energy addition.

Each fuel has a unique (a) heat of combustion (energy per unit mass of fuel) and a unique (b) fuel/air ratio that burns all of the oxygen in the air called the stoichiometric fuel/air ratio, f_s, see Table 4.1. When the heat of combustion and the fuel/air ratio are multiplied together, the result is the *Brayton cycle heat addition*, which is the energy added per unit mass of air. For the Brayton cycle heat addition, there are essentially two families of values of heat addition using conventional fuels: (1) hydrogen and acetylene, at 3498 kJ/kg and (2) hydrocarbons at 2954 ± 92 kJ/kg. There are indeed some exotic fuels at higher values, but these are very unstable or spontaneously ignite on contact with air. Since the total energy of the air (energy per unit mass of air) plus the square of the speed is a constant, there comes a speed when the energy of the air equals the energy added to the air by burning fuel. Clearly, the faster the aircraft flies, the smaller the fraction "fuel heat addition" becomes of the kinetic energy. Then, the ratio of the total enthalpy to the fuel heat addition ratio increases, as shown by Eqs. (4.3a)–(4.3c) for the fuel combustion energy (not including any losses):

$$\frac{h_t}{Q} = \frac{232.6}{Q} + \frac{500.0 \cdot V_0^2}{Q} \quad (V_0 \text{ in km/s}) \tag{4.3a}$$

$$\left(\frac{h_t}{Q}\right)_{\text{Hydrogen}} = 0.0665 + \frac{V_0^2}{6.995} \quad (V_0 \text{ in km/s}) \tag{4.3b}$$

$$\left(\frac{h_t}{Q}\right)_{\text{Hydrocarbon}} = 0.0787 + \frac{V_0^2}{5.907 \pm 0.18} \quad (V_0 \text{ in km/s}) \tag{4.3c}$$

From hydrocarbons to hydrogen, the Brayton cycle heat addition with Carnot losses equals the air kinetic energy between 2160 and 2351 m/s (7087–7713 ft/s). From hydrocarbons to hydrogen, the Brayton cycle heat addition with Carnot and non-uniform combustion losses equals the air kinetic energy between 2196 and 2019 m/s (6623–7208 ft/s). Then, for any speed above these speeds, the air kinetic energy is greater than the fuel combustion energy addition to the air stream. Second Law available energy losses make the problem a bigger problem because they limit the actual heat energy added to the air to less than the maximum values in Eqs. (4.3b) and (4.3c). For hydrocarbons, see Eq. (4.3c), there is a range in the heat of combustion (±0.18 range on the value in the denominator). With this, there is a practical limit to the combustion energy's ability to offset internal flow and frictional losses that can be determined from first principles. At that point, the airbreathing propulsion system can no longer accelerate the vehicle.

If we look at the other energy losses added to the Carnot loss, we see how much greater the air stream kinetic energy is compared to the fuel addition energy. This is what limits the application of airbreathing propulsion to space launchers. In terms of practical operational engines, the maximum flight speed is probably about 14,000 ft/s (Mach 12) and perhaps as much 18,000 ft/s (Mach 16.5) for research engines (that is, with no payload). The latter figure is 1/2 the specific kinetic energy (energy per unit mass) required to achieve orbit. Clearly, to achieve orbital speed with an airbreather propulsion system, a rocket is required for the final atmospheric acceleration in the trajectory (to obtain the ΔV required to reach orbit) and for all space operations due to lack of an atmosphere.

Table 4.1 Representative fuel properties

Fuel	Q_c (Btu/lb MJ/kg)	Q (Btu/lb MJ/kg)	Q carnot loss (Btu/lb MJ/kg)	Q carnot + non-uniform (Btu/lb MJ/kg)	Q_c·SG (Btu/lb MJ/kg)
Hydrogen	51,500	1504	1188	1038	3648
	119.95	3498	2763	2414	8485
Kerosene (JP-4)	18,400	1247	985.1	860.4	14,360
	42.798	2900	2291	2001	33,402
Methane	21,500	1256	992.2	866.6	8927
	50.009	2921	2308	2.015	20,765

4.4 Internal Flow Energy Losses

The performance of an airbreathing engine is primarily governed by the (a) state properties of air and by the vehicle characteristics that include (b) the captured inlet air mass flow, (c) the air kinetic energy entering the inlet, (d) the energy released to the cycle by combustion of the fuel, and (e) the internal drag and energy losses through the engine flowpath (Yugov et al. 1990). The energy losses in the air stream and the internal wave and friction drag of the engine module can dominate the energy budget. Evaluating these factors permits the establishment of performance boundaries based on first principles. The result is a representation of performance potential and constraints for Brayton cycle airbreathing engines defined by two parameters, altitude and velocity. As first introduced in Sect. 3.7.3, the vehicle performance is constrained by an *altitude boundary* (based on the entropy state of exhaust gas) and a *velocity boundary* (based on the air kinetic energy to combustion energy ratio), a visualization which is called the *flight envelope*, see Fig. 3.34. Both boundaries impact on lift available. In order to define these boundaries for the airbreathing hypersonic cruiser and accelerator, we need to first establish the magnitude of the engine internal flow losses.

Energy input into the combustion chamber must overcome all the losses that are a result of (1) the external drag of the vehicle, (2) the energy losses associated with the internal engine flow, (3) the irreversible losses in the thermodynamic cycle, and (4) it must as well supply the excess thrust minus drag ($T - D$) required for acceleration to orbital speed. As shown in Fig. 4.3, as the flight speed is increased, the kinetic energy becomes increasingly larger than the energy added by the fuel. As the flight speed is increased, the internal drag of the engine increases more rapidly than the airframe drag, so there is a point where the total drag is just equal to the thrust potential of the airbreathing propulsion system (decreasing with increasing speed because the fuel-added energy is becoming a smaller fraction of the air kinetic energy). That is then the maximum speed of the airbreathing flight vehicle. In Fig. 4.3, the losses are represented as a fraction of the flight kinetic energy. The drag losses are given as drag areas referenced to an area related to the propulsion system, see Fig. 4.2. Drag area is a universal way to represent drag energy losses. Multiplying the drag area by the local dynamic pressure, q, yields the first-order total drag which is defined as

$$D = C_D \cdot S \cdot q = C_D \cdot S \cdot \frac{\rho}{2} \cdot V^2 \tag{4.4}$$

The drag area is defined as

$$\frac{D}{q} = C_D \cdot S \quad (\mathrm{m}^2) \tag{4.5}$$

The first-order losses introduced above can be modeled as fractions of the flight kinetic energy. Those losses have been already introduced in Sect. 3.7.3 and are repeated here for convenience: (1) engine internal drag losses, (2) fuel/air mixing losses (after Swithenbank), (3) aircraft total drag, (4) kinetic energy added to the combustor flow by the hot gaseous fuel injection (not applicable for cold liquid-fuel droplet injection), and (5) energy required to accelerate the aircraft.

(1) Combustor drag losses:

$$\left(\frac{\Delta E}{\mathrm{KE}}\right)_{\text{combustor}} = -\left(\frac{V_c}{V_0}\right)^2 \cdot \left(\frac{C_D \cdot S}{A_1}\right)_{\text{eng}} \tag{4.6a}$$

(2) Fuel mixing losses:

$$\left(\frac{\Delta E}{\mathrm{KE}}\right)_{\text{mix}} = -k_{\text{mix}} \cdot \left(\frac{V_c}{V_0}\right)^2 \tag{4.6b}$$

(3) Vehicle drag losses:

$$\left(\frac{\Delta E}{\mathrm{KE}}\right)_{\text{vehicle}} = -\left(\frac{C_D \cdot S}{A_c}\right)_{\text{vehicle}} \tag{4.6c}$$

(4) Fuel injection losses:

$$\left(\frac{\Delta E}{\mathrm{KE}}\right)_{\text{fuel}} = +\phi \cdot f_s \cdot \left(\frac{V_{\text{fuel}}}{V_0}\right)^2 \tag{4.6d}$$

(5) Energy to accelerate:

$$\left(\frac{\Delta E}{\mathrm{KE}}\right)_{\text{accel}} = -\left(\frac{T}{D}\right)\cdot\left(\frac{C_{\mathrm{D}}\cdot S}{A_{\mathrm{C}}}\right)_{\text{vehicle}} \tag{4.6e}$$

In Eq. (4.6d), ϕ is the equivalence ratio.

The only positive term that adds to the available energy is the kinetic energy of the injected fuel. If the temperature of the fuel (in this case hydrogen) is scheduled so that the injected fuel velocity is equal to the flight speed, and the fuel injection angle is in the 6°–10° range, then the injected fuel energy to air stream kinetic energy ratio is 0.0292ϕ. For an equivalence ratio, ϕ, of 6, this provides an energy addition of 17.5% of the air stream kinetic energy. Consequently, recovering normally discarded energy as thrust is as critical as burning fuel in the engine in the first place. This will be discussed further on in this chapter, when identifying the operational zones available for Brayton cycle propulsion systems.

The principal culprit in the drag energy loss inside the combustion chamber, see Eq. (4.6a), is surface friction, and thus the wetted area of the engine (often referenced to the engine module cowl cross-sectional area), and the shock and wake losses from struts and injectors in the combustor flow. Note that friction scales directly with density and that must be minimized to maximize thrust. In order to keep the wetted area, and therefore skin friction loss, to a minimum, the combustor cross-sectional shape and length are critical. Cross-sectional shape is generally driven by integration considerations with the aircraft and has only limited variability, see Chap. 3. The combustor length used is based on both (a) experimental data (Swithenbank 1967; Swithenbank and Chigier 1969) and (b) Computational Fluid Dynamics (CFD) analyses where Second Law (available energy) losses must be considered (Riggins 1996). From both sources, the combustor length for maximum energy efficiency is about 0.40 m (15.7 in.). Swithenbank's measurements in a shock tube combustor test facility verified that for methane, atomized hydrocarbons, and hydrogen. With appropriate choice of injectors/mixers, the combustion time was 35 ± 5 μs (microseconds) over the combustor gas speed range of 6000–12,000 ft/s (1828–3658 m/s) (Swithenbank 1984).

With the wetted area minimized, the remaining task is to identify the shock wave and wake losses. This was done for four combustor configurations in Fig. 4.4 (Czysz and Murthy 1991). The total internal drag area for the four internal combustor geometries is shown in Fig. 4.5. In addition to the work by Czysz and Murthy, these were analyzed by students in the Parks College Hypersonic Propulsion and Integration class with the same results.

Case 2 is a set of five vertical struts with fuel or rocket injectors in the strut base, producing wake turbulence mixing that is characteristic of many ramjet/scramjet designs.

Case 1 is from Professor James Swithenbank of Sheffield University assembling a single horizontal strut with a line of trailing-edge triangles inclined a few degrees to the flow to form a lifting surface that create streamwise vortices for mixing. The fuel injection is from the strut base and at the base of each triangular "finger." The trailing-edge angle is sufficient to produce a subsonic trailing edge in the Mach 4 to 5 combustor flow. The trailing-edge vortex mixing is produced by a subsonic trailing edge on a lifting surface and was developed via experiments in the late 1960s.

Case 0 is an adaptation of the Swithenbank vortex mixing concept to a wall injector configured as a surface inclined to the wall with a subsonic trailing-edge angle, see picture on the right side in Fig. 4.4 (Swithenbank 1967; Swithenbank and Chigier 1969; Swithenbank 1984). The subsonic trailing edge produces the mixing vortex. The author (P.A. Czysz) was shown these injectors by Professor Swithenbank in 1988. The concept of a trailing-edge vortex on a lifting surface was also proposed by Townend (1986).

Case 3 is a shock-confined combustion zone formed between the body and the low-angle body shock wave when

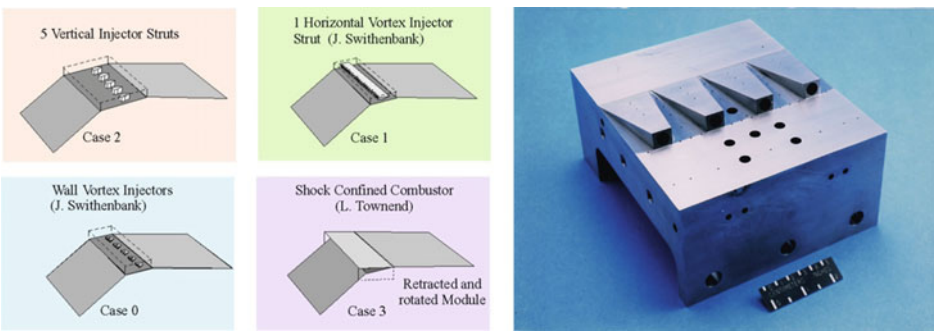

Fig. 4.4 Four representative ramjet/scramjet module configurations are presented schematically on the *left*. For clarity, the aircraft is compression side up, with the airflow from *right* to *left*. The picture on the *right* shows parallel fuel injectors. Their shape creates streamwise trailing vortices favoring mixing (*Courtesy* NASA)

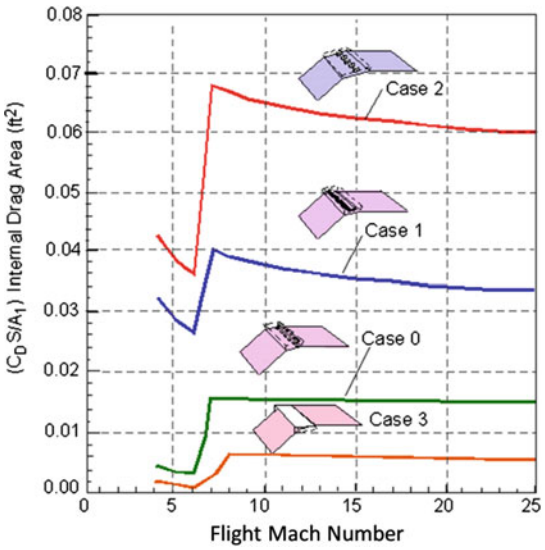

Fig. 4.5 Four very different internal drag areas divided by cowl area for the four combustor fuel injection configuration modules

the engine module is retracted. With Mach numbers on the order of Mach 10 or greater, the resistance of the shock system to normal flow is as great as a physical wall. This concept was successfully tested in an RAE facility by Leonard Townend in 1966 and offers the lowest losses of any configuration. It was also a configuration developed at McDonnell Aircraft under the leadership of H.D. Altis (Czysz 1999, Fig. 15).

For each of these cases, the internal drag area based on skin friction and shock wave drag ($C_D \cdot S$) was determined and referenced to the engine module cowl area as $(C_D \cdot S/A_1)_{engine}$ for each of the four engine module combustor configurations in Fig. 4.5 as a function of *flight* Mach number. Note that as the supersonic combustor through-flow begins (i.e., scramjet operation begins), there is a sharp increase in the internal drag. The stronger the shock waves and shock interference associated with the internal geometry, the sharper the drag rise.

With this information, it is possible to compare the magnitude of the internal engine drag to the external aircraft drag. The ratio of engine drag to aircraft drag can be determined casting the relationship as follows:

$$\frac{\text{Engine drag}}{\text{Aircraft drag}} = \frac{\left[\left(\frac{C_D \cdot S}{A_1}\right)_{eng} + k_{mix}\right] \cdot \left(\frac{q_c}{q_0}\right)}{\left(\frac{C_D \cdot S}{A_0}\right)_{air} \cdot \left(\frac{A_0}{A_1}\right)} \tag{4.7a}$$

$$\left(\frac{q_c}{q_0}\right) \leq \frac{A_0}{A_2} \cdot \frac{V_c}{V_0} \tag{4.7b}$$

$$\frac{A_0}{A_1} \approx \text{constant} \approx 7.0 \tag{4.7c}$$

The value for the aircraft drag area referenced to the geometric capture area $(C_D \cdot S/A_0)_{air}$ is essentially constant for the supersonic through-flow operation of the engine above Mach 6 and has a value of approximately 0.090. The engine airflow contraction ratio (A_0/A_2) depends on whether the engine is operating in supersonic or subsonic through-flow mode. Table 4.2 compares the combustor entrance conditions for the flight speed of 14,361 ft/s (4377 m/s). Once supersonic through-flow is established, the combustor static pressure and temperature remain essentially constant, as determined by Builder's thermodynamic analysis (Builder 1964). At 19,350 ft/s (5898 m/s), the contraction ratio for supersonic through-flow is 32:1, and for subsonic through-flow it is 128:1. Then, as the vehicle accelerates, the supersonic through-flow engine geometry and combustor are almost constant. For the subsonic through-flow engine, the combustor height becomes rapidly smaller and more intensely heated. The pressure and temperature are very high for the subsonic through-flow engine, to the point of being impractical-to-impossible to operate in a flight-weight combustor built from known materials.

Given the combustor conditions, it is now possible to determine the ratio of engine module drag to aircraft drag from Equation set (4.7a–4.7c).

The drag ratios for the four different combustor configurations of Fig. 4.4 are shown in Fig. 4.6. In steady flight, the mass flowrate entering the engine from the external free stream is constant while the density, velocity and flow area vary along the streamtube (flowpath) consistent with that constant mass flow. The result is that the dynamic pressure, q, of the flow, that is, the ability of the flow to generate force, is greatly increased, just as predicted by Eq. (4.5). That increase can be from 3 to 12 times the free stream value. That also means that the internal drag of the engine can exceed the external drag of the aircraft, which explains why internal drag losses are vital to the operation of the scramjet vehicle as shown in Fig. 4.6. This is a key result, because it quantifies how serious the engine drag can be as flight speed is increased, and why some historical engine programs struggled to exceed the Mach 10 to 12 regimes.

With a *retractable* vertical strut, it is possible to shift from the strut injector configuration to the wall injector configuration to maintain aircraft acceleration. If this configuration change is impossible, or is not made, accelerating much beyond Mach 10 is unlikely. It is therefore clear why engines with retractable strut concepts (Baranovsky et al. 1992a, b; Czysz and Vandenkerckhove 2000) are essential to high Mach number operation. The adaptation of the Swithenbank center strut to a wall-mounted vortex mixing injector was a significant improvement. Swithenbank developed the single horizontal strut with the trailing-edge delta fingers such, that although fixed, it had the potential to reach Mach 12. Townend's early pioneering in "shock-confined

Table 4.2 Combustor entrance geometry and conditions for 14,361 ft/s flight speed

Combustor conditions	A_0/A_2 (–)	V_c (ft/s; m/s)	P_c (atmosphere)[a]	T_c (K)	P_c (amagat)[b]
Supersonic through-flow	28.4	12,972 3954	1.10	1756	0.152
Subsonic through-flow	76.5	4495 1370	34.4	5611	1.325

V_0 = 14,361 ft/s, Z_0 = 124,000 ft, q_0 = 1122 lb/ft^2
V_0 = 4377 m/s, Z_0 = 37,795 m, q_0 = 57.72 kPa
[a]Referenced to sea-level pressure and density at 14.696 psia and 59 °F analogous to STP (standard temperature and pressure) conditions
[b]One amagat is local density divided by density at 14.686 psia and 0 °F, 0.002662 slugs/ft^3

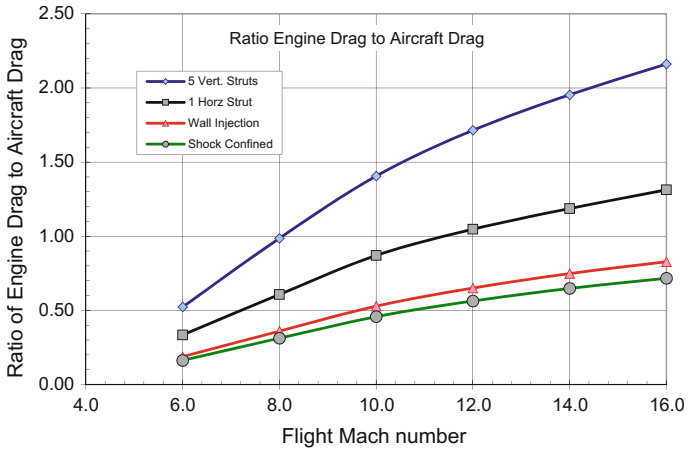

Fig. 4.6 Engine module configuration significantly affects performance

combustion" offered a significant reduction in propulsion system drag (Townend 1986). Ashford and Emanuel have compared the ejector ramjet to the Oblique Detonation Wave Engine (ODWE). The ODWE can represent one operating regime of a combined-cycle propulsion system (Townend and Vandenkerckhove 1994), when at high hypersonic speeds the internal drag of the engine module becomes as large as to significantly diminish thrust-to-drag ratio. The result is that the so-called propulsion acceleration specific impulse, or "effective specific impulse," based on thrust minus drag, is the important parameter for accelerating vehicles, not specific impulse alone as in cruisers. The effective specific impulse is given by

$$I_{spe} = \frac{T - D}{\dot{w}_{ppl}} \quad \left[\frac{\text{N}}{\text{kg/}s} = \text{m/s} \quad \text{(SI units)}\right] \tag{4.8}$$

We now have nearly everything necessary to determine what speed a scramjet-powered vehicle can reach based on available energy and thrust minus drag ($T - D$). There is one element missing, and that is altitude. Altitude is not limiting in the sense that combustion cannot be maintained; it can be limiting based on the value of the nozzle expansion entropy. Entropy is a thermodynamic quantity that relates to how much of the energy in the system is irreversible. That is, if energy (pressure) is expended to accelerate an airstream to supersonic speeds, then to slow it down sufficiently for mixing and combustion to take place, the air must be passed through a series ("train") of shock waves. The entropy-increase across the shock train determines how much of the initial pressure can be recovered. The greater the entropy rise, the larger the fraction of the initial pressure becoming unrecoverable (irreversible pressure loss). The same is true for any Brayton cycle engine (ramjet/scramjets and turbojets are Brayton cycles).

One characteristic of the atmosphere is that, as altitude increases, pressure decreases (at constant volume and temperature $\partial S/\partial p = -V/T$). As pressure decreases, entropy increases. The consequence for any propulsion cycle is that the higher the altitude, the higher the initial entropy in the atmosphere. Since most Brayton cycles have a constant increment of entropy across the cycle, this means that the higher the altitude, the larger the expansion-nozzle entropy. That entropy level determines how much of the chemical energy added to the air molecules through combustion can be recovered as exhaust velocity. The reason the combustion energy cannot be recovered as flow kinetic energy of the gas bulk motion (or flow velocity) is because the entropy limits the conversion of internal energy of the burnt gas (characterized by composition and temperature) to the molecules translation energy by collisions. To extract maximum momentum from high-temperature gas, this must be expanded down to the external pressure. Thermodynamically the driver of this process is the entropy gradient, and if atmospheric entropy is too high, expansion stops inside the

nozzle. The burnt expanding gas is said then to be "frozen." This "frozen" gas will be in a higher energy state compared to a gas in equilibrium with the atmosphere, which corresponds to the lowest internal energy and highest kinetic energy.

Equation (4.9) gives the critical entropy value based on the physical size of the nozzle and its expansion-nozzle half-angle determining expansion (Harney 1967). In the equation, (S/R) is the non-dimensional entropy, θ is nozzle half-angle, r^* is the radius of an equivalent sonic throat that would give the nozzle mass flow, static pressure, and temperature at the combustor exit, and r^*_{ref} is one inch (25.4 mm).

$$\left(\frac{S}{R}\right)_{\text{nozzle}} = \Sigma - 0.4 \cdot \ln\left(\frac{\tan\theta}{r^*/r^*_{\text{ref}}}\right) \tag{4.9}$$

with

$$\Sigma = 30.0 \quad \text{then there is no 'frozen' energy} \tag{4.10a}$$

$$\Sigma = 32.0 \quad \text{then about } 3\% \text{ of the dissociation energy is 'frozen'} \tag{4.10b}$$

$$\Sigma = 34.6 \quad \text{then about } 10\% \text{ of the dissociation energy is 'frozen'} \tag{4.10c}$$

If 10% of the chemical energy is "frozen" and cannot be recovered, there is a serious drop in exhaust gas velocity and a loss of thrust. Remember, in an airbreathing engine for thrust to be generated, the exhaust nozzle exit speed must be greater than the flight velocity. For the case presented in Table 4.2, the exhaust gas speed is just 9.7% greater than flight speed for the supersonic through-flow case and only 3.5% greater than flight speed for the subsonic through-flow case. Clearly, any loss of velocity producing energy is critical at this speed. For a particular engine, given the initial entropy of the atmosphere and the entropy increment of the engine, the onset of "frozen" flow can be identified (Glassman and Sawyer 1970). Then, the dissociation level becomes a function of altitude. We now have an altitude-sensitive or entropy-sensitive criterion for determining the physics of the flow and how it affects the magnitude of the net positive acceleration, see Fig. 4.7.

Above 175,000 ft, the static entropy increases to a level that makes continued control of the frozen dissociation by adding excess hydrogen improbable. There is a region where adding excess hydrogen can provide sufficient three-body collisions to reduce the degree of frozen oxygen and nitrogen dissociation. The excess hydrogen also is a better working fluid than air (its molecular weight is a factor 15 lower) and helps to contain the decrease in thrust from frozen chemistry effects. In the 170,000–180,000 ft altitude region, the atmospheric entropy is so large that even a large amount of excess hydrogen cannot control the irreversible effects. Above this altitude, it is probably not possible to achieve the desired airbreather performance.

With this understanding, we are finally able to determine the operating spectrum of a ramjet/scramjet propulsion system.

4.5 Spectrum of Airbreathing Operation

As introduced in Sect. 3.7.3, with increasing flight speed, the engine performance becomes characterized by energy conservation rather than by combustion; energy conservation becomes far more important than chemistry (Ahern 1992). Figure 4.8 presents a cross section of hypersonic glider trajectories and one maneuvering high L/D weapon (Boost Glide Reentry Vehicle, BGRV). Mercury, Gemini, and Apollo were ballistic capsules with very little lift. Shuttle and ASSET were hypersonic gliders with modest hypersonic L/D ratios (1.5–1.7). Model 122 was a precursor to BGRV to verify the trimmed rolling could be controlled by a nutating

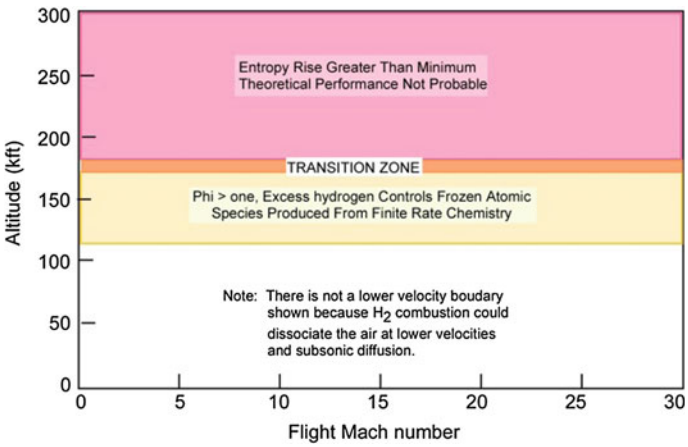

Fig. 4.7 Altitude boundaries determined by "frozen" chemistry

flare. Furthermore, rocket and airbreather exit trajectories are compared with the entry trajectories. The accelerating air breather launchers operate at the highest dynamic pressure (lowest altitude at a given speed). Then, entry heating for the airbreathing vehicle class is less than the exit heating. Cruise dynamic pressure is about equal to the capsule dynamic pressure. A cruise vehicle with a gliding return has less heating when gliding. In fact, one reason for boost-glide (BG) is that because of the pressure required to operate a scramjet, boost-glide always has less heating. Airbreathing exit operates at a greater dynamic pressure than even the BGRV maneuvering entry.

The result is a spectrum of operation over the speed regime developed by (Czysz and Murthy 1991) which is shown here again for convenience in Fig. 4.9. This figure illustrates the extent to which the kinetic energy of free stream air entering the vehicle inlet capture area and the fuel mass and kinetic internal energy become gradually more significant and critical as the flight speed increases. Thus, the operating limits of the airbreather can be clearly identified.

Figure 4.9 shows flight altitude versus flight speed, in kft/s. The corridor labeled "acceleration," which begins at zero speed and extends across the figure to nearly orbital speed (20 kft/s), is the flight corridor for airbreathing vehicles to reach orbital speed. This corridor is based on the dynamic pressure limits of accelerating airbreathing vehicles. The lower limit is based on structural weight and skin temperatures. The upper limit is based on having sufficient thrust to accelerate efficiently to orbital speed. The narrow corridor cutting across the acceleration corridor, labeled "cruise," is the corridor for hypersonic cruise vehicles to achieve maximum range. The vertical shaded area identifies the flight speeds at which a subsonic flow-through engine (ramjet) should transition to a supersonic flow-through engine (scramjet).

The shaded area between 5 and 7 kft/s is the transition region defined by Builder for hydrogen and hydrocarbon fuels as the region where kinetic compression to subsonic

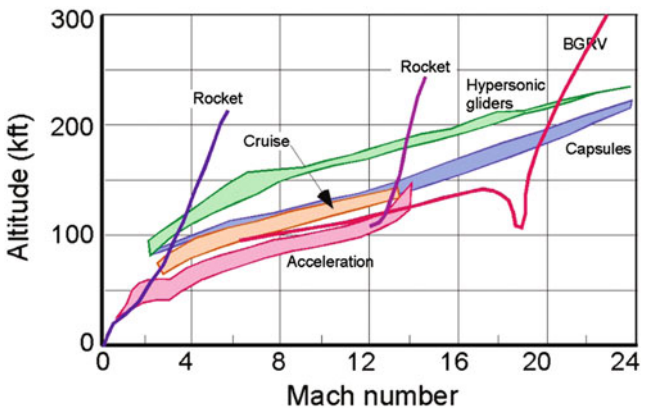

Fig. 4.8 Exit and entry trajectories overlaid

speeds ahead of the combustor alone yields optimum enthalpy compression ratio (Builder 1964). To the left of this area, mechanical compression is required to reach the optimum enthalpy compression ratio. In this area, engines are generally limited to the practical compression ratios achievable; they do not achieve the optimum enthalpy compression ratio. To the right of this area, the kinetic enthalpy compression ratio exceeds the value of the optimum enthalpy compression ratio. Then, diffusion of the air stream has to be limited in order to limit the enthalpy compression ratio (the engine through-flow speed is supersonic). This means that engine flow-through needs to remain supersonic, and flow-through speed increases as the flight speed increases.

The goal in limiting flow diffusion is to maintain a constant value for the optimum enthalpy compression ratio. Analysis of the Second Law of Thermodynamics by Builder does show that the engine design enthalpy compression ratio (rather than the design pressure ratio) and the fuel define the cycle efficiency. Hydrocarbon fuels are to the left side of the shaded area, and hydrogen is to the right side of the area. The vertical lines identified with the numbers 0.5, 1, 2, 4, and 7 represent the ratio of flight kinetic energy to the available fuel energy accounting for Carnot losses. As indicated by the arrows, to the left of the vertical shaded area engines are subsonic flow-through, and to the right of the vertical shaded area engines are supersonic flow-through. As pointed out in Eq. (4.6d), the kinetic energy of the injected, hot, gaseous fuel is a source of energy and momentum very useful to overcome the internal drag and mixing losses. As indicated by the arrows and text adjacent to the vertical lines, this energy addition becomes more critical to engine operation as the speed increases.

The speed regime to the right of the energy (airstream energy/chemical energy added) ratio = 4 line is questionable for an operational vehicle. It is certainly possible for a research vehicle to investigate this area but, as we shall see, at the energy ratio = 4 boundary, the airbreathing vehicle has achieved a significant fraction of the benefits from incorporating airbreathing in terms of the propellant required to achieve a given speed increment. As the energy ratio increases, the scramjet-powered vehicle thrust-to-drag ratio decreases. As the thrust-to-drag ratio decreases, the acceleration (effective) $I_{sp} \equiv I_{spe}$ decreases to the point where the high thrust-to-drag rocket uses less propellant for a given speed increment compared to the scramjet. At that point, the rocket engine is clearly a better accelerator than the airbreathing engine. From an energy viewpoint, a practical maximum airbreathing speed is about 14,200 ft/s (4.33 km/s).

Further to the right of this line, the payoff achieved compared to the resources required offers diminishing returns. That is, the velocity increment produced per unit propellant mass and volume flow is less for the airbreather. Beyond this point, a hydrogen/oxygen rocket requires less

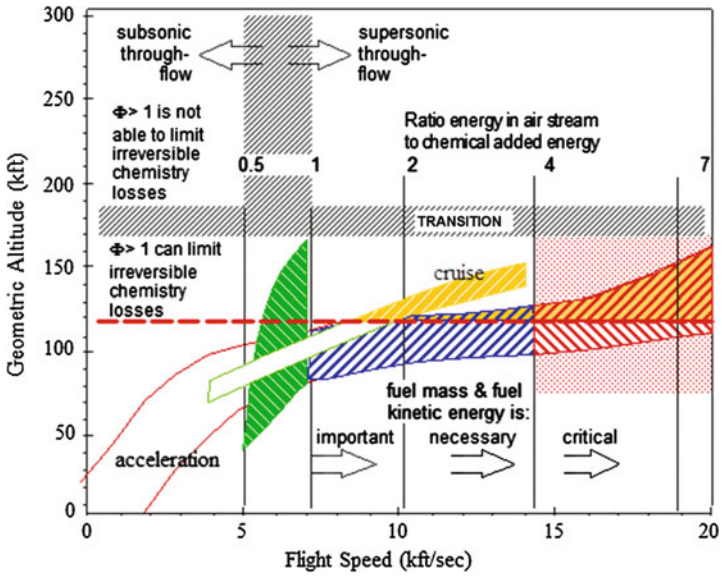

Fig. 4.9 Operating boundaries of Brayton cycle engines based on enthalpy and entropy analyses

propellant mass flow per velocity increment and less vehicle storage volume compared to the airbreathing engine. In terms of available energy and of the propellant required to produce a given velocity increment, the airbreather is outperformed by a hydrogen/oxygen rocket. This is a result of the fact that the thrust-to-drag ratio of the airbreather is diminishing as speed and altitude are increased, while the thrust-to-drag ratio for the rocket is increasing. For this operating regime, the acceleration (effective) I_{spe} of the airbreather falls below that of the rocket.

Returning to the consideration of entropy and applying the criteria from Eq. (4.9), the loss of exhaust velocity begins at about 120,000 ft (36,576 m), shown as a horizontal dashed line in Fig. 4.9. The altitude regime above 120,000 ft altitude produces a degradation of thrust because the increasing entropy levels limit the internal molecular energy that can be converted to kinetic energy and exhaust gas velocity. Dr. Frederick Billig of APL/JHU advocated the introduction of excess hydrogen in the flow to act as a molecular collision third body. In Eq. (4.6d), excess hydrogen means the equivalence ratio (ϕ) is greater than 1. For $\phi = 1$, nominally the fuel burns all of the oxygen available in the air. Excess hydrogen provides abundant third bodies for the dissociated product molecules to recombine to the minimum internal energy state (Billig 1989; Czysz and Murthy 1991). The hydrogen molecule dissociates into two hydrogen atoms. However, unlike other diatomic gases, atomic hydrogen in the exhaust has about 90% of the velocity potential as molecular hydrogen. Since it is a low molecular-weight gas, it is a better working fluid than air, producing pound-per-pound more thrust and higher specific impulse.

However, again due to entropy, adding excess hydrogen works up to a point. In terms of altitude, that point is about 170,000 ft (51,816 m). Between 120,000 ft and 170,000 ft, the excess hydrogen ameliorates the energy "frozen" in the non-equilibrium exhaust gas. Above that altitude, the entropy levels are such that, even with more third body collisions provided by hydrogen, the energy trapped in non-equilibrium products cannot be recovered and it is improbable that a Brayton cycle engine can produce sufficient thrust. Excess hydrogen fuel used in Brayton cycle engines below 150,000 ft and at less than 14,500 ft/s can convert a fraction of the aerodynamic heating into net thrust by soaking friction heating followed by injection and expansion of the heated hydrogen into the engine at a speed corresponding to flight speed. Note that cruise engines operate at greater cycle entropy levels compared to acceleration engines; they may therefore require a larger excess hydrogen flow compared to acceleration engines.

Up to this point, we have used first principles to determine that the vehicle will be stout, and not too small if it is to be built from available industrial capability, see Figs. 3.69–3.72. We have also established it is not practicable for an operational vehicle to exceed 14,200 ft/s in airbreathing mode, and apparently 12,700 ft/s would be less challenging while retaining the benefits of airbreather operation.

4.6 Design Space Available—Interaction of Propulsion and Materials/Structures

We have now established the most likely operational region for an airbreathing operational launcher from a first principles approach. The next question is: "*Are there materials available to operate in the Brayton cycle operating region?*" In this section, the role of coatings reducing heat transfer will not be discussed; while they can enhance structure survivability, most are proprietary and/or classified (for

instance, in the USA any related information is subject to ITAR). The approach taken here was first used in the 1965–1970 Hypersonic Research Facilities Study (HyFAC) for NASA (Pirello and Czysz 1970). The interest has been in identifying operational regions for different materials used on the compression side of hypersonic vehicles and near the nose, where radiation-cooled structures begin. Specifically, the heat transfer rate and surface temperature determined at a point 5 ft aft of the nose have been calculated for the vehicles in Fig. 3.13 as a function of Mach number, altitude, angle-of-attack and load factor and are shown in Figs. 4.10 and 4.11.

The load factor is the lift divided by the weight; in level flight, it is exactly 1. In a maneuver, such as a vertical or horizontal turn, or change in flight path angle, the normal load factor can be in the 2–3 range. The normal load factor, defined as the ratio of lift-to-weight, is usually expressed in units of g, the gravitational acceleration constant on the ground ($\approx$9.81 m/s^2). The angle-of-attack range has been selected from 1° to 20°, since this class of hypersonic aircraft develops their maximum lift-to-drag ratio at less than 20°. This range is much smaller compared to the reentry angle-of-attack range of the space shuttle (Jenkins 2001) or DynaSoar X-20 (Miller 2001) configurations that typically have glide angles in the 40°–45° range during the reentry phase. Correlating heating and lift results in an altitude versus Mach number chart for a particular material temperature, with load factor and angle-of-attack as parameters.

Figure 4.11 shows the assembled area plots for six representative radiation equilibrium temperatures (Pirello and Czysz 1970). Since 1970, the availability of materials has changed, so not all of the materials identified in the reference are available today. One notable example is Thoria-Dispersed Nickel (TD Nickel). Thoria is mildly radioactive and what was thought acceptable in 1967 is no longer acceptable 50 years later. Equivalent materials for 2100 °F (1147 °C) are carbon/carbon and silicon carbide/silicon carbide metal matrix composites manufactured in the USA and in the late 1980s by SEP at Bordeaux (later SNECMA, and currently Safran Snecma). TD Nickel was not considered for either Copper Canyon or the National Aerospace Plane (NASP or X-30). For a given material, the operational envelope and

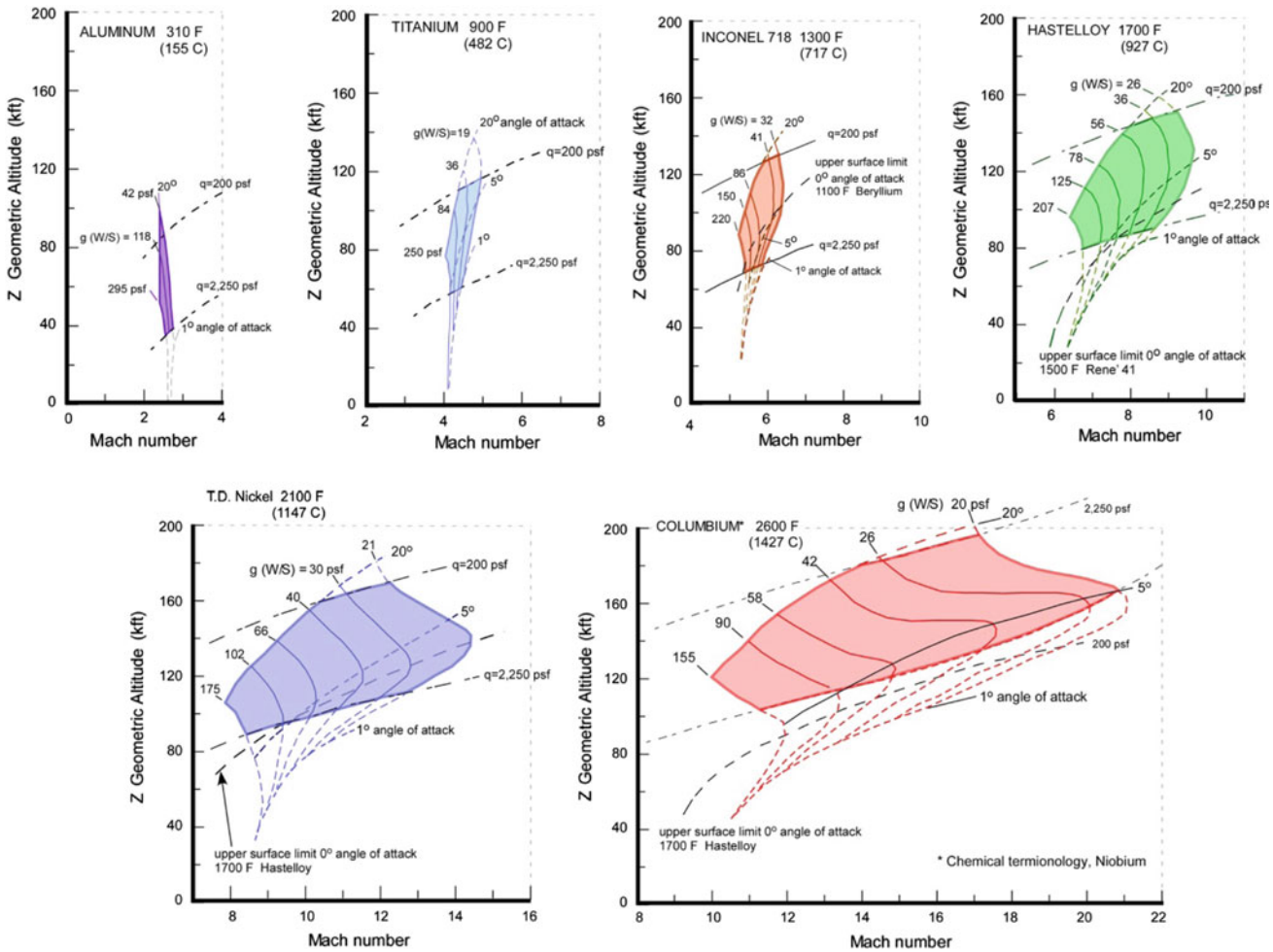

Fig. 4.10 Detailed performance envelopes for aluminum, titanium, inconel 718, hastelloy, thoria-dispersed nickel and columbium (niobium)

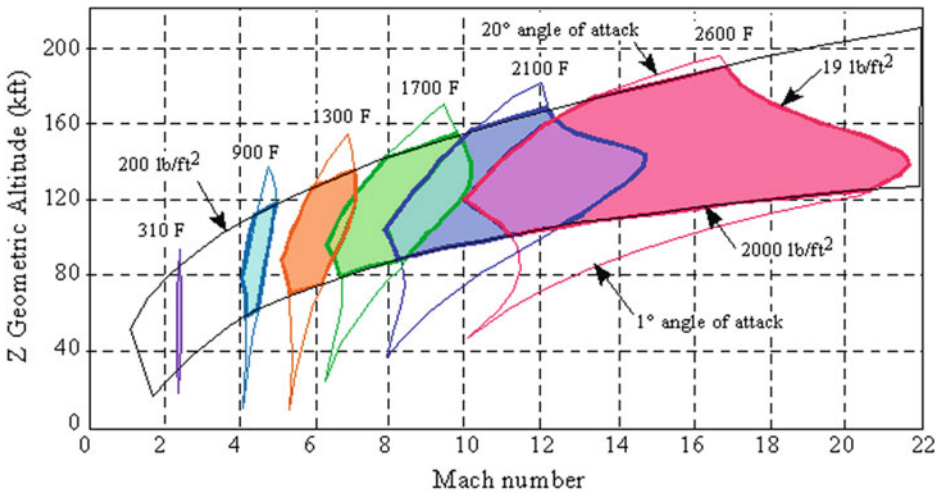

Fig. 4.11 Performance envelope of six materials. Temperature measured 5 ft (1.52 m) aft of the nose on a full-size operational vehicle

maximum speed for an aircraft has been determined as a function of angle-of-attack and load factor.

As shown in Fig. 4.10, each particular material has an operational region bounded by four limits. The left- and right-side limits are lift loading boundaries. Lift loading is defined as:

$$\frac{L}{S_{\text{plan}}} = N_z \cdot \frac{W}{S_{\text{plan}}} \quad (N_z \text{ is the normal load factor}) \quad (4.11)$$

with N_z representing the normal load factor and S_{plan} being the wing planform area. On the right side, this limit decreases as speed increases, because the aircraft becomes lighter as propellant is consumed and the aircraft accelerates toward orbital speed. The upper boundary of each area is determined by the 20° angle-of-attack, and the lower by 1° angle-of-attack. Note that the left boundary is not the same for each temperature area, because the aircraft becomes lighter as less propellant is consumed to reach cruise speed or orbital speed. The materials associated with each surface temperature and the magnitude of the maximum lift loading for each are given in Table 4.3.

Remember that the left and right boundaries are lift loads. If maneuvering at 3*g* is required (not impossible or unlikely for a hypersonic aircraft flying at high dynamic pressure), the wing loading corresponding to the minimum right-side lift loading becomes a maneuver lift loading three times the right-side minimum lift loading. In Fig. 4.10, that corresponds to 63 psf at Mach 10, instead of 21 psf at Mach 14 for the 2100 °F material at 0*g*, and to 78 psf at Mach 8, instead of 26 psf at Mach 10 for the 1700 °F material. Clearly, if a margin for an emergency maneuver is one of the operational requirements, then the maximum speed must correspond to the emergency lift load, not the 1*g* acceleration load.

The importance of lift loading in determining the maximum speed for a given surface temperature is not to be underestimated. If a vehicle is flying near its lift loading Mach limit, and for some reason the angle-of-attack, that is, the lift loading, must be changed, it may be mandatory to slow down before executing that maneuver. For an accelerating air-breather at 1500 lb/ft^2 (7.32 t/m^2) dynamic pressure, the 1*g* level-flight lift loading can be doubled by a 2° change in angle-of-attack, a very significant effect. Flight near a speed boundary could "over temperature," in pilot parlance, that is overheat, the windward compression surface (lower surface, or belly). Similarly, a reduction of the angle-of-attack to near 1° angle-of-attack could "over temperature" the expansion surface (upper surface). From this, for high-speed hypersonic flight it seems the straight and narrow flight path is the least demanding trajectory. With either the hypersonic glider or the airbreathing hypersonic cruiser and accelerator aircraft possessing a glide range approximately equal to the

Table 4.3 Material selections and maximum lift loading boundary for Fig. 4.11

Temperature (°F)	310	900	1300	1700	2100	2600
Temperature (°C)	154	482	704	927	1149	1427
Material	Aluminum	Titanium	RSR titanium[a] Inconel	RSR titanium[a] Hastelloy 1700	RSR MMC[a]	Coated niobium C–C C–Sic
Left boundary (lb/ft^2)	350	250	210	210	180	155
Limit (t)	1.71	1.22	1.03	1.03	878 kg/m^2	757 kg/m^2

[a]These materials are hot isostatically pressed, rapid solidification rate (RSR) titanium powders and metal matrix composites (MMC) made from RSR titanium powder with either silicon carbide fiber or Tyranno fiber reinforcement. Tyranno fiber and coating are patented materials of the UBE Corporation, Tokyo, Japan

circumference of the Earth, it may be better to continue around the Earth and land at the launch site, rather than attempting to turn back and overheat the structure.

An afterburning turbofan engine can increase its thrust by 42% by advancing the power lever to the afterburner position; additional fuel is then injected into the afterburner downstream of the turbine. This maneuver increases thrust by burning the oxygen left in the exhaust gas flow at the expense of increasing specific fuel consumption by 2.5 times (the I_{sp} is 40% of non-afterburning I_{sp}). In contrast, scramjets accelerate by increasing their angle-of-attack to increase the inlet mass capture and therefore thrust. The scramjet can easily double its thrust by an angle-of-attack increase of only a few degrees, at almost constant I_{sp}, by simply capturing more air flow. Then, while the afterburning turbofan in afterburner produces 1.42 times the thrust at 3.55 times the fuel flow, the scramjet produces 2.0 times the thrust at 2.1 times the fuel flow. Clearly, when a scramjet-powered vehicle chooses to accelerate, the pilot advances the throttle for the aircraft to increase its angle-of-attack in order to initiate and execute acceleration! This can produce very different reactions in human pilots who are not accustomed to see the angle-of-attack increase as the power lever is advanced. However, doing so can never give the automatic pilot any concern.

From Fig. 3.18 for the hypersonic glider, the maximum compression-side wall temperature is 2600 °F (1427 °C). This means that any vehicle achieving orbital speed with a vehicle in the FDL-7 class of performance must have materials capable of the same thermal performance on its compression side, whether rocket-powered or airbreather powered to orbital speed. In Fig. 4.11, the maximum temperature material is 4600 °F (2542 °C) for an airbreathing vehicle of either cruising or accelerating to orbit type. Clearly, an airbreathing vehicle capable of orbital speed must be built of the right materials to potentially achieve airbreathing operation in the Mach 12 to Mach 18 speed regime. Whether it is possible for the airbreather to operate in this range, considering what has already been said on Second Law energy losses, remains to be seen.

From a collaboration between P.A. Czysz and J. Vandenkerckhove in early 1984, practical maximum operational speeds for operational airbreathing launchers (Czysz 1992) have been established. These maximum operational speeds range between 3.9 km/s (12,700 ft/s, Mach 11.68) with the possibility to reach 4.27 km/s (14,000 ft/s, Mach 12.87) from a vehicle sizing, compression-side materials, and minimum dry weight approach (Czysz 1995). Many vehicles may not require operation above Mach 12. TSTO launchers concepts usually "stage" (i.e., release the second stage) in the Mach 6 to Mach 10 range, although some concepts stage at Mach 12. Hypersonic cruise vehicles are historically in the Mach 8 to Mach 12 range because of engine limitations, and also due to the very practical fact that flying faster does not improve block time, because of the longer climb and descent time and distances (Koelle 1989). For these cases, current titanium material systems match up well with the acceleration and cruise requirements.

Figure 4.12 shows two of these operational areas for two representative radiative equilibrium surface temperatures at 5 ft (1.52 m) aft of the nose, i.e., 1700 °F (927 °C) and 2100 °F (1149 °C). Radiative equilibrium occurs when the surface temperature is such that the total heat flux from the air above is radiatively rejected by the surface. These two temperatures are characteristic of hot isostatically pressed, rapid solidification rate (RSR) titanium powders, and of metal matrix composites (MMC) made from RSR titanium powder with silicon carbide fibers or Tyranno fiber/cloth reinforcement. These operational zones are from Fig. 4.11 with three values of lift loading shown. The lift loading lines have the same value in both operational areas. If the leading edges are thermally controlled by transpiration cooling or heat-pipe thermal pumping, then the materials shown are applicable for the primary metal thermal protection system based on shingles. The control surfaces will have to be fabricated with carbon–carbon or silicon carbide–carbon ceramic matrix materials because of their flow environment and also because of their structural thinness, as indicated in Fig. 3.18.

In Fig. 4.11, the cruise corridor corresponds to the highest flight Mach numbers for a given material. For instance, if an aircraft is flying at Mach 14 with a 1g wing loading of 19 lb/ft^2 (92.5 kg/m^2) and there is an operational problem that requires returning to base, unless the aircraft is slowed to about Mach 11 before attempting to climb, dive, or execute a 2g turn (lift loading now 38 lb/ft^2 (185 kg/m^2)), this maneuver will end in "over-temperaturing" the vehicle. This is one important reason to operate hypersonic vehicles with automatic controls, because actions consistent with instinctive subsonic or low supersonic aircraft piloting are fatal when flying hypersonic aircraft. Again, whether accelerating or cruising, any deviation from straight-line flight can be a source of "over-temperaturing" the thermal protection system (TPS).

4.7 Major Sequence of Propulsion Cycles

Section 3.7.3 introduced airbreathing propulsion systems in the context of parametric sizing and multi-disciplinary synthesis. The following expands the discussion to propulsion-integrated transatmospheric launchers.

There are a significant number of propulsion system options that have been studied and reported. In this chapter, 14 different classes of propulsion systems are discussed that are suitable for either hypersonic flight or transatmospheric

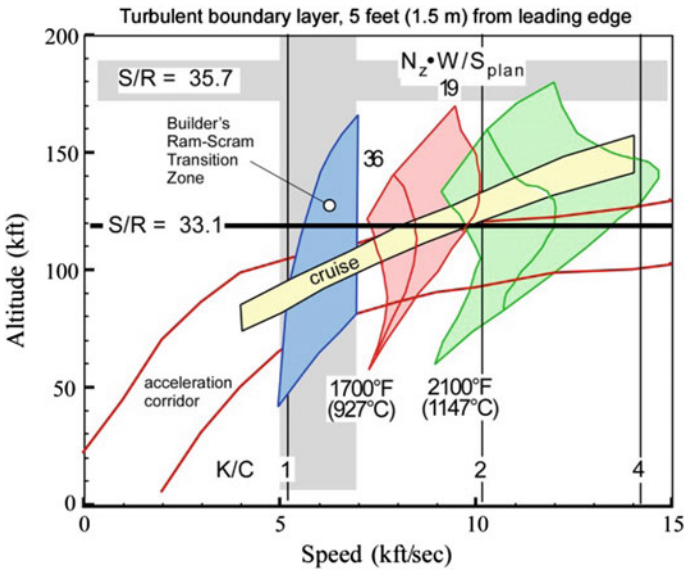

Fig. 4.12 Materials and engine operating regimes compared to the cruise and acceleration flight corridors. The ratio ($N_z \times W/S_{plan}$) is normal acceleration times wing loading in lb/ft^2

space launchers. The authors have focused on those that are applicable to SSTO and TSTO transatmospheric vehicles and hypersonic cruise vehicles. If the rocket ascent to orbit is deleted from the analysis, then a SSTO that uses airbreathing propulsion to Mach 10 is essentially the first stage of a TSTO vehicle. At the end of this chapter, SSTO and TSTO are compared following the work of the late Jean Vandenkerckhove in collaboration with the authors. The intent is to define the SSTO weight ratio and the onboard oxygen ratio carried by the vehicle.

As we have seen in Chap. 3, the smaller the weight ratio and the oxygen-to-fuel ratio, the smaller the size and gross weight of the resulting vehicle. In terms of mass ratio and oxidizer-to-fuel ratio to orbital speed, the authors examined 6 principal hydrogen-fueled propulsion categories, as shown in Figs. 3.4 and 3.5. The term "thermally integrated" is used in the description of these categories. "Thermally integrated" means that the hydrogen fuel has a role in all cycles integrating the combined-cycle engine; it collects thermal energy normally discarded as "cooling heat," finally turning that energy into useful work. This is accomplished by driving closed-loop power extraction units (Ahern 1983), or expansion turbines, or by converting heat into thrust via expansion. The combined-cycle concept dates back more than 50 years to The Marquardt Company (Escher 1998). Marquardt had a propulsion concept that would reach hypersonic speeds using a single engine (Escher et al. 1967; Escher 1995, 1996). One of The Marquardt Company's concepts incorporated folding rotating machinery (Escher and Czysz 1993) into their cycle; however, it was still a single engine that could go from takeoff to hypersonic speeds.

The following introduces seven principal airbreathing propulsion categories with hydrogen as fuel:

(1) The first category is the liquid-propellant, chemical rocket and rocket-derived air-augmented propulsion, where the primary propulsion element is a rocket motor. Solid rockets and hybrid rockets are not included as they are inherently expendable, limited-use engines not applicable to sustained-use vehicles.

(2) The second category is the airbreathing rocket, where the propulsion elements are a rocket motor and an air/fuel heat exchanger that supplies the rocket motor with atmospheric air as oxidizer over part of its trajectory. The British HOTOL, SKYLON, and further concepts developed by Alan Bond (Reaction Engines) represent such a propulsion system.

(3) The third category is the thermally integrated rocket–ramjet/scramjet engine, a combined-cycle propulsion system where the principal element is a rocket ejector ramjet/scramjet. The rocket ejector provides both thrust and low-speed compression. The rocket ejectors in the ramjet/scramjet are fuel ejectors when the thrust/compression augmentation is not required. Jean Vandenkerckhove's "Hyperjet" was in this class of engines.

(4) The fourth category is a combined-cycle based on a thermally integrated rocket and turbojet (often cited in the literature as "KLIN" cycle). In this case, thermal integration provides the turbojet pre-compressor air cooling for higher Mach number operation and greater thrust; the thermal energy recovered from the turbojet improves the rocket expander cycle operation. Invented by V.V. Balepin, formerly at the TsIAM Russian center, it is the only such known thermally integrated, turbine-based, combined-cycle propulsion system.

(5) The fifth category is a combined-cycle consisting of an airbreathing rocket thermally integrated with a rocket

ejector ram/scramjet. This system was first reported by Rudakov and Balepin (1991) at an SAE Aerospace America Conference in Dayton, Ohio.

(6) The sixth category is the thermally integrated engine combined-cycle propulsion analogous to the fifth category, except the thermally processed air is separated into nearly pure liquefied oxygen (so-called "enriched air") and oxygen-poor nitrogen, with the liquid oxygen-enriched air stored for later use in the rocket engine. The oxygen-poor nitrogen is introduced into the ramjet engine creating a bypass ramjet. With the greater mass flow and reduced exhaust velocity, the propulsion efficiency is increased.

(7) There is a seventh category spanning the above categories. In fact, the engines discussed in the above are all continuously running engines. In World War II, the V-1 flying bomb was powered by a pulsejet. This engine is an intermittently firing engine, consisting of an acoustically tuned pipe fed an explosive mixture that, when ignited, sends the combustion products wave traveling down the pipe. After the products exit the tube, the tube is effectively scavenged. New fuel is then injected and a new mixture forms, reloading the tube. The ignition process is then repeated, starting a new cycle. This periodic operation gives the pulsejet a characteristic cyclic rate and the characteristic sound that in the V-1's case gained it the nickname of the "buzz bomb," The modern development of the pulsejet is the pulse *detonation* engine, or PDE, where the volumetric explosion is replaced by a thin detonation wave, with a drastic increase of burning rate and power available, see for instance (Holley et al. 2012; Cocks et al. 2015). Three PDE versions of the continuous operation engines are included in the discussion at the end of this chapter. The first is a pulse detonation rocket (PDR) and the remaining two are the PDE-ramjet and the PDE-scramjet combined-cycles. More recently, rotating detonation engines (RDE) are being tested in the USA and France, where the detonation wave burns fuel and air while continuously rotating rather than by traveling axially (Cocks et al. 2016). Note that this subject is proprietary in France, being developed by MBDA for the military, and it is subject to ITAR (International Traffic in Arms Regulations) in the USA.

There is a discussion of each engine cycle in this chapter. However, before we can proceed, there are operational considerations giving additional insights into the application of the propulsion system to a launcher; these are presented in Table 4.4. There are three general performance groups: (1) one that has no airbreathing capability, (2) another that can reach Mach 5 to 6 airbreathing, and (3) the last group that can reach Mach 6 to 14, again in airbreathing operation. The nominal SSTO mass ratios to orbital speed and the normal airbreathing speeds at their transition to rocket propulsion are given in the top rows. As with all launchers, if the mass ratio is less than four, horizontal takeoff is not possible, and vertical takeoff with horizontal landing (VTHL) must be the takeoff and landing mode assumed.

In Table 4.4, the term "abortable on launch" is the capability of the launcher to safely abort the mission while being *on launch* and to *return* to the launch site. This does not just consist of an escape rocket firing and a payload capsule being recovered. It means, in aircraft terms, that the system aborts the launch and returns intact and functional to the launch or adjacent alternate site. The only vertical launch rocket that aborted its launch after an engine failure and landed vertically and safely on its launch pad was the McDonnell Douglas Astronautics experimental rocket, the Delta Clipper (Butrica 2003; Stine 1996; Hannigan 1994). The late astronaut Pete Conrad was flight director, and Dr. William Gaubatz was program manager. Other than current aircraft, no other space launcher has ever demonstrated that capability. One of the limitations to achieving abort on launch is indeed the mass of the oxidizer carried. The Delta Clipper had only a mass ratio of about 2.5. Had it been an operational orbital vehicle with a mass ratio of about nine, it may not have been abortable. If commercial space is to happen, in the authors' opinions it will be necessary to recover the launcher, functional and intact, and this capability is dramatically influenced by the oxidizer mass carried. It should be remembered that the oxidizer mass is always many times greater than the fuel mass; it is the oxidizer that affects the mass of the propellants the most.

Reuse and sustained operations imply that the returned vehicle is ready for another flight after an inspection. With today's rocket engines this is improbable, because they are designed for minimum weight and not for sustained use as aircraft engines are. Designing rocket engines for sustained use would require readopting the philosophy in place for the XLR-129. Flights before overhaul are indicative of an operational system that has sustained operational capability avoiding refurbishment after every launch. In 1964, the goals for the vehicle (McDonnell Douglas Model 176) to support the MOL and the XLR-129 were 100 flights before overhaul.

One of the serious impediments to commercial operations is that there is only one launch site available per launcher, with the exception of the Sea Launch platform, that can be towed to any oceanic location. This may be acceptable for the commercial communications satellite organizations, just as operations from one coal mine were acceptable for the first commercial railroad train in York, England. A commercial space transportation system will have to have the

Table 4.4 Comparison of continuous operation propulsion cycles

Characteristics	Continuous operation propulsion system concepts						
Propulsion concept	Rocket	Rocket-derived	Airbreather rocket	Turbojet-rocket combined cycle	Ejector rocket combined cycle	Airbreather rocket combined cycle	ACES
Candidate cycles	Topping, expander cycle	Air-augmented or ram rocket	LACE or deeply cooled	KLIN	Strutjet or ram/scram and rocket	LACE, or deeply cooled and ram/scram	LACE, deeply cooled and ram/scram
Category	First	First	Second	Fourth	Third	Fifth	Sixth
SSTO mass ratio (LEO) (–)	8.0–9.0	6.5–7.5	5.0–6.2	5.0–5.5	4.0–5.4	3.2–4.2	2.5–3.5
Airbreathing speed (Mach)	0	~5.0	5.0–6.0	~5.5	6.0–14	6.0–14	6.0–14
Abortable on launch	Improbable	Questionable	Possible	Possible	Likely	Yes	Yes
Reuse/sustained operation	No	Possible	Yes	Yes	Yes	Yes	Yes
Flights before overhaul (–)	100[a]	100	200	200	300	500	600
Onboard oxidizer (%)	Maximum	90	55	55	40	30	<10
Applicable to TSTO	Possible	Possible	Yes	Yes	Yes	Yes	Yes
Basing	Fixed	Fixed	Fixed	Multiple	Multiple[b]	Multiple	Multiple
Takeoff/landing	VTHL	VTHL	VTHL	VTHL	VTHL	HTHL option	HTHL
Configuration	External	External	Hypersonic	Hypersonic	Integrated	Integrated	Integrated
concepts	Tank + glider	Tank + glider	Glider	Glider	Airbreather	Airbreather	Airbreather

All can carry personnel or payload, but are automatic, autonomous vehicles
[a]80+ flight ground test without overhaul demonstrated by RD-0120
[b]Operates from numerous non-space launcher bases

characteristics of a UPS or Federal Express system to be truly commercial. Until the launchers are designed for a lower mass ratio, say, 4 or less, that will not be practicable. When a mass ratio of 4 or less is achieved, the entire concept of operations will change, because with the correct hypersonic configuration and propulsion system the time-consuming vertical assembly, fueling and month-long countdown will be eliminated. Runway operations will become the norm, opening more launch and return sites for distributed operations. Orbital plane changes and offset maneuvers will be far more economical when executed in ascent and not from orbit.

Another item in Table 4.4 is "applicable to TSTO." This is an important consideration. Most of the analysis discussed in this chapter is done for SSTO because this requires only one vehicle, it offers the best approach for sustained operations, and represents the most challenging. However, SSTO can create the impression of being a one-size-fits-all solution. The advantage of a TSTO solution is the payload to orbit flexibility. A SSTO with a 7 t (15,435 lb) payload to orbit is a hypersonic vehicle with an operational empty weight (OEW) of about 70 t (154,300 lb) and a gross weight (TOGW) of about 380 t (837,900 lb). That is a mass ratio to orbit of 4.9. The payload to Earth orbit is 10% of the vehicle empty weight that carries it. This means, whether people or support supplies, the payload is always 7 t. However, a hypersonic glider, that is the second stage of a TSTO, with a 7 t payload can be carried by a first stage that stages at Mach 11 and that has an OEW of about 35 t. Then, the payload to Earth orbit is 20% of the empty weight of the vehicle carrying it. The first-stage OEW is about 38 t, for a total empty weight of 73 t (161,000 lb). The total gross weight of the two stages is about 210 t (463,000 lb), with the second-stage gross weight at about 94.5 t (208,500 lb). That means a total mass ratio of 5.0. If the second stage is a cargo-only expendable cylinder, then for the same gross second-stage weight the payload would be about 17.5 t (38,600 lb). Then, the payload to Earth orbit is 50% of the vehicle empty weight that carries it. The gross weight is the same, so the mass ratio is the same. Thus, there is much more flexibility in the payload variety and weight that can be delivered to Earth orbit by the TSTO vehicle concept. In addition, the offset or orbital plane

maneuver would be carried by the first-stage flying as an aircraft in the atmosphere, not the stage reaching orbital speed and altitude (Czysz and Vandenkerckhove 2000). The propulsion conclusions apply to TSTO as well as SSTO.

4.8 Rocket-Derived Propulsion

Rocket-derived propulsion systems begin with the liquid-propellant rocket. Propellants are injected into a combustion chamber to burn at high pressure and temperature, and then their products exit via a sonic throat into an expansion nozzle that is designed to match the nozzle exit static pressure to the ambient atmospheric pressure, as shown in Fig. 4.2. For maximum performance, the nozzle exit pressure should be equal to the surrounding ambient pressure. However, atmospheric pressure ranges from 14.696 psi (101.3 kPa) at the surface to zero in space. Normally the nozzle size is specified by the area ratio, i.e., the exit area divided by the sonic throat area. The area ratio determines the ratio of the nozzle exit pressure to the chamber pressure. Once the chamber pressure is determined, then the exit pressure is determined. If the nozzle exit pressure is higher than the ambient pressure, the nozzle is termed "underexpanded" and the result is the nozzle flow suddenly expanding upon exiting the nozzle. When you see a picture of a rocket at high altitude or in space and see the exhaust blossoming into a large plume, this is an underexpanded nozzle. If the nozzle exit pressure is lower than the ambient pressure, the nozzle is termed "overexpanded" and the nozzle flow separates from the nozzle wall at a location that yields the approximate correct area ratio for the ambient pressure. If you see a picture of a rocket lifting off from a launching pad, you can see the flow exiting the nozzle is smaller in diameter than the actual nozzle diameter, a sign that this is an overexpanded nozzle.

Engines such as the Pratt & Whitney RL10-3 have a two-position nozzle. At lower altitudes, the nozzle area ratio is small (10–20). As the altitude is increased and the area ratio becomes too small, a nozzle extension slides over the nozzle increasing the area ratio (50–60). Thus, there are two altitude regions where the engine is correctly matched to the ambient pressure.

For most high-thrust rockets, the propellants are a fuel and an oxidizer. For some space maneuver and station-keeping rockets, the fuel is a monopropellant that is decomposed by a catalyst into gaseous products.

Rocket-derived propulsion involves installing the rocket as a primary nozzle in an air ejector system. The rocket induces airflow in the secondary air system, thereby increasing the total mass flow through the system. These systems are generally operated up to Mach 6 or less, because of pressure and temperature limits of the air induction system. At Mach 6, the inlet diffuser static pressures can typically equal 10–20 atmospheres and 3000 °R (1666 °K). These propulsion systems can offer major advantages when applied to existing rocket launchers (Czysz and Richards 1998) and are described below.

1. Chemical rocket. Figure 4.13 represents a typical turbopump-fed liquid-propellant rocket. A turbopump is generally a centrifugal compressor to pressurize the fuel, coupled to an expansion turbine driving the pump. The turbopump pressurizes the propellant feed system to the pressure required for engine operation. For the turbopump to function, some fuel and oxidizer are burned in a separate combustion chamber to generate the hot gases necessary to power the turbine, powering in turn the pump. Because this burned propellant does not contribute to the primary thrust of the rocket engine, the turbopump cycle rocket (such as the Rocketdyne J-2 for the Saturn V) has the lowest specific impulse, I_{sp}, for a given propellant combination.

A hydrogen/oxygen high-pressure engine has an I_{sp} of about 430 s. In the so-called "topping cycle" (such as in the Rocketdyne SSME), the turbopump exhaust, which is still rich in fuel, is introduced into the rocket motor, contributing to the engine total thrust. A hydrogen/oxygen high-pressure engine using this cycle has an I_{sp} of about 455 s. In an "expander cycle" (such as Pratt & Whitney RL-10), a liquid fuel, such as hydrogen, is vaporized and raised in temperature by passing through the engine cooling passages. The hot gases then drive an expansion turbine to drive the turbopump before being introduced into the combustion chamber. This engine has the highest I_{sp} for a specific propellant. A hydrogen/oxygen high-pressure engine has an I_{sp} of about 470 s. Some representative propellants are given in Table 4.5 with hypergolic propellants in bold. Hypergolic propellants are those that spontaneously ignite on contact with each other; monopropellants are in italics.

The chamber pressure assumed in Table 4.5 is 1000 psia (about 68 atmospheres), yielding the specific impulse values given in a nozzle with optimum area ratio. The I_{sp} is the thrust developed per unit mass flow and per second (lb/(lb/s)) or kg/(kg/s)). The I_{sp} is a function of the combustion temperature, chamber pressure, and the thermodynamics of the products of combustion. Since the thrust per unit mass flow is constant, the rocket engine thrust is a function of the total mass flow. Given the combustion temperature, the mass flow depends on chamber pressure and engine throat area. To obtain more thrust, either the pressure can be increased for the same size engine or the size of the engine can be increased. The rocket motor is necessary for space propulsion because it is independent of any atmosphere. Although a turbopump rocket engine is shown in Fig. 4.13, for some if not most, space applications, the propellant tanks are pressurized to feed propellant into the engine and there are no turbopumps.

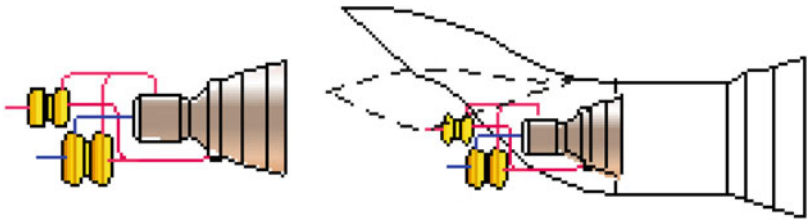

Fig. 4.13 Rocket-derived propulsion (*left* liquid-propellant rocket; *right* air-augmented rocket, ram rocket). *Blue* oxidizer. *Magenta* fuel. Pump and its turbine driver share a common shaft

Table 4.5 Representative propellants and their characteristics

Fuel	Oxidizer	I_{sp} (s)	SG·I_{sp} (–)[a]	*O/F* (–)
UDMH	**N_2O_4**	**319**	**390**	**1.23**
Hydrazine	**H_2O_2**	**304**	**375**	**2.04**
Hydrazine	**N_2O_4**	**312**	**365**	**2.25**
JP-4	LOX	329	330	2.40
Nitromethane	–	*273*	*308*	*Monoprop.*
Methyl alcohol	LOX	297	282	1.15
Methane	LOX	329	247	2.33
Hydrazine	–	*218*	*219*	*Monoprop.*
Hydrogen	N2O4	349	207	11.5
Hydrogen	LOX	455	170	6.00

[a]The product of specific impulse and the specific gravity (SG) of the propellant is termed density specific impulse and was used by the late V. Glushko of the GDL OKB to show the performance advantages of hypergolic propellants. All the I_{sp} are in vacuo

This is to clarify that the question of airbreather engines versus rocket applies only to flight in the Earth's atmosphere and concerns the large weight of oxidizer required by rockets, which increases the gross weight of the vehicle and increases the thrust of the rocket engines accordingly. Thinking along these lines, it appears intuitive that one way to increase the thrust of the rocket, for the same propellant flow, is to make it an "air-augmented" rocket.

2. Air-augmented rocket. Figure 4.13 employs the rocket motor as a primary ejector (Harper and Zimmerman 1942; Nicholas et al. 1996), so some of the external airstream can be mixed with the rocket exhaust to increase mass flow, thereby increasing thrust and specific impulse. These systems are generally operated up to Mach 6 or less, because of pressure and temperature limits of the air induction system. At Mach 6, the inlet diffuser static pressures can typically equal 10–20 atmospheres and 3000 °R (1666 °K). The rocket motor operates on its normal oxidizer-to-fuel ratio. The reduction of the mass-averaged exhaust velocity at low speed increases propulsion efficiency.

This simple concept is not designed to burn the oxygen in the entrained air. The weight ratio is reduced for an SSTO from 8.1 to 7.5. The sketch in Fig. 4.13 is notional, but the use of an inward-turning inlet with a variable capture area offers high mass capture tailored to the Mach number and provides high-pressure recovery. The retractable feature eliminates inlet drag at higher Mach numbers. True, the external air inlet system adds empty weight, but with a mass ratio reduction of 0.60, the air induction system weights less than the rocket, if the inlet system is less than 8% of the dry weight.

3. Ram rocket. Figure 4.13 is an air-augmented rocket cycle where the rocket is operated at a fuel-rich oxidizer-to-fuel ratio, so the oxygen in the entrained air can now burn the excess fuel at the normal airbreathing air/fuel ratios for the fuel used. Scherrer gives an excellent evaluation of the air-augmented rocket and the ram rocket based on ONERA research (Scherrer 1988). The external airstream is mixed with the rocket exhaust to increase mass flow. Combined with the combustion of the excess fuel, thrust and specific impulse increase at lower Mach numbers ($M < 6$). The weight ratio is reduced for an SSTO from 8.1 to 6.5. The sketch in Fig. 4.13 is notional, but the use of an inward-turning inlet with a variable capture inlet feature offers high mass capture tailored to the Mach number and provides high-pressure recovery.

The retractable feature eliminates inlet drag at higher Mach number. The external air inlet system adds empty weight. But with a mass ratio reduction of 1.6, the air

induction system weights less than the rocket if the inlet system is less than 24% of the dry weight. This is the better operational mode compared to the air-augmented rocket.

Neither of these latter two rocket configurations have found any significant applications yet, because of the opinion that the air-induction system might be too heavy for the benefit provided. That is very close to true for the air-augmented rocket, but it is not true for the ram rocket. A significant reduction in mass ratio can be realized for about a 5% increase in empty weight. Aircraft such as the SAAB-Scania Viggen, in fact, employ this method to increase the thrust of the gas turbine engine. The exhaust nozzle is an ejector nozzle, where the primary gas turbine exhaust induces ambient air into a secondary nozzle-mixer flow (Roed 1972).

4.9 Airbreathing Rocket Propulsion

Airbreathing rocket-derived propulsion systems are generally operated up to Mach 6 or less, because of pressure and temperature limits of the air-induction system (Miki et al. 1993). At Mach 6, the inlet diffuser static pressures can typically equal 20 atm and 3000 °R (1666 K). Airbreathing rocket propulsion concepts employ a method to reduce the temperature of air entering the inlet system; hence it can be compressed to rocket chamber operating pressures with reduced power requirements. There are two options: (1) One option is to deeply cool the air just short of saturation and use a turbo-compressor to compress the cold gaseous air to the rocket chamber pressure and inject it into the combustion chamber; (2) the second option is to liquefy the air and use a turbopump to pump the liquid air to rocket chamber pressure, then gasify it for injection into the rocket chamber, see Fig. 3.4. The rocket motor operates at nearly normal oxygen-to-fuel ratios, except that there is now a large mass of nitrogen also introduced into the combustion chamber. Again, the mass average exhaust velocity is reduced and the total mass flow increased, increasing thrust and propulsion efficiency.

4. Liquid air cycle engine, LACE rocket. Figure 4.14 is the rocket part of the Aerospace Plane propulsion concept developed by The Marquardt Corporation in the mid- to late-1950s, see Fig. 4.15.

The LACE (Liquid Air Cycle Engine) concept has been developed in Russia (Rudakov and Balepin 1991; Balepin and Tjurikov 1992; Balepin et al. 1993, 1995), Japan (Togawa et al. 1991; Miki et al. 1993; Ogawara and Nishiwaki 1989), and India (Gopalaswami et al. 1988). The thermodynamic principle of LACE is that a significant fraction of the energy required to liquefy the hydrogen is recoverable as available energy that can be converted to useful work. For a hydrogen-fueled aircraft, atmospheric air is an enormous source of energy, because of the 220–230 K temperature difference. Via a hydrogen/air heat exchanger, atmospheric air can be cooled as the liquid hydrogen is boiled, requiring no energy expenditure from the aircraft's systems. Ahern (1983, 1992) was associated with the development of the first LACE system in the USA when working with the scramjet team at The Marquardt Company in 1958. As part of that work, Ahern proposed a closed helium heat pump that avoided the problem of having two phase changes in the hydrogen/air heat exchanger (air being liquefied as hydrogen is gasified) and of having a hydrogen heat exchanger in the air inlet. To the author's knowledge, this concept has never been developed beyond the laboratory stage. Ahern also had a concept of recovering the aircraft aerodynamic heating with the hydrogen flow to the engine, and using that energy to create useful work (electrical, hydraulic, and air handling work) and engine thrust (thrust from supersonic hydrogen fuel jet injected into the scramjet combustor). This will be further discussed in the section on ramjets/scramjets.

As depicted in Fig. 4.14, this cycle employs a hydrogen/air heat exchanger in the air inlet to capture the inlet air kinetic energy from the incoming air and to cool it to nearly saturation. The cooled air is then pressurized to a few atmospheres and then flows into the pressurized liquefying heat exchanger. The total thermal energy collected from the incoming air and hydrogen combustion chamber is used to drive an expansion turbine, which in turn drives a turbopump that pumps liquefied air into the rocket motor. A rocket motor combustion chamber heat exchanger is necessary to provide sufficient energy to drive the turbomachinery (Tanatsugu et al. 1987). In effect the rocket becomes an airbreathing rocket for Mach numbers less than 6. In this concept, there is no need for another airbreathing engine. This cycle reduces the mass ratio to the 5.0–5.8 range and the oxygen-to-fuel ratio to about 3.5.

5. Deeply cooled rocket. As depicted in Fig. 4.14, this cycle employs a hydrogen/air heat exchanger in the air inlet to capture the inlet air kinetic energy from the incoming air and cool it to nearly saturation. Unlike the LACE cycle, the next step is to compress the cold air via a turbo-compressor. This controls the air temperature entering the compressor and limits the work of compression and the compressor corrected speed. The warmed hydrogen then enters the rocket combustion chamber to recover additional energy. The total thermal energy collected from the incoming air and hydrogen combustion chamber is then used to drive an expansion turbine, which in turn drives a turbo-compressor that compresses the cooled inlet air. That air can be cooled to nearly saturation by the hydrogen flow, then compressed to rocket operating pressures and introduced into the combustion chamber.

This cycle was independently developed at TsIAM (Rudakov and Balepin 1991) and by Alan Bond for

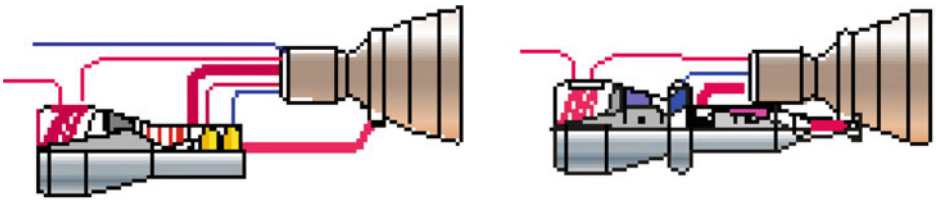

Fig. 4.14 Airbreathing rockets (*left* LACE rocket; *right* deeply cooled rocket). The cooling heat exchanger is the structure ahead of the compressor. See text for operation

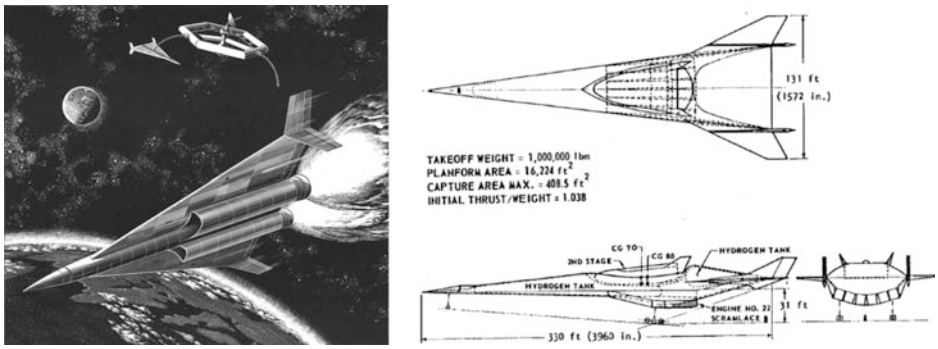

Fig. 4.15 Marquardt's first generation (1963) (Anon 1963) and second generation (1966) (Escher 1966) baseline Aerospace Plane (ASP) with scramjet engine

HOTOL. A rocket motor combustion chamber heat exchanger is necessary to provide sufficient energy to drive the turbomachinery in an expander cycle. Both Rudakov and Balepin of TsIAM and Tanatsugu of JAXA, Japan, employ heat exchangers in their rocket combustion chamber. Alan Bond did not for the HOTOL engine, as it could have adversely affected its performance at higher Mach numbers. In effect, the rocket becomes an airbreathing rocket for Mach numbers less than 6. In this concept, no other airbreathing engine is required. This cycle reduces the mass ratio to the 5.2–6 range and the oxygen-to-fuel ratio to about 3.4. There is a significant discussion of whether a liquefying system is equivalent in weight to a deeply cooled gaseous system. In most studies the authors are aware of, it is an even trade-off and other considerations should be used to make the selection.

With a suitable inlet system, airbreathing rockets can be integrated into flat-bottomed hypersonic glider configurations, see Fig. 3.9, as the forebody compression system required by a ramjet/scramjet, see Fig. 4.2, is not needed. Figure 4.16 shows such an inlet, an inward-turning, variable capture area inlet (DuPont 1999), that has been wind tunnel tested to Mach 5 plus. The mechanical details are not shown, but the mechanical actuation and integration is similar to the movable ramps on current supersonic military fighters. The movable lower inlet can be designed to retract flush with the lower surface when not in use. Since the outer surface of the lower cowl is the only surface that experiences entry heating, this system is much lighter than an outward-turning inlet. Note that in the low-speed position, the exit of the lower ramp flow is parallel to the lower vehicle moldline. Thus, all of the inlet structure is inside the fuselage moldline except the lower movable ramp. The inlet has the advantage of turning the flow inward, so there is no bulge in the moldline produced by an outward-turning inlet, such as the half-conical 2-D or pitot inlets on the Dassault Mirage aircraft. It also has the advantage of changing capture area to match the increasing corrected airflow requirement as speed is increased. The inlet meets or exceeds the military inlet recovery specification over the entire Mach range.

This class of propulsion systems can be airbreathers to Mach 5.5, and it is not necessary to have a fully developed airbreather configuration like the Mach 6 Lockheed Martin HTHL SSTC (single-stage to cruise) hypersonic cruiser SR-72, or the Mach 12 McDonnell Douglas HTHL SSTO accelerator, see Fig. 4 found in the *Introduction* chapter. Overall, a variable capture inward-turning inlet, integrated into a non-propulsion contoured flat-bottom hypersonic glider configuration, provides a satisfactory system (Balepin and Hendrick 1998). Figure 4.17 shows an inward-turning inlet incorporated into a hypersonic glider configuration with the engine system represented in Fig. 4.14, the LACE or deeply cooled rocket propulsion system. The rocket is installed much as it would be for an all-rocket configuration.

In 1983, McDonnell Douglas proposed the TAV (transatmospheric vehicle) concept incorporating the DuPont variable capture area, inward-turning inlet concept. The baseline airframe was the AFFDL developed FDL-7 flat-bottom hypersonic glider configuration. Figure 4.18 shows four artist sketches made for a USAF TAV competition in 1983. Note the retractable inlet for a powered

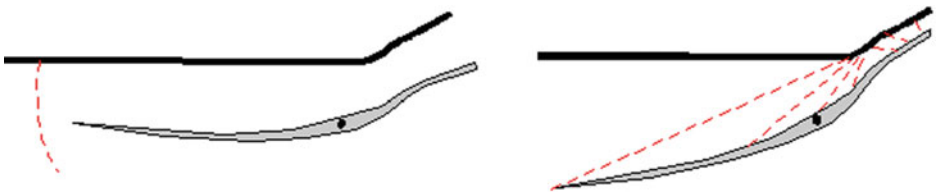

Fig. 4.16 Variable capture area, inward-turning inlet

landing with an airbreathing rocket. The USAF requested a horizontal takeoff machine (HTHL), and in doing so the gross weight increased by over a factor of 2. This is compared to the VTHL (vertical takeoff horizontal landing) configuration concept as implemented with the Boeing X-37 (Orbital Test Vehicle) (Weeden 2010) or the NASA selection of three private space companies including the Sierra Nevada Corporation Dream Chaser Spacecraft for commercial ISS resupply services as announced in early January 2016 (Morring 2016).

Note that the X-37 resembles a wing-body configuration, the Dream Chaser an all-body configuration (round-bottom lifting body), and the FDL-7 series an all-body configuration (flat-bottom lifting body). All three vehicle configuration concepts differ with respect to a multitude of attributes as introduced in Chap. 3. In summary, for a notional ISS return, all three vehicles would have significantly differing hypersonic glide and landing performances as expressed by down-range/cross-range capability, field performance, etc., overall dictating aspects like space operation (i.e., orbital waiting times), landing site selection and retrieval, and much more. The parametric sizing methodology introduced in Chap. 3 has been developed to correctly identify the *required* versus the *available* total vehicle solution space topography to directly support informed decision-making.

4.10 Thermally Integrated Combined-Cycle Propulsion

As the Mach number increases, the kinetic energy of the air increases with the square of the speed. As we have seen in Fig. 4.3, the kinetic energy of the air rapidly exceeds the thermal energy available to be transferred to the engine working fluid, air. The fraction of the combustion energy, rejected as unavailable for conversion to useful work, is also significant. In a modern turbojet engine, only about 23% of the fuel combustion energy is actually converted to thrust, and 44% is discarded out of the exhaust nozzle unused except to heat the atmosphere (Kroon 1952; Flack 2005). With commercial high bypass ratio engines, about 31% is converted to thrust. Then, it is critical to examine what part of the energy, which has been carried onboard the aircraft, has *not* converted to useful work or thrust. Any increase in the useful work conversion ratio reduces the propellant carried onboard, thus reduces the gross weight and the overall size of the vehicle. The result of this analysis and of many previous efforts has been the *thermally integrated* combined-cycle propulsion system.

The combined-cycle engine concept fundamental element began as a rocket ejector ramjet–scramjet (Stroup and Pontez 1968), thermally integrated into a rocket propulsion system, and that has a long history in hypersonics as early workers realized that the hypersonic vehicle in atmospheric flight must obey the rules of any thermodynamic cycle. An excellent discussion of the subject, by one who was already working in supersonic combustion engines in 1958, is by Curran (1993). Another early pioneer, Dr. Frederick Billig, added many insights into the advantages of thermal integration (Billig 1993). Other countries were also working on thermally integrated concepts, and one excellent source is from TsAGI (Lashin et al. 1993). In the class of integrated ejector ram–scramjet propulsion, the integral rocket ejectors provide both thrust and compression at lower Mach numbers (Buhlman and Siebenhaar 1995a, b). The combination of a separate ramjet and turbojet results in poor acceleration. However, the introduction of a deeply cooled turbojet thermally integrated with an expander rocket (KLIN cycle)

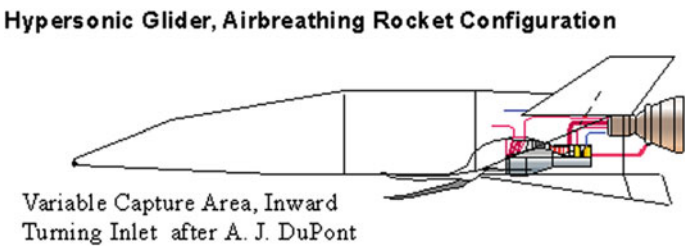

Fig. 4.17 Airbreathing rocket configuration concept

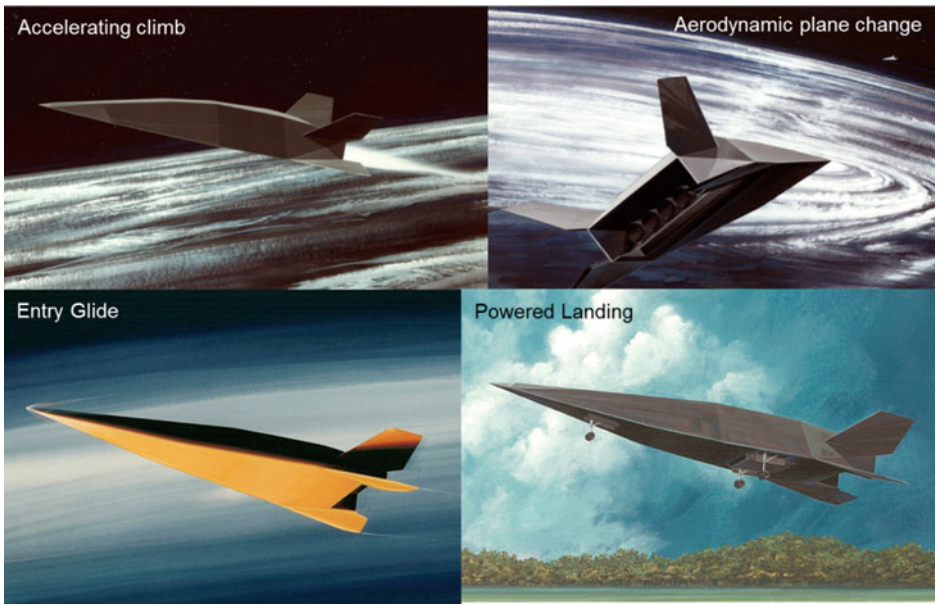

Fig. 4.18 McDonnell Douglas TAV concept from 1983

(Balepin and Hendrick 1998) is analogous to the rocket ejector ram-rocket–ramjet, with an additional benefit of excellent low-speed performance.

6. Deeply cooled turbojet-rocket (KLIN cycle). Figure 4.19 is an adaptation of Rudakov and Balepin's deeply cooled rocket ramjet into a deeply cooled turbojet-rocket. The turbojet and expander cycle rocket are thermally integrated (Balepin and Hendrick 1998). Unlike the ramjet, the pre-cooler on the turbojet keeps the compressor air inlet temperature low to reduce required compressor work and to increase mass flow and thrust. With the pre-cooler, the turbojet does not see the inlet temperature associated with higher Mach number flight, so it "appears" to be at lower flight speed. The pre-cooled turbojet provides a significant increase in transonic thrust. However, even with the increased transonic thrust, the turbojet remains a poor transonic accelerator. Clearly, the KLIN cycle operates with the rocket as a team. Whenever the turbojet thrust is not adequate to maintain a higher value of effective specific impulse, the rocket engine operates to add additional thrust and increases the effective specific impulse, as defined below. The specific impulse is given by

$$I_{\text{sp}} = \frac{\text{Thrust}}{\text{Propellant flow}} = \frac{T_{\text{rocket}} + T_{\text{airbreather}}}{\dot{w}_{\text{rocket}} + \dot{w}_{\text{airbreather}}} \tag{4.12}$$

We obtain the effective specific impulse

$$I_{\text{spe}} = \frac{\text{Thrust-Drag}}{\text{Propellant flow}} = I_{\text{sp}} \cdot \frac{\frac{T}{D} - 1}{\frac{T}{D}} \tag{4.13}$$

Because of its lower thrust in the transonic region, a hydrogen-fueled turbojet is about equivalent in effective specific impulse to a hydrogen-oxygen rocket. In afterburner operation, the rocket outperforms the turbojet. Thermally integrated together, the combination is better that the sum of the individual engines, as demonstrated in Fig. 4.20. The thermal energy from both rocket and turbojet is used to power the expansion turbines that drive the propellant turbopumps. If there is remaining excess energy, it can be added to a heat exchanger upstream of the turbojet combustor. The pre-cooled turbojet provides operation from takeoff to Mach 5.5 with rocket thrust augmentation when required, such as in the transonic region. Above Mach 5.5, the turbomachinery is shut down, and the rocket operates as a conventional cryogenic rocket.

7. LACE rocket-ram–scramjet. Figure 4.21 is the engine family in Fig. 4.14 integrated with a ramjet. As in Fig. 4.20, the results with a LACE rocket will be similar to the deeply cooled rocket. The airbreathing rocket operates only to Mach 6 or less, so the companion engine is a subsonic through-flow ramjet. In this cycle, the thermal energy from the incoming air and hydrogen combustion is used to drive an expansion turbine that in turn drives a turbopump. A rocket motor combustion chamber heat exchanger is

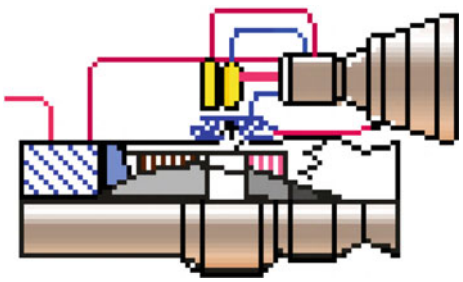

Fig. 4.19 Deeply cooled turbojet-rocket (KLIN cycle, thermally integrated turbojet-rocket)

necessary to provide sufficient energy to drive the turbomachinery. After leaving the expansion turbine, the hydrogen is introduced into the ramjet combustion chamber. The inlet air is cooled to nearly saturation by an air-hydrogen heat exchanger, and then pressurized to a few atmospheres. It then flows into the pressurized liquefying heat exchanger. The turbopump pressurizes the liquid air to rocket operating pressures, so it can be introduced into the rocket combustion chamber. After exiting the turbomachinery, the hydrogen is introduced into the ramjet combustion chamber.

At Mach 6 or less, the rocket is essentially an airbreathing rocket operating in parallel with a ramjet. The ramjet can convert to a supersonic through-flow engine (scramjet) at Mach numbers above Mach 6, but the rocket is now a conventional cryogenic rocket, not an airbreathing rocket. Above Mach 6, the rocket is normally not used when the scramjet is operating. After scramjet shutdown, the rocket operates as a conventional expander cycle cryogenic rocket.

8. Deeply cooled rocket-ram–scramjet. Figure 4.21 shows the integration of the deeply cooled cycle developed by Rudakov and Balepin at TsIAM and Alan Bond for HOTOL (Parkinson 1991) with a subsonic flow-through ramjet. In this cycle, the recovered thermal energy from the incoming air and hydrogen combustion in both, the rocket and the ramjet, is used to drive an expansion turbine, which in turn drives a turbo-compressor. The incoming inlet air is cooled to nearly saturation in an air-hydrogen heat exchanger, and then compressed to rocket operating pressure by the turbo-compressor so it can be introduced into the rocket combustion chamber. A rocket motor combustion chamber heat exchanger is necessary to provide sufficient energy to drive the turbomachinery. After leaving the expansion turbine, the hydrogen is introduced into the ramjet combustion chamber. At Mach 6 or less, the rocket is essentially an airbreathing rocket operating in parallel with a ramjet. Above Mach 6, the rocket is normally not used, and the ramjet operates as a supersonic through-flow ramjet (scramjet). After scramjet shutdown, the rocket operates as a conventional cryogenic rocket.

4.11 Engine Thermal Integration

When discussing propulsion, hypersonic flight or atmospheric entry, the question of cooling is always prominent; *cooling* implies discarding the rejected energy (Ahern 1983, 1992). *Thermal management* implies that a fraction of the rejected energy creates useful work or thrust (Barrère and Vandenkerckhove 1993). The concept of thermal management begins typically with two separate engines that are thermally integrated by having the fuel (in this case hydrogen) flowing through both engines before a portion of the collected thermal energy is extracted as useful work. This first example is limited to an airbreathing Mach number of 6, and the airframe is not a part of the thermal integration concept.

Figure 4.20 is from (Rudakov and Balepin 1991) and shows the performance of a Japanese LACE rocket with a pressurized liquefier, as part of a SCRJ-LACE system (Aoki and Ogawara 1988; Togawa et al. 1991; Yamanaka 2000, 2004), and of a Russian deeply cooled rocket, integrated with a ramjet (Rudakov and Balepin 1991). The solid line identifies the deeply cooled rocket by Rudakov. The central dashed line identifies a hydrogen ramjet by Rudakov. When simply *operated independently*, the combined thrust and fuel flow produces about a 500 s I_{sp} increase, as indicated by the lower dashed line identified as combination of rocket/ramjet. When *thermally integrated*, the fuel flows through both engines, collecting thermal energy from both rocket and ramjet, which is used to power the expansion turbines driving the turbo-compressor. The same two engines, when thermally integrated, provide a 1500 s increase in I_{sp} over the combination of rocket/ramjet, as indicated by the top dashed line.

Then, between Mach 2 and Mach 6, it is possible to have the thrust of a rocket and the specific impulse of a military subsonic turbofan, e.g., 4500–4000 s (specific fuel consumption from 0.8 to 0.9 kg/s per kg of thrust). This concept could be preceded by the development of the airbreathing rocket, which does produce a tangible benefit for operational

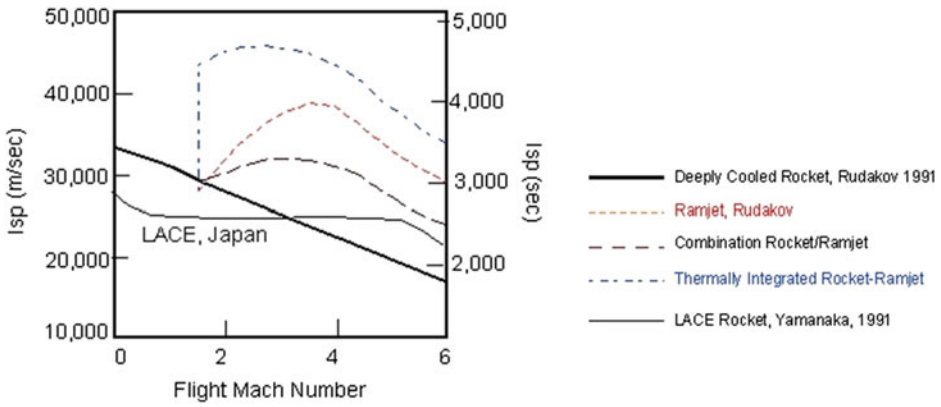

Fig. 4.20 Benefits of thermal integration from Rudakov and Balepin (1991)

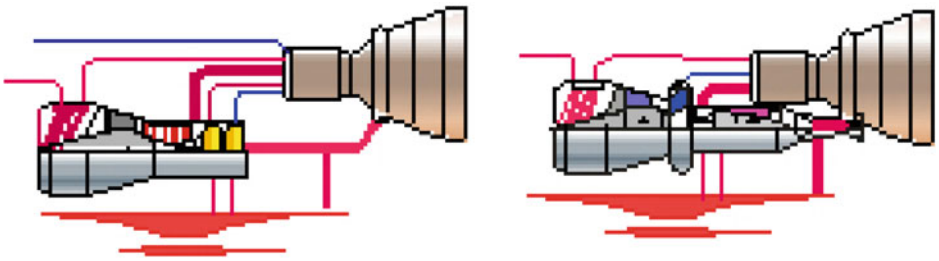

Fig. 4.21 Airbreathing rocket thermally integrated combined cycle. *Left* LACE-based combined-cycle. *Right* deeply cooled combined-cycle

launchers based on existing rocket engines and hardware technology. This initial step could deliver an interim operational capability in terms of a sustained-duration-use rocket launcher, in parallel with the development of the ramjet engine to be incorporated later into this propulsion system, eventually developing into a scramjet version of the ramjet. When these principles are applied to SSTO and TSTO launchers, size and weight (both dry and gross weights) are reduced.

These three propulsion systems could profoundly affect the size and weight of both SSTO and TSTO launchers if they were applied. Their advantage is that they are fabricated of tested and demonstrated hardware utilizing current industrial capability. Alan Bond and Alexander Rudakov were pioneers in the construction of actual hardware with operational potential; current work by Reaction Engines for the SABRE engine documents that it is possible to build integrated engines with technology already available (Davies et al. 2015). Unfortunately, today's status quo environment in aerospace propulsion steadfastly maintains rocket engines as the primary known standard, thus better than new concept solutions. Today, we observe a prevailing rocket advocacy to the exclusion of all or most else. A promising development in the UK has been the November 2015 announcement by BAE Systems plc and Reaction Engines Limited for BAE Systems of a strategic joint investment and collaboration to accelerate Reaction Engine's development of SABRE (Gallagher and Webster-Smith 2015). SABRE (Synergetic Air-Breathing Rocket Engine) resides in category (2) out of the 7 categories discussed here. It is an airbreathing rocket, where the propulsion elements are a rocket motor and an air/fuel heat exchanger that supplies the rocket motor with atmospheric air as oxidizer over part of its trajectory.

4.12 Total System Thermal Integration

When discussing propulsion in the context of hypersonic flight or transatmospheric vehicle ascent/entry, the question of cooling must be examined in the context of total energy management or integration. In the case of the SR-71, aerodynamic heating was mostly absorbed by the structure, having the surface operate at radiative equilibrium temperature. Then, the SR-71 is classified as a hot structure vehicle and therefore it required a material that maintained its strength at high temperature (i.e., in the 660 °C range and that was beta-titanium). During flight, the thermal energy had to be removed from the crew compartment and equipment bays. That thermal energy plus the thermal energy rejected by the engine both were transferred to the fuel. Discussions of the SR-71 design state that the fuel temperature entering the engine was over 600 °C (Merlin 2002; Goodall and Miller 2003). In this case, all of the thermal energy was discarded as hot fuel; note that hot fuel itself does not provide useful work or engine thrust. With a high-temperature coking hydrocarbon as fuel used as heat sink, this was a rational approach (utilizing the fuel as the heat sink for cooling purpose) as there was hardly any option to extract the recovered energy (heat) from the liquid hydrocarbon.

Let us now consider a system-level thermal integration approach. When synergistically utilizing fuel as a very capable heat transfer medium, the structural concept should be unlike the SR-71 *hot structure* and more like a *cold structure* protected by a combination of metal radiation shingles, radiating about 95% of the aerodynamic heating back to space. Structure cooling includes a *thermal management system* that converts about half of the thermal energy entering the airframe into useful work and thrust. Figure 4.22 illustrates a system-level thermal integration approach (Ahern 1992). The skin panels in the nose region, engine ramps and nozzle region, and the combustion module are one side of a heat exchanger system, which "pumps" aerodynamic heating into an energy extraction loop. The very cold hydrogen passes through skin panels that absorb the incoming aerodynamic heating. The energy extraction loop lowers the heat-absorbing hydrogen temperature and then passes it to another heat exchanger panel. Consequently, the liquid hydrogen goes through a series of energy additions and subtractions until it reaches the combustion chamber where it is injected as a high-speed hot gas producing thrust, see Figs. 4.4 and 4.23. This concept goes back to the original Aerospace Plane (ASP) effort for the US Air Force, to which The Marquardt Corporation was one of the

contractors, see Fig. 4.15. At that time, John Ahern worked with Charles Lindley, Carl Builder, and Artur Magar, who originated many of these concepts.

Figure 4.23 depicts a typical closed-loop heat pump loop identified in Fig. 4.22 as a rectangle with "EX" (exchanger) inside, and the fuel wall injection system. This particular loop is for one of the inlet ramps ahead of the engine module. The three heat exchangers form a closed-loop system, where thermal energy extracted from the skin panels is used to power an expansion turbine that drives the working fluid compressor. The *net work* extracted can be used to power electrical generators, hydraulic pumps, refrigeration units, or fuel boost pumps. With hydrogen as fuel, the vehicle is independent of ground power sources and can self-start as long as there is hydrogen in the fuel tanks. Eventually, the fuel reaches the engine module where it picks up the heat transferred to the combustor walls. When the hydrogen reaches its maximum temperature, it is injected into the combustion chamber via series of Mach 3 nozzles at a low angle to the wall. The size of the nozzles can be small and approach the equivalent of a porous wall. The result is that the hydrogen acts as film cooling for the wall, reducing the wall friction as well as the heat transfer rate. For a Mach 3 wall nozzle, the kinetic energy of the injected fuel also creates thrust.

The thrust per unit fuel flow, I_{spf}, is given in Eqs. (4.14a) and (4.14b) for hydrogen.

$$I_{spf} = 9.803 \cdot T^{0.5197}\ (\text{s})\ T \text{ in Rankine} \tag{4.14a}$$

$$I_{spf} = 13.305 \cdot T^{0.5197}\ (\text{s})\ T \text{ in Kelvin} \tag{4.14b}$$

At 2000 °R (1111 K), the hydrogen specific impulse is 509 s, or better than a hydrogen/oxygen rocket. For a scramjet engine with an equivalence ratio larger than one, this can produce 30% or more of the engines net thrust (Novichkov 1990a, b). Applying this approach and using Builder's Second Law, the impact of fuel temperature injected through Mach 3 nozzles in the combustor wall, see Fig. 4.24, can be assessed.

One measure of airbreathing engine performance is the energy conversion efficiency θ. The energy conversion efficiency is defined here as follows:

$$\theta = \frac{V \cdot T}{Q_c \cdot \dot{w}_{fuel}} \tag{4.15a}$$

$$\theta = \frac{V \cdot I_{sp}}{Q_c} \tag{4.15b}$$

$$\theta = \frac{V \cdot T}{Q \cdot \dot{w}_{air}} \tag{4.15c}$$

with

$$I_{sp} = \frac{\theta \cdot Q_c}{V} \tag{4.16}$$

and V the flight speed. At hypersonic speeds, the value of θ is almost constant, ranging between 0.55 and 0.60 from Second Law analysis (Builder 1964). That means that as speed is increased, the specific impulse must decrease. Figure 4.24 shows three I_{sp} values, decreasing from upper left to lower right. The top solid line is for an ideal engine with no internal losses. The middle solid line shows the I_{sp} from Builder's analysis including the losses from Swithenbank's injector system (Case 0, Fig. 4.5). This is the value of the I_{sp} if the vehicle was in cruise mode; that is, thrust equal to drag ($T = D$), with no acceleration. The bottom solid line shows the effective or acceleration I_{sp} based on engine net thrust minus aircraft drag, I_{spe}; this is the I_{sp} for an accelerating aircraft that must have thrust greater than drag. If there is no acceleration (that is, $T - D = 0$), then the value of effective I_{sp} is zero ($I_{spe} = 0$). The gray band is the sizing breakeven I_{sp} for a hydrogen/oxygen rocket and a hydrogen-fueled airbreather. Since the bulk volume of 100 kg of 6:1 liquid oxygen–hydrogen is 0.26 m^3, and that of 100 kg of subcooled liquid hydrogen is 1.34 m^3, the breakeven I_{sp} is a function of volume and I_{sp} together. As Mach 12 (13,050 ft/s) is approached, the propulsion system efficiencies become similar. That is, the propellant masses required to achieve a unit change in velocity are equal.

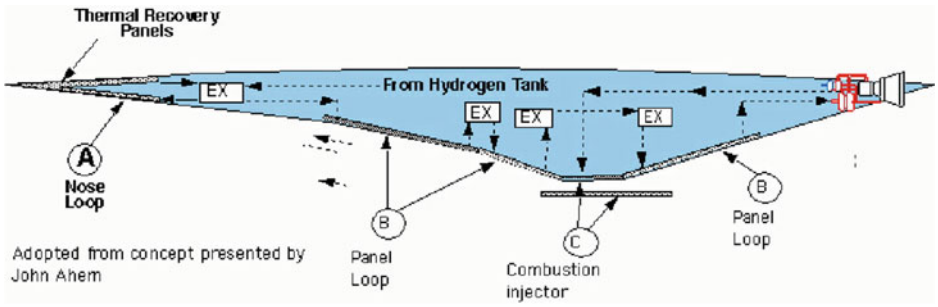

Fig. 4.22 System thermal integration

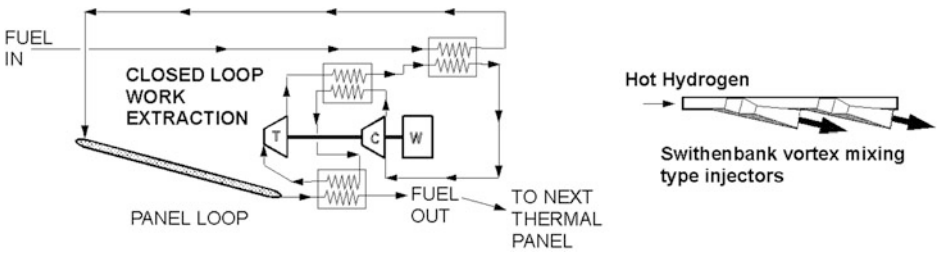

Fig. 4.23 Closed cycle heat pump (after Ahern) and combustor fuel injection. The external appearance of the Swithenbank injectors is shown in Fig. 4.4

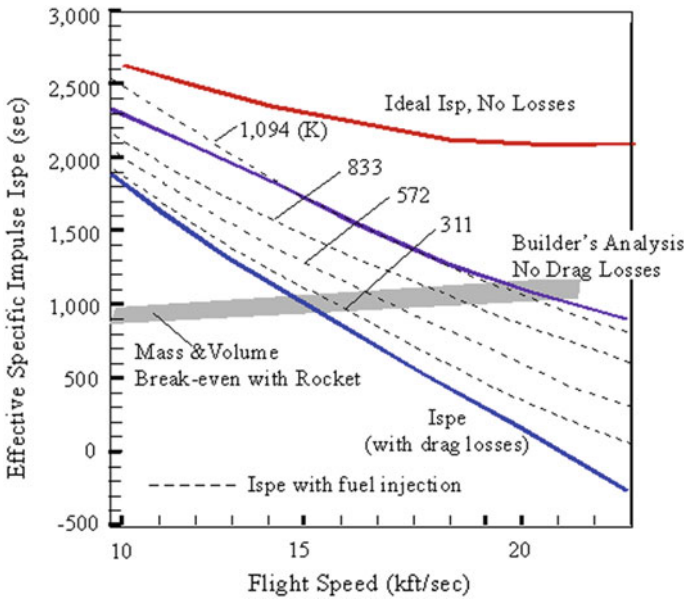

Fig. 4.24 System thermal integrated specific impulse

For some airbreathing systems, the rocket propellant mass required to achieve a unit change in velocity is less than for the airbreathing system, and so the volume requirements for the rocket propellant are about 1/5th that for the airbreather system. For the Swithenbank injectors, that breakeven speed is Mach 15.0 (16,312 ft/s). However, at the breakeven speed, the airbreather is just equal to the rocket, and even if no higher speed is sought, a higher I_{sp} is always welcome. That higher I_{sp} comes through system thermal management.

The impact of thermal management is illustrated in Fig. 4.24 by the four dashed lines for the specific impulse of the thermally integrated system. The temperature of the injected hydrogen is given in Kelvin. As the injected fuel temperature increases, the injected fuel energy offsets a greater fraction of the internal drag losses. If the injected hydrogen temperature can reach 1094 K (1969 °R), then all of the internal drag losses generated by the Swithenbank injector concept have been compensated for. The airbreathing engine energy and entropy limitations presented in Fig. 4.9 are still in effect. At Mach 15 flight speed, the effective I_{sp} can be increased by over 600 s. It requires a detailed engine analysis to quantify a specific value for a given system, but the general trend is correct. Recovered thermal energy can be converted into useful work and thrust to increase performance (Ahern 1992; Barrère and Vandenkerckhove 1993; Novichkov 1990a, b).

9. Ejector ram–scramjet-rocket. Figure 4.25 is an ejector ramjet thermally integrated with a rocket. The ejector may be a hot gas ejector and/or a rocket ejector. Remember, if the ramjet is a subsonic through-flow engine, then the scramjet is simply a supersonic through-flow engine. The maximum airbreathing speed can be selected from Mach 6 to at least Mach 14.5. At Mach less than 2, the system is an ejector ramjet analogous to a ram rocket system, except the rocket ejectors are distributed in the struts inside the ramjet engine module (Stroup and Pontez 1968). At Mach numbers greater than 2, the engine is a conventional ramjet with the rocket injectors now functioning as hot hydrogen injectors. Subsonic thrust is generated in the same manner as a ramjet, and the supersonic hydrogen injection acts as an aerodynamic isolator. Above Mach 6, it is a conventional scramjet engine with variable configuration injectors to minimize internal drag as discussed earlier in this chapter (Gounko et al. 2000).

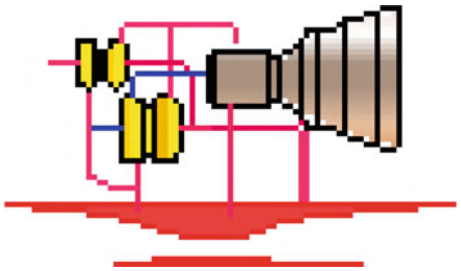

Fig. 4.25 Integrated ejector ram–scramjet-rocket

This propulsion concept was the backbone of the effort to create an airbreathing launcher and hypersonic cruiser discussed in conjunction with Fig. 3.13, and it represented the Marquardt effort from 1959 until 1963 to achieve the first aerospace plane (ASP) for the US Air Force shown in Fig. 4.15, and the effort of the Applied Physics Laboratory, Johns Hopkins University, to achieve a scramjet missile for the US Navy (Rife and Cantelon 2010; Werrell 1985). In all cases, the rocket community argumentations overpowered those supporting the advantages of airbreathing propulsion, and an all-rocket solution was adopted in every case.

There have always been, and still remain, arguments that scramjets will not work, and that the [notorious] analogy is with trying to light a match in a supersonic wind tunnel. However, Professor James Swithenbank of Sheffield University has the correct analogy, and that is lighting a match inside a Concorde traveling at Mach 2. Both, the surrounding air and the match are at the same relative velocity, as is the hot hydrogen which is injected into the engine via the injection devices, and assuming the supersonic flow-through airflow velocity and hydrogen injection velocity are matched to be the same. For the Mach 13 (14,137 ft/s) case shown in Table 4.2, the hydrogen injection velocity and the combustor through-flow speed would be the same at a gas temperature of 660 °C (933 K, 1220 °F). For a slower Mach 8 (8700 ft/s) case, the combustor through-flow speed is 7100 ft/s (Mach 6.53, 2164 m/s) and the hydrogen gas temperature required is a modest 293 °C (566 K, 585 °F). Then, in reality, the fuel and air are essentially at static conditions with very little differential speed and shear. Clearly, Swithenbank's analogy, that the scramjet is like lighting a match for a cigar while tasting *Champagne* on Concorde, is the correct one.

When one of the authors (P.A. Czysz) was a young engineer at Wright Patterson Air Force Base, he was assigned as Chief Engineer to the high temperature hypersonic tunnel at Hypervelocity Branch, Aircraft Laboratory at the Wright Air Development Division. The high-temperature hypersonic tunnel was a nominal Mach 4 wind tunnel heated with a zirconia pebble bed. Nominal air temperatures were in the range 2500–1500 K (4500–2700 °R). The pressure, temperature, and velocity in the test section were very close to those of a scramjet operating at a Mach 8 flight condition. The Aero-Propulsion Laboratory assigned Paul James Ortwerth and then Squadron Leader E. Thomas Curran to investigate the possibility of testing a scramjet combustor in the high-temperature hypersonic tunnel.

Squadron Leader Curran was familiar with the work Professor James Swithenbank was doing in a similar facility in Montreal, Canada. The result was an experiment that used the test section of the high-temperature hypersonic tunnel as a scramjet combustor. A 7.6-cm-wide flat plate model, 19 cm long with five hydrogen injection ports, located at 1/4th of the model length from the model nose, was placed in the 12.7 cm test section (Burnett and Czysz 1963). The model was installed on an injection system, so the duration of the time in the test section could be controlled. There were a series of pressure taps running down the model centerline. The gas plenum chamber in the model was equipped with thermocouples to measure the hydrogen temperature. Both color Schlieren and infrared ciné film (motion picture film format) recordings of the flow field were made. The infrared film was filtered to center on the high-temperature water emission radiation. Figure 4.26 shows two of only a few surviving photographs from the test; all of the original ciné film was burned to recover the silver.

In Fig. 4.26, the left picture is a color Schlieren with a horizontal knife-edge. The red above the model indicates a reduction in density, whereby the green/blue does indicate an increase in density. The shock waves from the model and gas injection are clearly visible. The red hydrogen injection is also clearly visible. The model plenum chamber thermocouple gave a hydrogen temperature of 300 ± 15 °C (573 ± 15 K), which is an indicator that the test section air and hydrogen speeds were very similar. From Table 4.2, the 7100 ft/s test section speed corresponds to a flight speed of 8000 ft/s as does the 2500 K stagnation temperature. The picture on the right is from the infrared film camera and clearly shows the water formation approaching the hydrogen injection holes, an indicator that combustion delay was minimal. Professor Swithenbank's data correlations for over 1000 test runs give a time to complete combustion of 35 ± 5 μs for gaseous fuels. At this airflow speed, the distance traveled is about 2.98 ± 0.4 in. (6.6–8.6 cm) and is very close to the data from the pictures. A later analysis showed a very close correlation between the schlieren and infrared pictures and thus confirmed the combustion distance from pressure measurement (Czysz 1993b). Then indeed, hydrogen will burn very well in a scramjet!

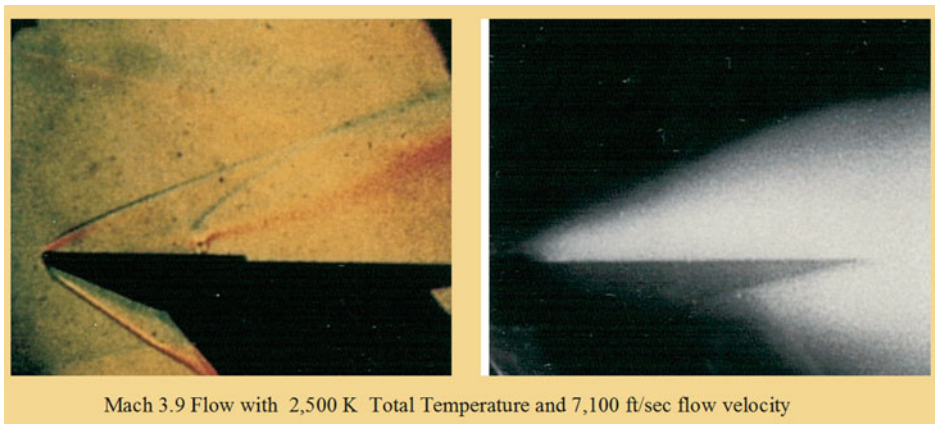

Fig. 4.26 300 °C hydrogen injected into supersonic air stream at flight conditions corresponding to a scramjet combustor for an aircraft flying at Mach 8 (tests circa 1962)

4.13 Thermally Integrated Enriched Air Combined-Cycle Propulsion

These cycles are thermally integrated combined-cycle propulsion systems analogous to the *LACE rocket-ram–scramjet* and the *deeply cooled rocket-ram–scramjet*, except the thermally processed air is separated into nearly pure liquefied oxygen (LEA: Liquid Enriched Air; LACE: Liquid Air Cycle Engine; and ACES: Air Collection Enrichment System) and gaseous nitrogen (OPA: Oxygen-Poor Air). This is possible because the boiling point of liquid oxygen is 90.03 K, and the boiling point for liquid nitrogen is 77.2 K. Just as in a fractionating tower for hydrocarbons, where hydrocarbons of different boiling points can be separated, the oxygen can be liquefied while the nitrogen remains gaseous.

This means that most of the oxidizer carried onboard the launcher is not loaded at takeoff but loaded during the flight to orbit. The result is that the carried oxidizer-to-fuel ratio at takeoff is less than for a non-ACES system. Thus, the takeoff gross weight and engine size are reduced. Whether also the volume (size) of the launcher is reduced depends on the volume of the ACES system (Bond and Yi 1993). The maximum weight of the launcher is then near the ascent climb to orbital speed and altitude, rather than at takeoff. The process is executed in steps, through temperature gradients where a fraction of the oxygen is liquefied at each step. As in all chemical processes, the difficulty increases as the oxygen purity increases, and for a flight-weight system there is a practical limit. The liquid-enriched air has purity in the 85–90% oxygen range and is stored for use in the rocket engine during the rocket ascent portion of the ascent trajectory. The oxygen-poor air contains 2–5% oxygen and is introduced into the ramjet, creating the equivalent of a mixed-flow bypass turbofan. That is, the mass-averaged exhaust velocity is reduced but the specific impulse rises, overall increasing engine mass flow and thrust.

Thermal integration means that the fuel passes through both rocket and scramjet to scavenge rejected heat and convert it into useful work before entering the combustion chambers. This increases the specific impulse while at the same time oxidizer is being stored for the ascent to space. Just as for the LACE and deeply cooled rocket, both rocket and ramjet must operate as an acceleration system until efficient scramjet operation is reached. The Mach number for air separation and collection is usually in the Mach 3 to Mach 5 region. The ACES cycle is a very good cycle for launchers that require a launch offset to reach an optimum launch latitude and time window, for instance, when the vehicle must cruise some distance until the ascent to orbit point is reached. This approach is applicable to SSTO vehicles. The ACES cycle has more significant payoffs for TSTO launchers that must fly an offset, because the air separation plant is in the first stage, not in the stage that continues its ascent to orbit.

A good example of this is reaching the ISS at 55° orbital inclination from Cape Canaveral, at 28.5° latitude. The Space Shuttle loses a significant fraction of its payload because of the propellant required to move the orbital plane during a rocket ascent. In order to rotate the orbital plane 26.5° requires a significant weight ratio increase to achieve low Earth orbit (this will be further discussed in Chap. 5). However, a "first stage" or carrier vehicle (with second-stage release at subsonic to hypersonic velocities utilizing an air-breathing engine) flying in the atmosphere can achieve the plane change with a much smaller fraction of the propellant required compared to the plane change using rocket thrust (Space Shuttle), because the first stage accomplishes the turn simply using aerodynamics. The rocket, during the acceleration-turning flight, has thrust at least twice its weight with an effective I_{sp} of around 400 s, while the aircraft has the thrust of 1/6th its weight with a specific impulse about 10 times larger, see Fig. 4.20. This expands the launch window because the launcher can fly to intercept the ascending node

of the desired orbit and not be confined to when the ascending node and launch site latitude coincide. The figure of merit for these systems is the weight of LEA collected per weight of hydrogen. A practical value is 6 kg of LEA per kg of hydrogen; for more details see (Czysz and Vandenkerckhove 2000). Examples of the thermally integrated enriched air combined-cycle propulsion are as follows:

10. ACES-LACE ejector ram–scramjet-rocket. Figure 4.27 shows an air collection and enrichment system (ACES) (Ogawara and Nishiwaki 1989) added to propulsion system #6. The liquid air is not pumped to the rocket immediately, but passed through a liquid fractionating system to separate the oxygen component as liquid-enriched air (LEA contains 80–90% oxygen) and nitrogen component as liquid oxygen-poor air (OPA contains from 2 to 5% oxygen) (Balepin 1996). The oxygen component is then stored for later use in the rocket ascent portion of the flight. The oxygen-poor nitrogen component is injected into the ramjet, to create a hypersonic bypass engine that increases engine mass flow, thrust and reduce the mass-averaged exhaust velocity. In the 1960s, hardware development was undertaken by the Linde Corporation under an Air Force contract. Sufficient hardware was fabricated to design the operational system and confirm performance. ACES most significant penalty is the volume required for the fractionating separator. For hydrogen-fueled hypersonic cruiser and transatmospheric space launchers, volume is a critical parameter, when increasing it becomes a significant size and weight penalty. However, this propulsion strategy can significantly reduce the takeoff perceived noise. ACES was invented for the same reasons a conventional mixed-flow bypass gas turbine was invented. ACES was originally proposed by the Air Force Aero-Propulsion Laboratory for the space plane of the late 1950s (Leingang et al. 1992; Maurice et al. 1992) and was the subject of intense investigation in the 1960–1967 time period (Leingang et al. 1992). Most of the original Air Force work was for a TSTO vehicle, although application to SSTO was investigated. For airbreather operation to the 12,000–14,000 ft/s range, its cycle can achieve weight ratios less than 3 with oxygen-to-fuel ratios approaching one-half.

11. ACES-deeply cooled ejector ram–scramjet-rocket. Figure 4.27 is an ACES option added to propulsion system #7. Even in the 1950s, the paramagnetic properties of liquid oxygen were noted by the LACE and ACES investigators (Leingang 1991). Patrick Hendrick was a graduate student under the late Jean Vandenkerckhove in 1988, when he observed that Siemens sold an exhaust gas analyzer measuring gaseous oxygen based on its diamagnetic properties. The magnetic susceptibility of oxygen at its boiling point (90.03 K) is 7699×10^{-6} in cgs units (centimeter-gram-second system of units), that is, as large as some chromium and nickel compounds.

During a visit to Jean Vandenkerckhove at his Brussels residence, Hendrick (1996) discussed his concept of gaseous air separation using the magnetic properties of oxygen. Collaboration with Vladimir V. Balepin resulted in the addition of a vortex tube pre-separator based on the small temperature difference in the liquid temperature of nitrogen and oxygen. The result was a new approach to the ACES concept with much lower total volume requirements than the liquid fractionating equipment. The deeply cooled gaseous air is not pumped to the rocket immediately, but passed first through a vortex tube initial separator (at this stage the LEA contains about 50% oxygen) (Lee et al. 2003a, b), and then into a cryogenic magnetic oxygen separator. The oxygen component is then liquefied as LEA (LEA contains 80–90% oxygen) and stored for use in the rocket ascent portion of the flight. The gaseous nitrogen component of oxygen-poor air (OPA) contains from 2 to 5% oxygen. The oxygen-poor nitrogen component is injected into the ramjet, to create a hypersonic bypass engine that increases engine mass flow, thrust and reduce the mass-averaged exhaust velocity.

At takeoff, this system can significantly reduce takeoff noise, for the same reasons a conventional mixed-flow bypass gas turbine was invented. This system is in the laboratory phase consisting of studies and testing, but has not as yet been developed as propulsion hardware. At this point in time, it has the potential to significantly reduce the volume and weight required for an ACES system, but is not yet proven. For airbreather operation to the 12,000–14,000 ft/s range, this cycle can achieve weight ratios less than 3 with oxygen-to-fuel ratios approaching one-half (1/2).

4.14 Comparison of Continuous Operation Cycles

To compare the continuous operation cycles, Fig. 3.5 is repeated as Fig. 4.28. In Fig. 4.28, weight ratio to LEO, that is the takeoff gross weight divided by the on-orbit weight, is represented for different engine cycles as a function of the net oxidizer-to-fuel ratio. These may be divided into two groups represented by (a) rocket-derived propulsion and (b) airbreathing rockets.

The rocket-derived propulsion class is represented by cycles: (1) rocket, (2) air-augmented rocket, and (3) ram rocket. For this class, the oxidizer-to-fuel ratio is essentially constant at a value of 6. As a ram rocket, the weight ratio to LEO decreases from 8.1 to 6.5. There is only a minimal payoff for the air-augmented rocket; without burning the oxygen in the air, there is insufficient thrust increase to make a significant difference in weight ratio.

There is a discontinuity in the oxidizer-to-fuel ratio curve between the rocket-derived propulsion value of 6 and where airbreathing propulsion begins, at a value of 4. The second

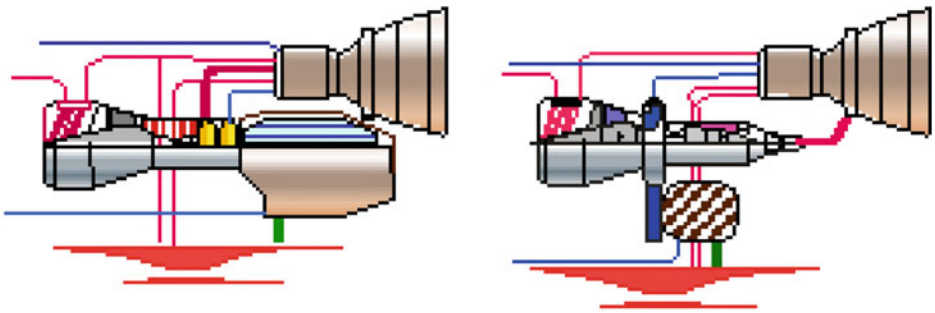

Fig. 4.27 Air collection and enrichment cycle (ACES). *Left* LACE-based combined-cycle. *Right* deeply cooled combined cycle

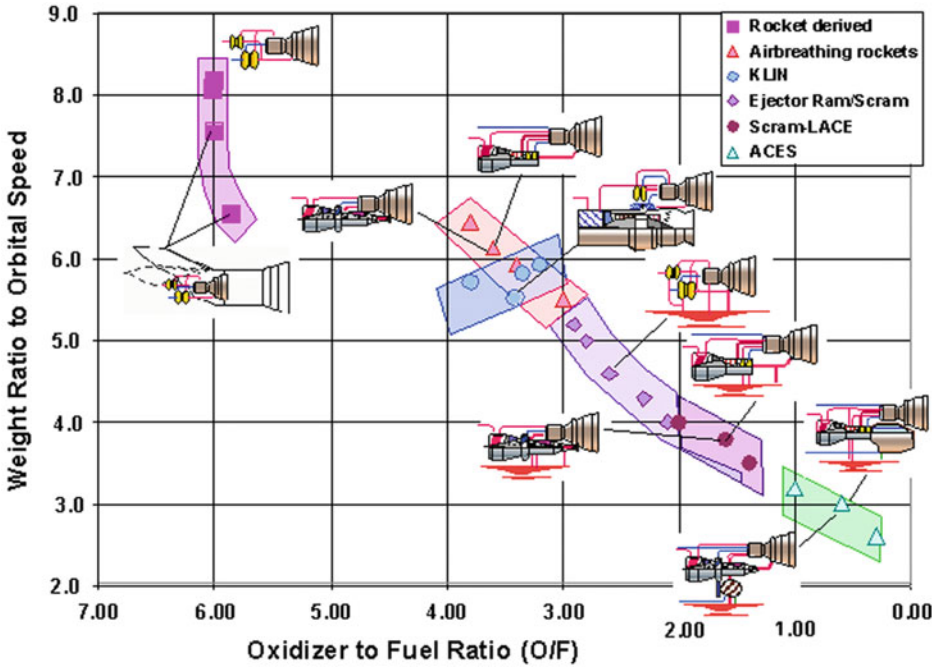

Fig. 4.28 The less oxidizer carried, the lower the mass ratio

class, represented via the airbreathing propulsion cycles, moves down to the right reducing in weight ratio and oxidizer-to-fuel ratio to values 2.5 and 0.5, respectively.

From Eq. (3.4), the relationships involving weight ratio are:

$$W_{\mathrm{R}} = 1 + \frac{W_{\mathrm{ppl}}}{W_{\mathrm{OWE}}} \tag{4.17a}$$

$$W_{\mathrm{R}} = 1 + \frac{W_{\mathrm{fuel}}}{W_{\mathrm{OWE}}} \cdot \left(1 + \frac{O}{F}\right) \tag{4.17b}$$

The TOGW is defined as

$$W_{\mathrm{TOGW}} = W_{\mathrm{R}} \cdot W_{\mathrm{OWE}} \tag{4.18a}$$

$$W_{\mathrm{TOGW}} = W_{\mathrm{OWE}} \cdot \left[1 + \frac{W_{\mathrm{fuel}}}{W_{\mathrm{OWE}}} \cdot \left(1 + \frac{O}{F}\right)\right] \tag{4.18b}$$

Equation (4.17b) directly links the weight ratio to orbit to a function of the oxidizer-to-fuel ratio and the weight of fuel divided by the operational weight empty (dry weight plus trapped fluids, crew, and payload). Then, the $W_{\mathrm{fuel}}/W_{\mathrm{OWE}}$ ratio is multiplied by 1 + (O/F) to produce the weight ratio (W_R). If the $W_{\mathrm{fuel}}/W_{\mathrm{OWE}}$ ratio is approximately constant, then there is a direct benefit in incorporating airbreathing propulsion. The gross weight is reduced and the total engine thrust is reduced, greatly reducing the size, complexity, and cost of the propulsion system. If the $W_{\mathrm{fuel}}/W_{\mathrm{OWE}}$ ratio is approximately constant, then increased engine and turbopump size and weight are a consequence of continuing with rocket propulsion systems.

When rearranging Eq. (4.17b), we obtain

$$\frac{W_{\mathrm{fuel}}}{W_{\mathrm{OWE}}} = \frac{W_{\mathrm{R}} - 1}{\left(1 + \frac{O}{F}\right)} \tag{4.19}$$

Remember, in this equation the oxidizer/fuel ratio is the oxidizer/fuel ratio carried on the launcher with its associated weight ratio, not the rocket engine oxidizer-to-fuel ratio. The importance of Eqs. (4.17b) and (4.18b) and of the chart is

that it shows the gross weight is a function of one airframe parameter, W_{OWE}, and of two propulsion parameters, and that it is directly proportional to the carried oxidizer-to-fuel ratio. When reducing the carried oxidizer, and the gross weight and resultant engine thrust decrease proportionately.

Beginning with the rocket point in Fig. 4.28 at a weight ratio of 8.1 and ending at the ACES weight ratio of 3.0, a straight line connects all hydrogen-fueled propulsion systems except the air-augmented rocket and ram rocket. The reason these two lie outside is because the engine oxidizer-to-fuel ratio stays essentially unchanged and the reduction in weight ratio comes from the air entrained, but not burned, in the ejector system.

Analyzing the data in Fig. 4.28, the result is a value for $W_{\text{fuel}}/W_{\text{OWE}}$ equal to 1.05 ± 0.06. Then, regardless of the propulsion system, the quantity of fuel carried by a hydrogen-fueled launcher that achieves LEO lies between 99 and 111% of the W_{OWE}. This only holds true for a hydrogen/oxygen propulsion system with a 6:1 oxygen/fuel ratio and a stoichiometric air/fuel ratio of 35.4:1. A hydrogen/oxygen rocket with a 7:1 oxidizer/fuel ratio will have a different value. This is an important result of the governing equations, as it fixes the fuel weight regardless of the propulsion system and focuses on the real problem, the weight of the oxidizer carried.

As shown by Eq. (4.17b), the launcher weight ratio is only a function of the carried oxidizer-to-fuel ratio, and the weight ratio is determined by the propellant combination. From the propellant combinations in Table 4.5, the value of $W_{\text{fuel}} = W_{\text{OWE}}$ for the different rocket propellant combinations has been calculated and given in Table 4.6. Note that hydrogen carries the least fuel per W_{OWE}. With an oxidizer-to-fuel ratio of 6, that means the propellant load is 7.3 times the W_{OWE}. The hydrocarbons are five times greater and with an oxidizer-to-fuel ratio about 2.35, the propellant load is 17 times the W_{OWE}. The propellant load of hypergolic propellants ranges from 19 to 20 times W_{OWE}. From Table 4.6, we can see why one of the famous Russian rocket engine designers, Valentin Petrovich Glushko, chose the room temperature liquid UDMH and N_2O_4 for Proton and the submarine-launched ballistic missiles (Chertok 2011).

The importance of this relationship is that with minimal information, a reasonable estimate of the fuel and propellant weight compared with W_{OWE} is available. Hydrogen provides the least weight ratio to orbit. Because the density of hydrogen is low, the volume required is the greatest.

The weight ratio is decreasing because the oxidizer weight is decreasing as a direct result of the oxidizer-to-fuel ratio. Then, from Fig. 4.28, when using hydrogen fuel, (A) an all-rocket engine can reach orbital speed and altitude with a weight ratio of 8.1. (B) An airbreathing rocket (AB rocket) or KLIN cycle can do the same with a weight ratio about 5.5. (C) A combined-cycle rocket/scramjet with a weight ratio of 4.5–4.0, and (D) an ACES has weight ratio of 3.0 or less. Clearly, an airbreathing launcher has the potential to reduce the mass ratio to orbit by 60%! It becomes obvious that a significantly smaller launcher is the result, both in weight and size, and presumably also less expensive. In order to achieve this operationally, the design goal must be to *reduce the carried oxidizer*.

It is more difficult if not impossible to achieve this continuous progression of propulsion systems with fuels other than hydrogen. Methane is a cryogenic fuel, but it does not have the thermal capacity to liquefy or deeply cool air, so the hydrocarbon equivalent of a LACE or deeply cooled cycle is not possible. Ramjet/scramjet engines are possible with most of the liquid fuels, although hydrocarbons decomposition into carbon-rich compounds (coking) will limit the temperature, which ultimately limits the maximum speed obtainable.

Examining the operational regions for each cycle, note that:

(1) *Chemical rocket, air-augmented rocket, and ram rocket* maintain essentially a constant oxidizer-to-fuel ratio, with the weight ratio to achieve orbit decreasing because of the increased thrust produced by the air ejector system. For a vehicle with a rocket W_{OWE} equal to 76 t and assuming the W_{OWE} of other propulsion systems at 76 t (plus any differential weight for the propulsion system), the W_{TOGW} for the three systems is:

Cycle	W_R (–)	O/F (–)	W_{TOGW} (–)	Savings[a] (t)	Payload (t)
Rocket	8.10	6.00	616 t	0	7.0
Air-augmented rocket	7.50	6.00	616 t	0	6.0
Ram rocket	6.50	5.80	543 t	73	15.4

[a]With respect to an all-rocket SSTO launcher

For the same liftoff weight of 616 t, the payload for the three systems is 7.0, 6.0, and 15.4 t, respectively. As is usually the case for the air-augmented rocket, the increased system weight is not offset by the increase in thrust, unless the oxygen in the secondary air is burned. For the ram rocket, the payload is more than doubled. The ram rocket is not any kind of technology challenge, as many afterburning turbojet engines have ejector nozzles (such as the mentioned Saab J-35 Viggen). The ram rocket is a simple way to increase payload to orbit using the same rocket engine, or to reduce the size and cost of the rocket engines for a fixed payload.

(2) *LACE rocket, deeply cooled rocket, and cooled turbojet-rocket (KLIN cycle)* are other propulsion system concepts that build onto the basic rocket engine for increased performance. This propulsion system creates

Table 4.6 Fuel weight to operational weight empty for propellant combinations from Table 4.5

Fuel	Hydrogen	Hydrogen	Kerosene	Methane	Hydrazine	UDMH
Oxidizer	O_2	N_2O_4	O_2	O_2	N_2O_4	N_2O_4
Relative fuel volume (–)	14.83	16.24	6.51	13.47	6.20	10.73
Relative oxidizer (–)	5.25	7.73	2.09	2.05	1.52	0.819
W_{fuel}/W_{OWE} (–)	1.05	1.15	5.02	5.12	6.20	8.42
W_{ppl}/W_{OWE} rocket (–)	7.35	14.4	17.0	17.1	20.2	18.7

UDMH = unsymmetrical dimethyl hydrazine

an airbreathing rocket operating to about Mach 5.5. All of the hardware required for the thermodynamic processing of the air has been built in one form or another over the last 55 years. No differentiation in weight is made for the liquid air cycle versus the deeply cooled. Historical data suggests that these two systems are essentially equal in total system weight.

One of authors (P.A. Czysz) saw a 1 m^3 liquid hydrogen/air heat exchanger operate for 1 min at Mitsubishi Heavy Industries in 1988 at outside air conditions of 38 °C and 90% relative humidity without any water condensation on the heat exchanger tubes. The runtime was short because the container capturing the liquid air was overflowing and running down the ramp. So again, this is not a technology issue, but (rather disappointingly) simply a decision-to-proceed issue. The KLIN cycle has the advantage of thrust for landing without the operation of a heat exchanger to provide the rocket with airbreathing capability. For a rocket vehicle with W_{OWE} equal to 76 t and assuming the same W_{OWE} for other propulsion systems plus any system-specific differential, the W_{TOGW} for the two systems is:

Cycle	W_R (–)	O/F (–)	W_{TOGW} (t)	Savings[a] (t)
LACE-deeply cooled rocket	6.40	3.85	476	140
LACE-deeply cooled rocket	6.00	3.60	443	173
LACE-deeply cooled rocket	5.50	3.10	404	212
KLIN cycle	5.70	3.40	432	184

[a]With respect to an all-rocket SSTO launcher

Even considering the weight of the heat exchangers, the conversion of the rocket to an airbreathing rocket to Mach 5.5 offers considerable savings in weight and engine thrust. This straightforward improvement to the rocket engine offers major cost reductions (Czysz and Richards 1998). For the same liftoff weight of 616.2 t, the payload for the airbreathing rocket systems and the KLIN cycle is between 24 and 38 t. Had the Delta Clipper program survived and, had an airbreathing rocket been considered, the payload could have been increased and the gross weight reduced. Instead, Delta Clipper employed four RL-10A-5 liquid-fueled rocket engines.

(3) *LACE rocket-ram–scramjet and deeply cooled (DC) rocket-ram–scramjet* have the advantage of providing a weight saving equal to the ejector ram–scramjet, but with an intermediate step. For the ejector ram–scramjet propulsion system, the benefits cannot be realized until an operational scramjet is developed and qualified for flight operations. The advantage of the airbreathing rocket is that it can be an effective first step based on existing hardware arranged in a different manner, and that can achieve approximately 60% of the eventual scramjet benefit without any new engine development. An operational system can be operating and realizing this benefit while the scramjet is being developed at its own pace, to be integrated later into the airbreathing rocket system (as envisioned by A.S. Rudakov), in order to realize the final 40% improvement. During that time, the airbreathing rocket system and the air vehicle have been proven in operation. No differentiation in weight is made for the liquid air cycle versus the deeply cooled. Historical data suggests that the systems are essentially equal in total system weight. For a vehicle with a rocket W_{OWE} equal to 76 t, and the W_{OWE} of other propulsion systems also fixed at 76 t plus any differential for the propulsion system, the W_{TOGW} for the two systems is:

Cycle	W_R (–)	O/F (–)	W_{TOGW} (t)	Savings[a] (t)
LACE rocket-ram–scramjet	4.00	2.00	283	334
LACE-DC rocket-ram–scramjet	3.50	1.40	245	372

[a]With respect to an all-rocket SSTO launcher

Integration of the ram–scramjet into the airbreathing rocket system realizes the gains Rudakov reported in Fig. 4.20, by reducing the gross weight by more than half. We are now approaching the weight of a vehicle that can safely abort on launch. With a weight ratio of 4 or less, the potential for horizontal takeoff becomes a real possibility, and a true, safe abort-on-launch capability, could be reality.

(4) *Ejector ram–scramjet-rocket* operational area overlaps the airbreathing rocket and airbreathing rocket-ram/scramjet operational areas. The complete spectrum for the ejector ram–scramjet-rocket is given below. At the higher weight ratios, the ejector ram–scramjet overlaps the airbreathing rockets. The advantage of the latter is that it can be developed from existing hardware and does not require the development of a new engine, the scramjet, for operational application.

There is a clear advantage for the application of airbreathing rockets to launcher before the application of scramjets. The lower weight ratios overlap those of the airbreathing rockets integrated with the ejector ram–scramjet engine. Again, the initial operating capability offered with the airbreathing rocket is built onto, rather than being replaced by, a new system. Building on the airbreathing rocket offers the advantages of expanding the capability of a proven operational system rather than introducing a new vehicle, an important advantage for this propulsion system. If the scramjet was a developed propulsion system at this point in time, beginning with the airbreathing rocket might not be the preferred choice. However, attempts to take this path began in the late 1950s and have yet to yield even a small-scale operational weight engine.

Recent developments are encouraging (Gallagher and Webster-Smith 2015; Davies et al. 2015; Norris 2015). But as of today, there is neither an operational size scramjet nor research and development size scramjet that has the necessary maturity for integration into an operational vehicle. One author (B. Chudoba) is involved to develop the logic successor to the X-51 scramjet demonstrator (Osborn 2015). Clearly, with the availability of rocket ejectors, the ejector ram–scramjet has low-speed thrust and does not require an additional propulsion system for takeoff and low-speed acceleration. If propellant remains after entry, the engine can provide landing and go-around thrust.

For a vehicle with a rocket W_{OWE} equal to 76 t and the W_{OWE} of other propulsion systems also at 76 t, plus any differential for the propulsion system, the W_{TOGW} for these systems is:

Cycle	W_R (–)	O/F (–)	W_{TOGW} (t)	Savings[a] (t)
Ejector ram/scramjet-rocket	5.50	3.40	396	220
Ejector ram/scramjet-rocket	5.20	3.00	372	244
Ejector ram/scramjet-rocket	5.00	2.80	365	260
Ejector ram/scramjet-rocket	4.50	2.50	317	299
Ejector ram/scramjet-rocket	4.23	2.00	296	320
Ejector ram/scramjet-rocket	4.00	1.75	278	338
Ejector ram/scramjet-rocket	3.50	1.40	241	375

[a]With respect to an all-rocket SSTO launcher

The ejector ram–scramjet, operating to airbreathing Mach numbers from 6 to 14, offers the ability to reduce the gross weight by more than 50%.

(5) *ACES-LACE ejector scramjet-rocket*, *ACES-deeply cooled ejector scramjet-rocket* is another concept that dates back to the late 1950s, and, like the scramjet, has not proceeded beyond the ground test phase. This concept did have much full-sized, flight-weight hardware built and tested successfully in the 1960s. The difficulty has always been the sensitivity of SSTO space launchers to volume demands. This propulsion system is very attractive for TSTO launchers with the air collection and separation system in the first stage (Rudakov et al. 1991). A number of these have been designed, but none have proceeded beyond the concepts stage. This will be discussed later in the chapter dealing with mission-sized launcher systems.

If indeed there is a problem with this propulsion system concept, it is the volume required for the liquid air separator. For volume-limited applications, the size and weight of the airframe increase. It remains to be designed and demonstrated that the volume reduction potential of the deeply cooled gaseous separation is real (Lee et al. 2003a, b). As a result, both systems are being treated as equal-size, equal-weight, and equal-performance systems.

For a vehicle with a rocket W_{OWE} equal to 76 t and the W_{OWE} of other propulsion systems also defined to 76 t, plus any differential for the propulsion system, the W_{TOGW} for this system is:

Cycle	W_R (–)	O/F (–)	W_{TOGW} (t)	Savings[a] (t)
ACES-scramjet	2.90	0.50	252	364

[a]With respect to an all-rocket SSTO launcher

Even though the weight ratio is less than for the ejector ram–scramjet-rocket, the gross weight is not due to the air separation system volume.

4.15 Conclusions with Respect to Continous Operation Cycles

Carl Builder was one of The Marquardt Company's team members that developed the Air Force scramjet program. Carl Builder, Lindley (1965), and John Ahern were responsible for developing the thermodynamic analysis for the scramjet. The standard approach for the ramjet and its extension to scramjets was based on an isentropic stagnation conditions analysis, where First Law inefficiencies were evaluated in terms of stagnation pressure losses, and of aerodynamic analysis of the engine flow path based on local Mach numbers and aerodynamic characteristics. For a subsonic flow-through engine (ramjet), where the heat addition is done at subsonic speeds, and where maximum pressure and temperatures do not exceed (typically) 20 atm and 1800 K, this type of approach is quite acceptable.

However, for supersonic through-flow engines (scramjet), the heat addition is at supersonic Mach numbers and the Fanno and Rayleigh solution characteristics change sign (Scott and Riggins 2000). The isentropic stagnation pressure and temperature can reach 1000 atm and 6000 K. For this case, a different approach was sought. It was based on static conditions, not stagnation, the cycle being analyzed using a Second Law approach based on un-recovered (lost) available energy and entropy increases (Builder 1964). The original work was done in the late 1950s. By 1960, the Air Force scramjet program associated with the aerospace plane began falling apart, and this group sought employment elsewhere. Builder joined the Rand Corporation in the strategic planning department, giving up on further scramjet work because his work had been so close to completing a successful program and yet it was to be scrapped arbitrarily in favor of rockets.

At the urging of The Marquardt Company scramjet manager, Artur Magar, Builder finally published in 1964 a partial description of the approach (Builder 1964). One of the authors (P.A. Czysz) and a colleague from Douglas Aircraft Company, Gordon Hamilton, visited Builder in 1984 to discuss the unfinished portion of his work. As a result, a paper was prepared that documented the complete approach (Czysz 1988a). Although the original paper is now over 50 years old, the conclusions reached by Builder are as applicable today as then. In fact, in reading this book, the reader should come to the same conclusions. The tragedy is that in the intervening 55 years, there has been no change in the space launchers propulsion systems, design, or fabrication. Forty years after the Wright Brothers' first flight, jet power aircraft were flying in both Great Britain and Germany and by 50 years the first British commercial jet transport was approaching operational status. As in the past, each rocket still flies for the first, last, and only time. The following paragraphs are Builder's conclusions from 1964, verbatim.

Before summarizing, it would be well to note that the analyses and figures presented are based upon an ideal gas analysis. It is well recognized that the behavior of air is not ideal at high temperatures, above about 3500 or 4000 °R. However, this analysis is restricted to the static conditions throughout the cycle, so the errors due to non-ideal behavior may not be as large as they would if stagnation conditions were being used. For example, the optimum compression enthalpy ratios determined in this analysis are generally under ten, which means that the temperatures at the end of the compressive device would be under 4000 °R, because of this, it is believed that the trends and characteristics which have been presented for the Brayton Cycle family are quite valid, even if the specific values or curves are subject to adjustment for non-ideal gas effects.

What conclusions can be drawn from this treatment of the Brayton Cycle family of airbreathing engines? First: we should note that a thermodynamic analysis on Mollier coordinates for the static gas conditions provide a consistent treatment of the complete spectrum of engines in this family.

Second: an optimum amount of compression can be defined which depends only upon the overall processing efficiency of the heat-energy input of the cycle. That optimum amount of compression is compared to that available from ram stagnation of the engine airflow, a clearer insight is gained into the factors, which are common to the natural evolution of the turbojet, the conventional ramjet, and the supersonic combustion ramjet.

Third: the energy conversion efficiency of the Brayton Cycle appears to continuously improve with speed, even approaching orbital velocities. It has been shown that the amount of compression is an important consideration in determining the energy conversion efficiency. Thus, we should not be overly preoccupied with the efficiency of compressive devices or the attainment of the maximum amount of compression possible. It is over-compression which causes the drop-off of conventional ramjet efficiencies above 10,000 fps.

Finally, what does this analysis tell us with respect to potentially new engines lurking in the spectrum of chemical airbreathing propulsion? The turbojet, conventional ramjet, and supersonic combustion ramjet are clearly the dominant occupants of the three distinct regions of desired compression: mechanical, stagnation, and partial diffusion. However, we seem to lack engines for the transition regions. The turbo-ramjet is a hybrid, which spans two of the three regions, but is probably not the best possible choice for the

region in-between. In the Mach 3 to 5 regime, an engine having very modest mechanical compression with high processing efficiencies might be very attractive. In a sense, a fan-ramjet might be a suitable name for such a cycle; the duct-burning turbofan and the air-turborocket could be considered close cousins to this hypothetical engine. At the higher speed end, around Mach 10, we can postulate a very efficient engine called the transonic combustion ramjet. There is still another important class of possibilities offered just outside the confines of the Brayton Cycle family: engines with non-adiabatic compression and expansion processes as a result of heat exchanges between the air and fuel. We might find a complete new spectrum of such engines awaiting our discovery.

At the time Builder wrote the AIAA-64-243 paper, a major effort was underway to develop, in a single engine, the characteristics of the combined turbojet and ramjet. The concept was called a turbo-ramjet (Doublier et al. 1988; Escher 1966).

4.16 Pulse Detonation Engines

4.16.1 Engine Description

Based on non-continuous through-flow, a pulse detonation engine (PDE) is a cyclical operation engine analogous to the World War II pulse jets (Neufeld 1995; Hellmold 1999). This engine fires cyclically, resulting in an intermittent engine thrust. The engine consists of an acoustically tuned pipe, fed by a detonable mixture inside that, when ignited, sends the combustion products wave traveling down the pipe ahead of a detonation wave. After the products exit the tube, the tube is effectively scavenged, new fuel is then injected, and a new mixture forms, sort of reloading the tube. The ignition process is then repeated, starting a new cycle. This periodic operation gives the PDE a characteristic cyclic rate and the characteristic sound that, in the V-1 case, gained it the nickname of "buzz bomb."

A comparison of the pulse detonation rocket engine (PDRE) or pulse detonation engine (PDE) with today's standard rocket and turbojet cycles can show the potential of this propulsion system. A PDRE is a cylindrical tube with a defined length. The PDRE is an intermittent internal combustion/detonation engine with three strokes, namely *injection*, *detonation*, and *exhaust*, as shown in Fig. 4.29. The PDRE is characterized by mechanical simplicity, and high compression ratio compared to continuous combustion engines. The PDE/PDREs have the potential to significantly reduce the cost and complexity of today's liquid-propellant rocket engines; they present novel alternatives to current gas turbine and/or rocket engines. The PDE/PDRE has the potential to provide dramatic improvements in both costs and performance for space propulsion applications. This is due primarily to the fact that detonations provide a more efficient mode of combustion over the conventional constant pressure approach of current engine technology. Large reductions in pumping, plumbing, and power requirements appear also possible with the PDE/PDRE. The self-compressing nature of the detonation combustion could dramatically reduce the need for massive oxidizer/fuel turbopumps. Pump pressure is 10 atm instead of 300 atm. Corresponding reductions in plumbing, structural requirements and pumping power are thought possible with the PDE/PDRE. Practical engineering issues and subsystem technologies still need to be addressed to ensure that this potential is realized.

The PDE/PDRE possesses a significantly higher power density compared to conventional rocket designs. Detonation combustion produces large pressure increases in the combustion chamber (over and above those produced by pre-combustion turbopumps), creating large thrust forces at the chamber thrust wall. The result is a very high thrust for an engine of equivalent dimensions compared to today's state-of-the-art propulsion systems, provided of course that the repetition rate is sufficiently high. Alternatively, an equivalent amount of thrust could be generated with a more compactly designed PDE/PDRE. Because additions in PDE/PDRE load-bearing structure do not increase proportionally with gained chamber thrust forces, the PDE/PDRE does also possess a much higher thrust-to-weight ratio than current chemical rocket engines.

As shown in Fig. 4.29, the basic cycle has one detonation wave traveling down the tube. One way to increase the thrust is by making a multiple-tube engine (Norris 2003) as was being developed by Pratt & Whitney. Note that in the referenced article, a single detonation wave tube is shown, which is satisfactory for sea-level testing. In all of the work done on PDEs for this chapter, they have been equipped with expansion nozzles just as in the case of a rocket engine, see Fig. 4.30. Another approach is to operate the detonation wave tube so there are multiple pulses traversing the tube (Norris 2003).

The flow characteristics in a pulse detonation engine have been modeled previously using a variety of methods including zero-dimensional, one-dimensional, and two-dimensional unsteady analyses. All three of these levels are useful, but provide different types of information. Zero-dimensional analyses provide fast, global parametric trends for the unsteady operation of a PDE. One-dimensional models provide a first indication of the dominant wave processes and the manner in which they couple with the

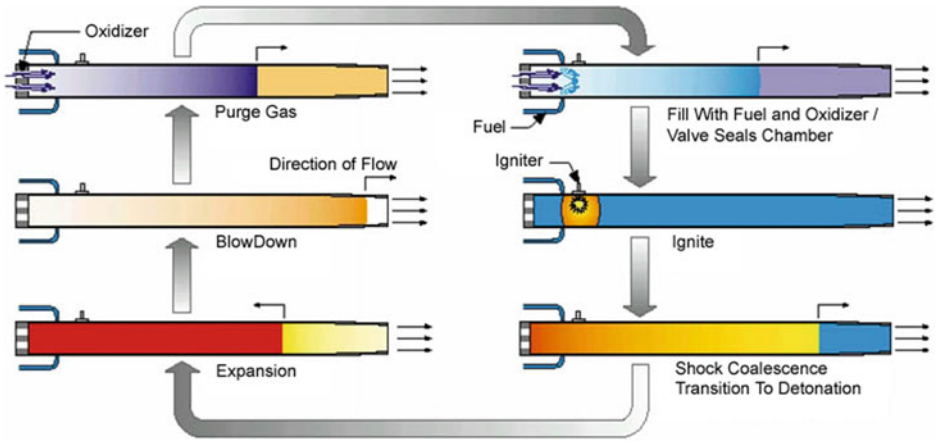

Fig. 4.29 The pulse detonation rocket engine (PDRE) operational cycle

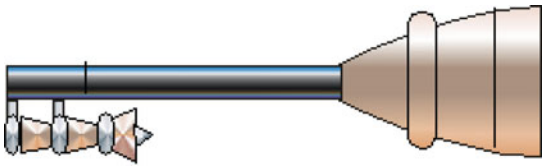

Fig. 4.30 Pulse detonation rocket engine (PDRE)

overall engine/vehicle system at a cost that is intermediate between zero- and two-dimensional models. Two-dimensional models have the capability of identifying the dominant multi-dimensional effects (e.g., fuel/air mixing) and their level of importance. However, multi-dimensional modeling requires a substantial investment in computational resources. Some specific areas of PDE/PDRE operation are inherently dominated by multi-dimensional phenomena, and the only way to address these phenomena is by modeling the entire multi-dimensional process.

4.16.2 Engine Performance

Analysis of engine flowpath physics, anchored to available experimental and CFD data, has shown performance to be dependent on the propellant combination, the feed system, and other design parameters. It is only through detailed component energy balancing, coupled with unsteady detonation analysis and modeling of losses, that accurate estimates of the PDE/PDRE performance may be obtained. Three key parameters that determine performance are *nozzle length* compared to the detonation tube length, *fill fraction* (i.e., whether there are multiple detonation waves present in the engine), and *detonation frequency*.

The first factor is *nozzle length*. Nozzle lengths can double the I_{sp} for a hydrocarbon-fueled PDRE (Kailasanath 2002). Data from (Daniau 2002) indicates that a divergent nozzle does not adversely affect the cycle time. Detonation frequencies in the 140 Hz range for hydrogen-oxygen and 110 Hz for hydrocarbon-oxygen mixtures are possible. The importance of the information is that for a fully airframe-integrated PDE with the aft-body forming the nozzle, a beta parameter in the 5–6 range enhances PDE performance. Beta is the ratio between nozzle length and combustion chamber length. The combustion chamber length is not the entire tube length, the forward part of the tube being where the fuel and oxidizer mix and combustion is initiated, as shown in Fig. 4.29.

The second factor that affects the performance of the PDE is the *fill fraction*. In an ideal detonation wave tube, see Fig. 4.29, the products of combustion exit the tube and the tube is purged before the next charge is introduced. An option is to introduce a new charge into the tube before the cycle is complete. In this case, the fill fraction is less than 100%. That is, only a certain fraction of the tube receives a new charge. A reduction in the fill factor directly affects the I_{sp} of the engine, no matter at what frequency. In this chapter, a 100% fill and a 60% fill fraction were used. The partial fill case provides 38% greater I_{sp} when compared with the full fill case. The former is referred to as "full fill," and the latter is referred to as "partial fill" in the propulsion characteristics and sizing results.

The third factor affecting performance is the *detonation frequency*. In a chart shown by Kailasanath (2002), the real difference in the performance of the PDE versus the ramjet is governed by the detonation frequency of the PDE. The chart depicts experimentally determined thrust versus the frequency for the PDE compared to a ramjet. For the PDE, as the frequency is increased, the thrust increases almost linearly. For a modest frequency PDE operating at one-half the maximum frequency of 35 Hz, the thrust is 2.25 times the ramjet thrust. Since the reason for rocket-driven ejectors in the ramjet engine is to obtain greater thrust at low-speed, the pulse detonation engine has significant potential to increase low-speed performance over that of a ramjet. For this chapter, a thrust of twice the subsonic through-flow ramjet engine has been used, see Fig. 4.31.

In the low-speed flight regime, there is insufficient kinetic energy to produce a static compression enthalpy ratio, Ψ, sufficient to sustain ramjet operation. The rocket ejector ramjet is a means of providing sufficient nozzle enthalpy and pressure ratio to have an efficient ramjet at speeds lower than Mach 2.5. The PDRE does not depend on ram pressure; with the PDE ejector, it has sufficient pressure ratio to operate at zero flight speed as either a pulse detonation rocket or as an airbreathing pulse detonation engine analogous to the rocket ejector ramjet. So, the question was to predict its potential performance using Builder's analysis.

The original Brayton cycle analysis by Builder (1964) was based on the static enthalpy rise within the engine. Builder called the term (Ψ) the static enthalpy compression ratio h/h_0, where h_0 is the freestream static enthalpy. If C_p = constant, then $\Psi = T/T_0$. The extension of Builder's original work by Czysz (1988a) has continued that nomenclature. Heiser and Pratt (2002) and Wu et al. (2003) use static temperature ratio for the value of Ψ, so there is about one-unit difference between the two definitions of Ψ in the 5000–6000 ft/s range, with the temperature ratio definition being the lower value. The comparison in performance is made using the energy conversion efficiency θ, that is, what fraction of the input fuel energy is converted into useful thrust work.

The energy conversion efficiency has been already defined before with Eqs. (4.15a)–(4.15c); we further have:

$$\theta = \frac{V \cdot T}{\frac{\text{Fuel}}{\text{Air}} \cdot Q_c \cdot \dot{w}_{\text{air}}} \tag{4.20a}$$

$$\theta = \frac{V \cdot T_{sp}}{Q} \tag{4.20b}$$

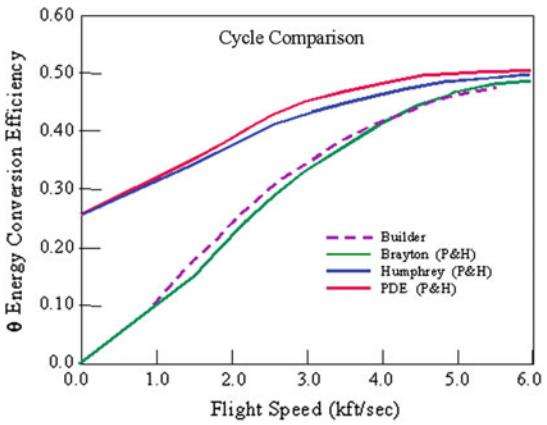

Fig. 4.31 The pulse detonation engine (PDE) cycle compared with the Brayton cycle. P&H indicates the (Heiser and Pratt 2002) paper

With specific impulse and specific thrust defined as

$$I_{sp} = \frac{\theta \cdot Q_c}{V} \tag{4.21}$$

$$T_{sp} = \frac{\theta \cdot Q}{V} \tag{4.22}$$

It is important to observe that as velocity is increased, both the specific impulse, I_{sp} (thrust per unit fuel flow) and specific thrust, T_{sp} (thrust per unit air flow) decrease inversely proportional to velocity, even though θ may increase with velocity to a plateau value. Making a direct comparison between the energy conversion efficiency of Builder (θ) using the enthalpy ratio Ψ and the temperature ratio definition of Ψ by Wu et al. (2003) and Heiser and Pratt (2002) did not produce a clear cut conclusion. The comparison for θ between (Builder 1964) and (Heiser and Pratt 2002) is rather good, considering that the values for Builder were independently done prior to 1964 using a Second Law approach that minimized the cycle entropy rise. Nevertheless, the clear advantage in the lower speed range for the PDE is shown in Fig. 4.31.

The Humphrey cycle is a cycle that has been used as a surrogate for the pulse detonation cycle to estimate performance. As shown in Fig. 4.31, it provides a good representation of the PDE energy conversion efficiency. The energy conversion efficiencies were converted into I_{sp} values, see Eq. (4.16), and the PDEs compared with conventional ram–scramjets. The more informative parameter, for an acceleration-dominated SSTO application, can be obtained from a comparison of effective specific impulse, that is, the acceleration specific impulse using the $T - D$ difference rather than thrust, T, alone. For I_{spe} estimations, the aircraft drag was determined from historical data for the two configurations of interest (Pirrello and Czysz 1970).

12. Pulse detonation rocket engine (PDRE). Figure 4.30 depicts a rocket PDE (or PDRE). The PDRE usually is charged with a near stoichiometric mixture of fuel and oxidizer, and they can be any detonable fuel and oxidizer combination. For estimating the performance of launchers, only hydrogen has been used here as fuel. The primary advantage of this system is reduced complexity and weight in the propellant fluid pressurization systems. The PDR is charged with fuel and oxidizer to generally less than 10 atm. The resulting pressure peak behind the detonation wave can exceed 1000 atm. The very uniform pressure behind the detonation wave yields a constant thrust pulse.

In one of the research institutes located outside Beijing, China, and at The University of Texas at Arlington's (UTA) Aerodynamics Research Center (ARC), there are

high-performance shock tube wind tunnels driven by a detonation wave tube, rather than the conventional hydrogen/oxygen combustion driver. The result is a very uniform drive-pressure profile and longer run times. The advantages are that the charge to the driver tube is a few atmospheres compared to the conventional tens to a hundred atmospheres. The detonation wave itself delivers compression and heating without a mechanical pump. Made flight weight, the PDR is a device which is operating at a cyclic rate rather than with a single firing. It can be installed in any rocket-powered aircraft or launcher, just as the rocket engine was installed, with the expansion nozzles located at the same place.

13. Pulse detonation rocket/ramjet engine. The evolution of a PDRE/PDE-based combined-cycle engine is reported as a Russian concept (Kailasanath 2002). This Russian concept can operate over a range of flight conditions going from takeoff to hypersonic flight. The PDE can be integrated into an airframe in the same manner as a rocket and ram–scramjet. For the low-speed flight regime, and until there is sufficient kinetic energy to produce a static temperature ratio, Ψ, sufficient to sustain PDE operation, a strut-integrated PDRE functions very much like a rocket ejector strut, except with less complexity and high-pressure fluid systems.

Figure 4.32 shows a Russian concept for a PDRE/ramjet PDE that is equivalent to a rocket–ramjet system, which can operate as an airbreathing system up to Mach 6 (Kailasanath 2002). (1) In the first operating region, to about Mach 2.3, the engine operates as a pulse detonation rocket ejector ramjet with the PDR replacing the rocket ejector. (2) Above Mach 2.5, the PDR acts as an ejector and is a hydrogen ejector, with a downstream-pulsed oxygen injection which stabilizes a periodic detonation wave in the engine ahead of the nozzle contraction. In this case, the ramjet nozzle is driven by a detonation wave process. The shock system around the PDR ejector and the ejected hydrogen pressure isolates the detonation process from the inlet, and prevents regurgitation of the shock system. (3) Above Mach 6, the PDR is the propulsion system, analogous to the airbreathing rocket or ejector ramjet–rocket. A representative installation is shown in a hypersonic glider (FDL-7 family) at the top of Fig. 4.32.

14. Pulse detonation rocket/ramjet–scramjet engine. Figure 4.33 shows a Russian concept for a PDE/ramjet/ODWE equivalent to a rocket-ram–scramjet system as described in Kailasanath (2002). The PDE module is shown integrated into a blended-body configuration airbreathing vehicle much as a rocket ejector ramjet–scramjet is integrated. Except for the pulsed nature of the ejector strut operation, the engine is essentially a rocket ejector ramjet. The engine spans the operational envelope from takeoff to perhaps a little above Mach 15.

(1) The PDRE operation is confined to the strut during the low-speed phase of the operation. (2) For the PDE engine above Mach 6 flight, the propulsion configuration is an airbreathing PDE that incorporates elements of the rocket PDE, with the kinetic compression of the rocket ejector ramjet producing a pulsed detonation wave within a steady flow device. This concept is equivalent to a LACE or deeply cooled airbreathing rocket. (3) For speeds greater than Mach 6, the propulsion converts to a steady-state operation as an oblique detonation wave engine (ODWE), as it is necessary to transition the detonation wave from an oscillating (back and forth) wave structure to a steady oblique detonation wave structure. In this operating mode, it is equivalent to a scramjet (Kailasanath 2002). In this latter mode, the engine works using a continuous detonation process and is now a steady-state engine. (4) Above the maximum airbreathing speed, the PDR provides the thrust to orbital velocity. At the top of Fig. 4.33, a representative installation in a propulsion-configured airbreathing configuration is shown. Externally there is little difference in the configuration compared to the conventional scramjet installation, except for perhaps a longer engine cowl.

The pulse detonation propulsion systems offer considerable promise to reduce weight and propellant pumping challenges. Note that PDREs are in a period of experimentation and development, and most of the engineering is still classified. The question remains: Can the eventual operational hardware developed capture the promise shown in the analytical studies? In the following section, we assume that operational hardware has captured the promised performance, so a valid measure of the propulsion system potential is presented.

4.17 Conclusions with Respect to Pulse Detonation Cycles

The three pulse detonation engine systems are compared in a single table in a similar manner to the continuous engine cycles. For a vehicle powered by a conventional continuous rocket engine, the W_{OWE} is 76 t (metric tons); the equivalent PDR W_{OWE} is 70 t because of the lesser total vehicle volume and the lesser propellant pumping hardware and weight. The assumption has been that the engine weight is the same as an equivalent thrust conventional rocket engine. This is yet to be demonstrated with operational engine weights, but it is a reasonable expectation considering the much less complicated hardware required. With these considerations, the W_{OWE} of 70 t is equivalent to the conventional all-rocket.

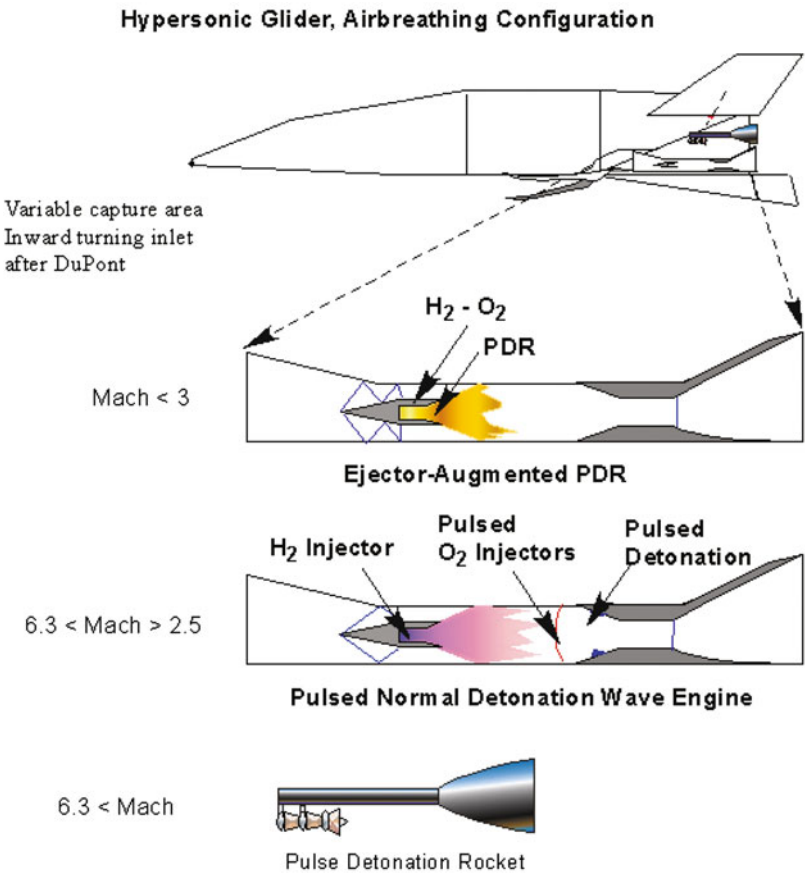

Fig. 4.32 Integrated PDRE ramjet combined cycle

For other propulsion systems, the W_{OWE} is 70 t plus any differential weight for the propulsion system. The W_{TOGW} for the three systems is:

Cycle	W_R (–)	O/F (–)	W_{TOGW} (t)	Savings[a] (t)
Pulse detonation rocket	8.10	6.00	567	49
Pulse detonation rocket/ramjet	5.10	4.60	357	259
Pulse detonation rocket/ram/scramjet	3.20	1.80	224	392

[a]With respect to an all-rocket SSTO launcher

Perhaps the PDEs are the beginning of the Builder conclusion more than 50 years ago, "*There is still another important class of possibilities offered just outside the confines of the Brayton Cycle family: engines with non-adiabatic compression and expansion processes as a result of heat exchanges between the air and fuel* and engines with non-steady *operation* (non-italics by the authors). *We might find a complete new spectrum of such engines awaiting our discovery.*" (Builder 1964)

4.18 Comparison of Continuous Operation and Pulsed Cycles

Adding the PDEs to the results in Fig. 4.28, the result is Fig. 4.34 that gives the SSTO mass ratio (weight ratio) to reach a 100 min (185 km) orbit with hydrogen fuel as a function of the maximum airbreathing Mach number for both continuous and cyclic operation engines. Seven classes of propulsion systems are indicated: (1) rocket-derived, (2) airbreathing (AB) rocket, (3) so-called KLIN cycle, (4) ejector ramjet, (5) scram-LACE, (6) air collection, and enrichment systems (ACES) and (7) pulse detonation derived engines (PDR/PDRE). As in Fig. 4.28, there is a discontinuity in the results. If the mass ratio to orbit is to be significantly reduced, the carried oxidizer-to-fuel ratio (oxygen and hydrogen) must be reduced to 5 or less. That means at least an airbreathing rocket or airbreathing PDR is required to achieve that threshold.

The weight ratio, hence the takeoff gross weight, is a direct result of the propellant weight with respect to the W_{OWE}. As introduced earlier (Sect. 4.14), the propellant weight is a direct function of the oxidizer-to-fuel ratio (O/F):

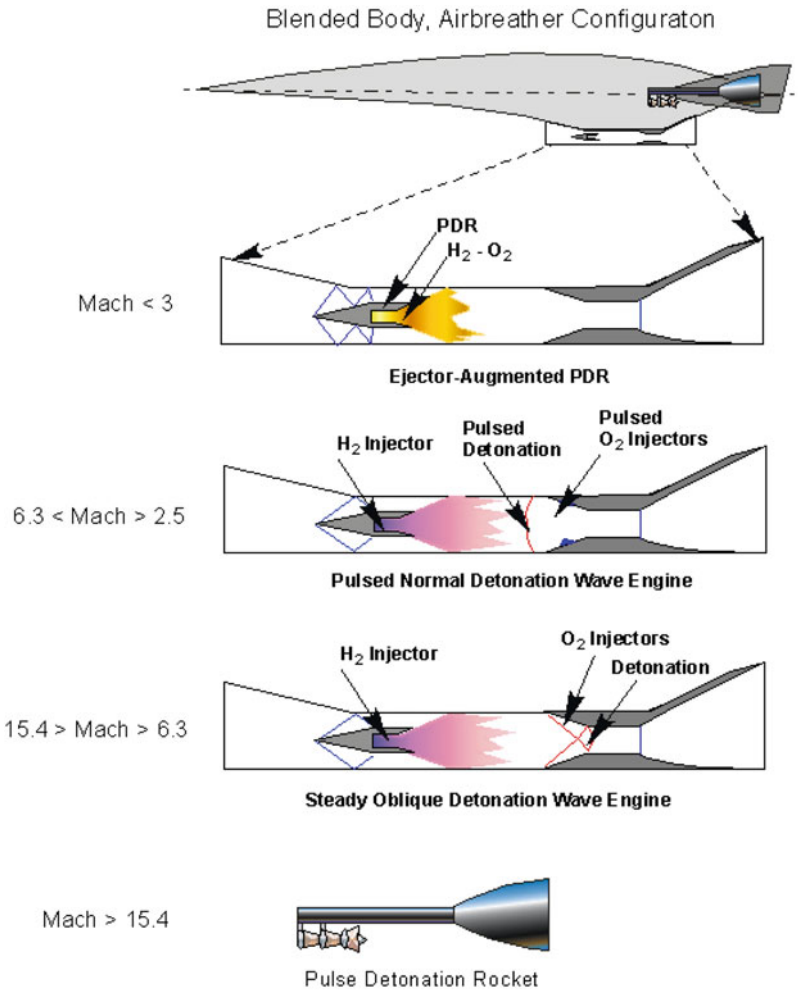

Fig. 4.33 Integrated PDRE ram–scramjet combined cycle

$$W_{\mathrm{R}} = 1 + \frac{W_{\mathrm{ppl}}}{W_{\mathrm{OWE}}} \tag{4.23a}$$

$$W_{\mathrm{R}} = 1 + \frac{W_{\mathrm{fuel}}}{W_{\mathrm{OWE}}} \cdot \left(1 + \frac{O}{F}\right) \tag{4.23b}$$

The TOGW = W_{TOGW} is defined as usual

$$W_{\mathrm{TOGW}} = W_{\mathrm{R}} \cdot W_{\mathrm{OWE}} \tag{4.24a}$$

$$W_{\mathrm{TOGW}} = W_{\mathrm{OWE}} \cdot \left[1 + \frac{W_{\mathrm{fuel}}}{W_{\mathrm{OWE}}} \cdot \left(1 + \frac{O}{F}\right)\right] \tag{4.24b}$$

$$\frac{W_{\mathrm{fuel}}}{W_{\mathrm{OWE}}} = \frac{W_{\mathrm{R}} - 1}{\left(1 + \frac{O}{F}\right)} \tag{4.24c}$$

Remember, in these equations, the oxidizer/fuel ratio is the oxidizer/fuel ratio carried on the launcher with its associated weight ratio, not the rocket engine oxidizer/fuel ratio. The importance of the equation set is that the gross weight is a function of one airframe parameter (W_{OWE}) and two propulsion parameters, and that the gross weight is directly proportional to the carried oxidizer-to-fuel ratio (O/F). Reduce the carried oxidizer, and the gross weight and resultant engine thrust decrease proportionately.

Beginning with the rocket point in Fig. 4.34 at a weight ratio of 8.1, and moving to the ACES with weight ratio of 3.0, a straight line between these points connects all of the continuous hydrogen-fueled propulsion systems. The exception are the PDRs, lying below the continuous propulsion curve: hence, their $W_{\mathrm{fuel}}/W_{\mathrm{OWE}}$ ratio is *less than one*.

The PDR is essentially equivalent to the rocket in terms of weight ratio to orbital velocity. The PDE/ramjet is equivalent to a rocket–ramjet system and lies in line with the thermally integrated KLIN cycle at a higher oxidizer-to-fuel ratio and lower weight ratio. Clearly, the PDE/ramjet has an oxidizer-to-fuel ratio about one unit greater than the KLIN cycle, and about one-half unit less in terms of weight ratio.

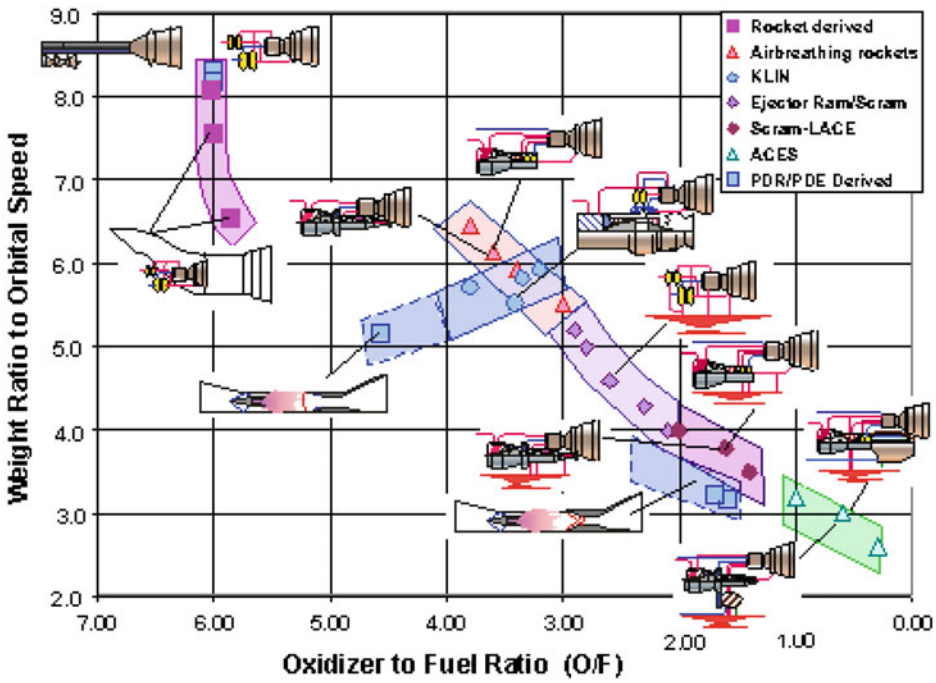

Fig. 4.34 The PDE improves the total weight ratio

In terms of characteristics, the PDE/ramjet appears to be more like a thermally integrated rocket/turbojet than the airbreathing rocket propulsion systems. In terms of the impact on operational systems, the next set of charts will size launchers to the same mission and payload to enable us to evaluate the propulsion system differences in terms of launcher system size and weight.

The PDE/ram–scramjet system is equivalent to the thermally integrated airbreathing rocket-ram–scramjet systems. It lies to the left (greater *O*/*F* ratio) of the thermally integrated ram–scramjet cycles at a slightly lesser weight ratio to orbital speed near the RBCC propulsion systems of Yamanaka (scram-LACE), Builder (ejector ram–scramjet), and Rudakov (deeply cooled-ram–scramjet). From the cycle analysis, the PDE appears to have performance advantages and disadvantages with respect to the continuous cycles (lesser weight ratio but greater oxidizer-to-fuel ratio), trades that must be evaluated in the context of launcher-sizing programs.

These three propulsion configurations have been further evaluated in detail. The overall process of exploring the thrust-to-weight ratio, cost of development, and overall payload capability for the variety of propulsion systems and matching flight vehicle integration has to examine the configurations without bias. Only such "generic" parametric modeling approach is able to correctly determine the relative merits of the "best" configuration implementation. At this point in our discussion, these ideas require further parametric investigation to finalize the comparison.

Clearly, while most conventional propulsion systems have fuel weights approximately equal to the W_{OWE}, the PDE propulsion systems have fuel weights that are less than W_{OWE}, hence the advantage of PDE systems. This weight advantage appears to represent a simple and fundamental correlation facilitating to judge hydrogen/oxygen propellant SSTO results. As shown in Table 4.6 for other fuels, the ratio will not be one.

In determining the launcher size for each propulsion system concept, an important parameter is the installed engine thrust-to-weight ratio. A non-gimbaled (that is fixed and not steerable by pivoting the engine) rocket engine for space operation could have an engine thrust-to-weight ratio as large as 90. For a large gimbaled engine, such as the space shuttle main engine (SSME), that value is about 55 for the installed engine. We use this value as the reference value for our comparisons. The liftoff thrust generally determines the maximum engine thrust for the vehicle. For a given vehicle thrust-to-weight ratio at liftoff or takeoff, $(T/W)_{\mathrm{TO}}$, the weight of the engines is a function of the required vehicle thrust-to-weight ratio at liftoff, the thrust margin, the weight ratio, and the W_{OWE}. Thus:

$$W_{\mathrm{engine}} = W_{\mathrm{R}} \cdot \left(\frac{T}{W}\right)_{\mathrm{TO}} \cdot \frac{W_{\mathrm{OWE}}}{\left(\frac{T}{W}\right)_{\mathrm{engine}}} \qquad (4.25)$$

The weight ratio is the total mission weight ratio including all maneuvering propellant. For vertical liftoff, the launcher thrust-to-weight ratio is at least 1.35. For horizontal takeoff, the launcher thrust-to-weight ratio is in the 0.75–0.90 range. Usually, if the horizontal takeoff thrust-to-weight ratio exceeds one, there is a significant weight penalty (Czysz and Vandenkerckhove 2000). The engine thrust-to-weight ratio, $(T/W)_{\text{engine}}$, has been a constant source of controversy and discussion for airbreathing engines. One approach to avoid such arguments before the actual sizing procedure begins, and that has stopped the sizing process from assessing the true potential in the past, is to find a suitable relationship for determining the engine thrust-to-weight ratio. For the authors' purpose, that procedure is to assume the total installed engine weight is a conservative constant equal to that of the all-rocket launcher. The resulting engine thrust-to-weight ratio, $(T/W)_{\text{engine}}$, for all other propulsion systems, can then be determined as:

$$\left(\frac{T}{W}\right)_{\text{engine}} = \frac{W_{\text{R}}}{W_{\text{R}_{\text{rocket}}}} \cdot \frac{(T/W)_{\text{TO}_{\text{vehicle}}}}{(T/W)_{\text{TO}_{\text{rocket}}}} \cdot \frac{W_{\text{OWE}}}{W_{\text{OWE}_{\text{rocket}}}} \cdot \left(\frac{T}{W}\right)_{\text{rocket}} \tag{4.26a}$$

$$\left(\frac{T}{W}\right)_{\text{engine}} = \frac{W_{\text{R}}}{8.1} \cdot \frac{(T/W)_{\text{TO}_{\text{vehicle}}}}{1.35} \cdot 1.55 \tag{4.26b}$$

$$\left(\frac{T}{W}\right)_{\text{engine}} = 5.03 \cdot W_{\text{R}} \cdot \left(\frac{T}{W}\right)_{\text{TO}_{\text{vehicle}}} \tag{4.26c}$$

Evaluating Eqs. (4.26a)–(4.26c) for the data in Fig. 4.34 results in Fig. 4.35, showing the engine thrust-to-weight ratio, $(T/W)_{\text{engine}}$, as a function of weight ratio to orbital speed, W_{R}, with minimum maneuver propellant. There is one calibration point in the open literature from 1966: William J. Escher completed the testing of the SERJ (supercharged ejector ramjet) to flight duplicated engine entrance conditions of Mach 8, the maximum airbreathing speed for SERJ (Escher et al. 2000, 2001). In those tests, the flight-weight engine would have had an installed thrust-to-weight ratio of 22, had it been installed in an aircraft. From Fig. 3.4, the mass ratio for an airbreathing speed of Mach 8 is 5. From Fig. 4.35, the range of values for a weight ratio of 5 is 25–27. Clearly, the SERJ engine would have had a weight just slightly larger than the assumed all-rocket engine weight.

The simple approach above estimates the operational weight of an arbitrary propulsion system. However, a word of caution: This approach estimates the installed engine thrust-to-weight ratio for an integrated propulsion system. It will not estimate the weight of the engine airbreather approach shown in Fig. 2.15, as that is an impracticable system by any standard. It is very easy to have estimates that destroy an airbreathing approach in that, to some, they appear perfectly reasonable when in fact they are based on misinformation. The relationship given with Eqs. (4.26a)–(4.26c) will give a realistic and obtainable value, given the industrial capability available today and based on the history of actual integrated airbreathing cycles.

Figure 4.35 shows that air-augmented rockets and ram rockets have lower engine thrust-to-weight ratios because of the secondary air duct weight. The ACES system has a lower engine thrust-to-weight ratio because of the weight of the air separation hardware. And, as postulated, PDEs have a higher *engine* thrust-to-weight ratio because the pumping hardware is lighter than the conventional rocket turbopumps, with a lower required launcher *takeoff* thrust-to-weight ratio. One of the advantages of wing-supported horizontal takeoff is an acceptable lower engine thrust-to-weight ratio. As discussed earlier in conjunction with Fig. 3.29, if the mass ratio permits horizontal takeoff without serious weight penalty, it has the operational advantage to open up more launch sites coupled with less strenuous engine thrust-to-weight requirements.

4.19 Integrated Launcher Sizing with Different Propulsion Systems

The real measure of a propulsion system performance, when installed in a vehicle and sized to a defined payload and mission, is when being compared to other propulsion systems. For the evaluation of the propulsion systems in this chapter, the reference mission is a SSTO mission, launching into 200 km (108 min) orbit with a 28.5° inclination and carrying a 7 t payload with a carried net density of 2.83 lb/ft^3 (45.33 kg/m^3). The sizing has been accomplished using the sizing program described in Chap. 3 (Czysz and Vandenkerckhove 2000) and using the configurations in Fig. 3.13. Hypergolic propellants are carried for in-orbit maneuvering, corresponding to a ΔV of 490 m/s. That results in a weight ratio for in-orbit maneuvering of 1.1148. The orbital maneuvering propellant includes propellant to circularize the orbit and a retro-burn to deorbit the vehicle.

All of the weight ratios presented in this chapter include the orbital maneuvering weight ratio of 1.1148, a value assumed constant for all propulsion systems. That is, the weight ratio of 8.1 for the all-rocket includes the 1.1148 weight ratio, so the actual weight ratio just to achieve orbital velocity is 7.2659. The primary sizing equations are repeated here for convenience. For details of the range of values, and

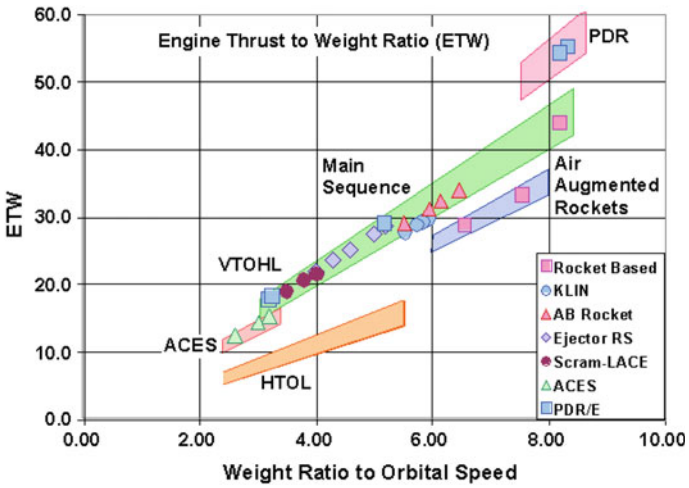

Fig. 4.35 Engine thrust-to-weight ratio decreases with weight ratio

the definition of the terms, see Chap. 3 and (Czysz and Vandenkerckhove 2000). The equations are solved simultaneously for the planform area and Küchemann's τ. Then, the other vehicle characteristics can be determined for that specific solution.

The weight budget is given by:

$$W_{\mathrm{OEW}} = \frac{I_{\mathrm{str}} K_{\mathrm{w}} S_{\mathrm{plan}} + C_{\mathrm{sys}} + W_{\mathrm{cprv}} + \frac{(T/W)_{\mathrm{TO}} \cdot W_{\mathrm{R}}}{(T/W)_{\mathrm{engine}}} \left(W_{\mathrm{pay}} + W_{\mathrm{crew}}\right)}{\frac{1}{1+\mu_{\mathrm{a}}} - f_{\mathrm{sys}} \cdot \frac{(T/W)_{\mathrm{TO}} \cdot W_{\mathrm{R}}}{(T/W)_{\mathrm{engine}}}} \tag{4.27}$$

The volume budget is given by:

$$W_{\mathrm{OWE}} = \frac{\tau \cdot S_{\mathrm{plan}}^{1.5}(1 - k_{\mathrm{vv}} - k_{\mathrm{vs}}) - (V_{\mathrm{crw}} - k_{\mathrm{crw}}) \cdot N_{\mathrm{crw}} - W_{\mathrm{pay}}/\rho_{\mathrm{pay}}}{\frac{W_{\mathrm{R}}-1}{\rho_{\mathrm{ppl}}} + k_{\mathrm{ve}} \cdot (T/W)_{\mathrm{TO}} \cdot W_{\mathrm{R}}} - W_{\mathrm{pay}} - f_{\mathrm{crw}} \cdot N_{\mathrm{crw}} \tag{4.28}$$

with

$$W_{\mathrm{OWE}} = W_{\mathrm{OEW}} + W_{\mathrm{pay}} + W_{\mathrm{crew}} \tag{4.29a}$$

$$W_{\mathrm{OEW}} = W_{\mathrm{OWE}} - (W_{\mathrm{pay}} + W_{\mathrm{crew}}) - W_{\mathrm{trapped\ fluids}} - W_{\mathrm{consumed\ fluids}} \tag{4.29b}$$

The above-summarized approach was originally developed for application to "Copper Canyon" and the National Aerospace Plane (NASP) programs (Schweikart 1998). It was used in the Phase 1 screening of 32 high-speed civil transport concepts (Douglas Model 2229) for the effort NASA sponsored with Douglas Aircraft Company (Bunin 1991; Graf and Welge 1991). The solution was adapted to MathCad by a Parks College graduate student, Ignacio Guerro, for use in the Senior Capstone Aerospace Design Course. Douglas Aircraft checked the solutions against a number of subsonic transports, and the author (P.A. Czysz) checked the solutions against the hypersonic aircraft concept of McDonnell Aircraft Advanced Engineering. Overall, the comparisons between this approach and specific converged design data are very close.

The three key determinants of the airframe empty weight are the (1) total volume, the (2) total surface area, and the (3) structural index. The first two are geometry-determined, and the latter is the total airframe structure (no equipment) divided by the total wetted area. Table 4.7 gives data related to 10 different structural approaches developed over the past 45 years and their impact on the empty weight of a launcher with a 7 t payload and a weight ratio of 6. They are listed in increasing weight per unit wetted area.

Except for structures 8 and 10, all are cold primary structure constituted by an internally insulated cryogenic integral propellant tank, protected by internally insulated metal thermal protection shingles that stand off from the structure/tank wall and provide an insulating air gap. The metal shingles are formed from two sheets of metal with a gap filled with a high-temperature insulation material. The edges are sealed so a multi-layer vacuum insulation can be employed, if needed. Structure 8 has the same thermal protection system, but the propellant tank and primary structure are separate, that is, representing a non-integral tank. Structure 10 is a non-integral tank concept with an external hot structure, separated from the propellant tank by insulation and air gap (like the fuselage of the X-15) (Jenkins 2007). The SR-71 and X-15 wings are hot structures that are not protected by insulation, and the structure and fuel soak up all the aerodynamic heating. In these cases, the determining structural parameter is the hot strength and stiffness of the material. In all other cases, the determining structural parameter is the cold strength and stiffness of the material. All the concepts protect the structure or tank with passive insulation, except concept 1 that uses propellant (fuel) to pump (convect) heat away from the structure and convert it into useful work, see Figs. 4.22 and 4.23.

Table 4.7 Specific weights of structures and associated structural indices

Source	I_{str} (metric) (kg/m^2)	I_{str} (imperial) (lb/ft^2)	W_{OWE} (t)
(1) NASA, active, 1993 (Pegg et al. 1993)	13.8	2.83	33.3
(2) NASA, passive, 1993 (Pegg et al. 1993)	16.6	3.40	43.4
(3) HyFAC, passive, 1970 projection to 1985	17.1	3.50	45.5
(4) VDK, passive, future	18.0	3.68	49.6
(5) VDK, passive, current	21.0	4.30	65.8
(6) HyFAC, passive, 1970 1970 industrial capability	22.0	4.50	72.1
(7) HyFAC, passive, 1970 1966 industrial capability	22.7	4.66	76.7
(8) HyFAC, passive, 1970 non-integral tank	25.4	5.20	96.5
(9) HyFAC, passive, 1970 1970 hypersonic demonstrator	29.3	6.00	130.6
(10) HyFAC, hot structure, 1970 non-integral tank	32.5	6.66	163.4

4.20 Structural Concept and Structural Index

Structures 1 and 2 in Table 4.7 are from reasonably recent reports (1993) concerning metal thermal protection systems (TPS) with current advanced titanium and metal matrix composite materials. Structures 3, 6, 7, 8, 9, and 10 are from the seminal Hypersonic Research Facilities Study (HyFAC) conducted for NASA by McDonnell Aircraft Company, Advanced Engineering Department, from 1968 to 1970 (Pirrello and Czysz 1970). One of the authors (P.A. Czysz) was the Deputy Study Manager for that program. Except for structure 3, which anticipated the development of advanced titanium, metal matrix composite materials, and high-temperature plastic matrix materials, the other concepts employ high-temperature chrome-nickel alloys and coated refractory metals for the thermal protection shingles that enclosed the vacuum multi-layer insulation. Structure 9 represents an effort to minimize the cost of a short flight time research vehicle (5 min) at the expense of increased weight by using more readily available high-temperature materials.

Structures 4 and 5 have been the work of the late Jean Vandenkerckhove (VDK) and the late author (P.A. Czysz) to characterize the high-temperature metal and ceramic materials available at the time in Europe. Carbon/carbon, silicon carbide/carbon, and silicon carbide/silicon carbide structural material from SEP, Bordeaux (now SAFRAN/SNECMA, Bordeaux), and metal matrix composites from British Petroleum, Sudbury, along with the conventional aircraft materials, have been characterized from information supplied by the major European aerospace manufacturers. At that time, no materials from the former Soviet Union were included. Notice that the structural concepts center on the HyFAC study structural data. These representative values have been used in most of the work completed by the authors.

The two structural indices used by J. Vandenkerckhove for a weight ratio 6 launcher result in a W_{OEW} of 49.6 t employing VDK *future,* and 65.8 t employing VDK *current*. The same vehicle using the 1970 McDonnell Douglas structural index results in 72.1 t *current* and 45.5 t *future* (projected to 15 years in the future, to 1985). Assuming the current availability of materials and manufacturing processes equivalent to 1970, then the vehicle empty weight ranges between 65.8 and 72.1 t. Assuming the current availability of materials and manufacturing processes equivalent to the 1985 projection (and from what the authors saw at SEP, Bordeaux, BP, Sudbury, and NPO Kompozit, Moscow), then the vehicle empty weight ranges between 45.5 and 49.6 t. Note that these values should span what is possible with readily available materials today, as much as the Saturn V was constructed from what was available in 1965. As we see from Table 4.7, the non-integral structural concepts are not competitive, resulting in a W_{OEW} of 96.5 t for a passively insulated tank, and 163.4 t for a hot structure concept. The 1993 results from (Pegg et al. 1993) show some weight reduction in the passive structural concept of the order of about 5%, not a critical item. The focus on future launcher must be durability over a long period of use, not one-time lightness. The design, build, and operations philosophy must be akin to that of the Boeing B-52, not of an ICBM.

The cold, insulated integral tank structural concept employed in these studies remains appropriate and valid. The concept has withstood the test of many challenges, but remains the lightest and lowest-cost approach to high-temperature, hypersonic aircraft structure that has been established by practice (Pirrello and Czysz 1970). The primary structure is principally aluminum with steel and titanium where strength is a requirement. The aerodynamic surface is made by interleaved smooth shingles with standoff

and insulation material that provide a high-temperature radiative surface to dissipate to space most of the incoming aerodynamic heating. Less than 3% of the incoming aerodynamic heating reaches the aluminum structure. The HyFAC data dates back to circa 1968 and is built on the materials and insulation available then. With advanced RSR materials and superplastic forming with diffusion bonding, together with silicon carbide and carbon fiber reinforcements to fabricate metal matrix composites (MMC), the values in Table 4.7 should be conservative.

The active TPS values are from a more recent source, as given by Pegg et al. (1993). Depending on the duration of the flight, that heat can be absorbed in the airframe thermal capacitance or removed by an active thermal management system (see Figs. 4.22 and 4.23). For some short duration (10 min or less) research flights and some orbital ascent flights, no active thermal management system is necessary. For a long-duration cruise flight, some means of moving the incoming thermal energy to a site where it can be disposed of or used to perform mechanical work is required. The original concept from the 1970s has been implemented, using high-temperature refractory metals such as columbium (niobium), tantalum, molybdenum, and Réne 41 and other refractory alloys, which have densities larger than steel (9000–17,000 kg/m^3).

Clearly, today's RSR titanium, RSR metal matrix composites (MMC), titanium aluminide, carbon/carbon, and silicon carbide/silicon carbide composites can achieve the same temperature performance at much less weight. The weight estimates based on scaling of the 1970 data are therefore very conservative. The configuration concept uses conventional aircraft construction techniques for most of the aircraft; the shingles are well within the current manufacturing capabilities considering the hot isostatic pressing, superplastic forming, and diffusion bonding available in the gas turbine industry. For longer-duration flights required for long-range cruise, the advantages of active thermal management are clear. With current materials, whether actively thermally managed for cruise, or passively thermally managed for exit and entry, it should be possible in the 2016-plus timeframe to build a structure for a hypersonic aircraft that is between 3.0 lb/ft^2 and 4.0 lb/ft^2 (14.6 and 19.5 kg/m^2) using materials and processes available today.

The W_{OWE} is a function of the structural index, I_{str}, and a weak function of the weight ratio to orbit W_R, see Fig. 4.36. There is a 15% margin on the W_{OEW} assigned by the sizing equations. The W_{OWE} that applies to the sizing results in this book is given by Eq. (4.30):

$$W_{OWE} = 65.8 \cdot [0.003226 \cdot (I_{str})^2 - 0.04366 \cdot (I_{str}) + 0.4943] \cdot (0.02369 \cdot W_R + 0.8579) \tag{4.30}$$

4.21 Sizing Results for Continuous and Pulse Detonation Engines

For the evaluation of the different propulsion systems, see Table 4.7, structural concept 5 (VDK *current* at 21.0 kg/m^2) has been used. The propulsion systems, see Fig. 4.34, have

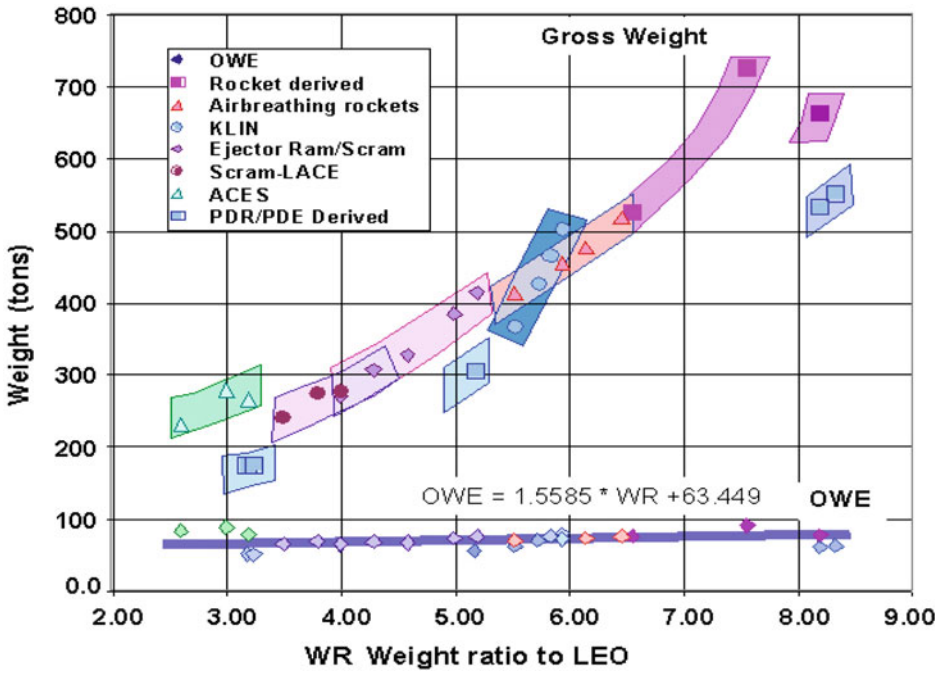

Fig. 4.36 Gross weight decreases significantly as weight ratio decreases. Operational weight empty is almost constant

been installed in the appropriate configuration concept and sized to mission. Figure 4.37 presents W_{TOGW} and W_{OWE} as a function of oxidizer-to-fuel ratio, and Fig. 4.36 presents W_{TOGW} and W_{OWE} as a function of weight ratio. Each of these presentations provides different perspectives of the sizing results and the characteristics of the propulsion systems.

Whenever presenting results as a function of oxidizer-to-fuel ratio, Fig. 4.37, there is always the discontinuity between the rockets and the airbreathing systems. For the rocket-derived systems, the all-rocket is not the top point, but the second from the top. The air-augmented rocket is heavier than the all-rocket, because the thrust increase and reduced oxidizer-to-fuel ratio do not offset the weight of the ejector system. This is clearly shown in Fig. 4.36, as the air-augmented rocket has a mass ratio of 7.5 and is heavier than the all-rocket. Below that point, the W_{OWE} value is on top of the correlation line indicating a heavier empty weight. The ram rocket, in which the oxygen in the ejector secondary air is burned, is a different case, and the weight and oxidizer-to-fuel are less than the all-rocket. The ram rocket has a gross weight similar to the PDE. The difference is that the ram rocket is at the end of its improvement capability while the PDE is just at the beginning of its potential improvement cycle. The pulse detonation rocket (PDR) has a gross weight similar to the ram rocket, with much less complexity. The important result is that either can reduce the gross weight by 200 t! This is comparable to the highest values of the airbreathing rockets and the KLIN cycle.

Clearly, the incorporation of some airbreathing in the rocket, whether an ejector burning fuel in the secondary air stream (ram rocket) or by direct airbreathing rocket (LACE, deeply cooled rocket or KLIN cycle), results in a significant advantage in gross liftoff weight and engine size and thrust reduction (in fact, a 28% reduction).

Direct airbreathing rockets (LACE, deeply cooled rocket, or KLIN cycle) form a group in the center of both charts (Figs. 4.36 and 4.37) and are in the 3–4 oxidizer-to-fuel ratio and in the 5.5–6.5 weight ratio area. These propulsion cycles form the first steps in airbreathing propulsion and are capable of reducing the gross weight from nearly 700 t (metric tons) to 400–500 t. Their maximum airbreathing Mach number is in the 5–6 range.

The important aspect is that this is a beginning capability that, with adaptation to further airbreathing (scram-LACE), can achieve gross weights in the 200–300 t range. As shown in Fig. 3.4, as the airbreathing speed is increased, both the oxidizer-to-fuel ratio and mass ratio decrease until Mach 12 airbreathing speed is reached, when further increase of airbreathing speed does not result in additional decrease in the mass ratio. This results from the fact that, as shown in Eqs. (4.12) and (4.13), both thrust and specific impulse for an airbreathing system decrease with the inverse of speed while drag could increase. When the effective specific impulse (based on thrust minus drag) falls below the effective specific impulse of a rocket, the rocket is a better accelerator. As a consequence, attempting to fly to orbital

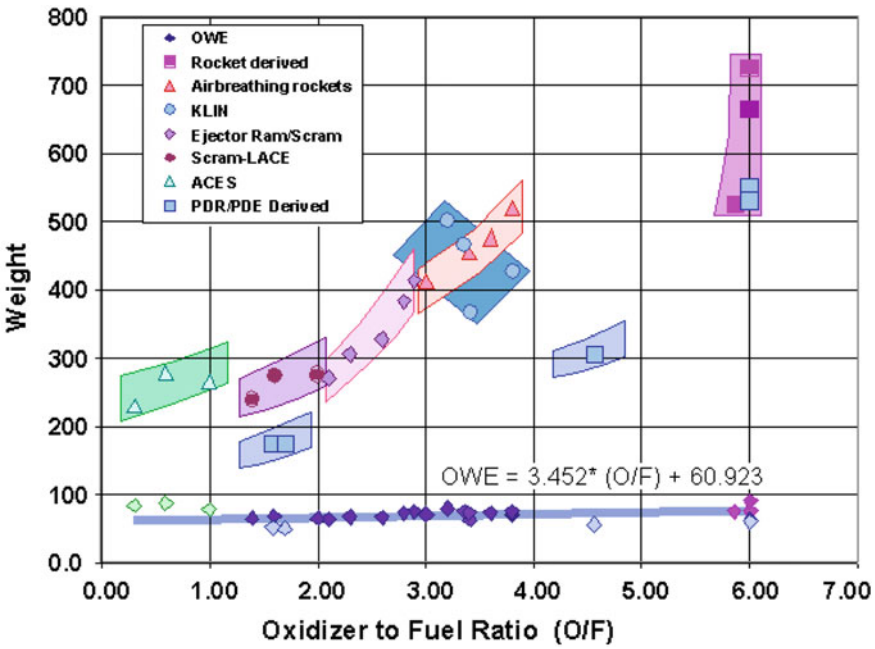

Fig. 4.37 Gross weight decreases significantly as oxidizer-to-fuel ratio decreases. Operational weight empty (empty weight plus payload) is nearly constant

speed with an airbreather will result in a larger vehicle that requires more propellant.

Air collection, enrichment, and separation (ACES) began as a recommended system beneficial for TSTO launchers. As discussed in Chap. 2 and later in this chapter, for the TSTO application the ACES system presents significant advantages. However, for the SSTO configuration implementation, the additional volume requirement in the orbital vehicle can carry penalties, depending on the system design chosen. Even though ACES has both a lower weight ratio and lower oxidizer-to-fuel ratio, its gross weight is about the same as the ejector ram–scramjet and the scram-LACE and scram–deeply cooled. In both plots (Figs. 4.36 and 4.37), the W_{OWE} is heavier than (above) the correlation line, as was the air-augmented rocket.

What does fall below the W_{OWE} correlation line are the PDE points. That is for two reasons: (1) less volume required and (2) lower weight of propellant pumping systems. In Fig. 4.35, it is almost possible to envision a new main sequence of PDEs parallel and lower than the continuous operation engines. As this class of engines is developed into operational systems, the potential exists for this class to reduce both, the rocket class and airbreather class, in gross weight and empty weight. What is not clear at this point is, whether the cyclic engine can have variants equivalent to the airbreathing rocket and its ACES derivative. These latter engine types may remain as continuous operation engine cycles only.

If we take the W_{OWE} results and subtract the 7 t payload to yield the W_{OEW}, then it is possible to see how volume affects the magnitude of the empty weight. Figure 4.38 shows the empty weight value as a function of the total vehicle volume. The correlation is rather good. First, notice that the triangles representing the ACES propulsion system have almost the largest volumes. The largest is the air-augmented rocket. This clearly explains the W_{OWE} values in the previous two graphs where the W_{OWE} values were greater than the correlation curve through the other cycles. It is also clear that the PDEs have some of the lowest volume values for the propulsion systems presented. Clearly, the variation in empty weight can primarily be explained by variation in total volume. The W_{OWE} is also a function of the structural index and the weight ratio to orbit, see Fig. 4.36. As given in Eq. (4.30), we now can determine the mean W_{OWE} for any other structural index than the VDK *current* at 21.0 kg/m^2 and any mass ratio.

When representing the data in Fig. 4.36 in terms of total volume rather than weight, this results in Fig. 4.39. Clearly, the ACES systems lie above the main sequence of propulsion systems (large shaded area) and the PDEs lie below the main sequence of propulsion systems. Whether the PDE-ramjet and PDE-scramjet areas can be connected remains to be seen, there should be no technical reason why future PDE systems would not span that area.

What we can conclude so far is:

(1) The structural concept for an insulated cold primary structure is an important decision that can have a significant impact on vehicle empty weight. For launchers, passive thermal protection is more than adequate. However, for a cruising vehicle, passive insulation permits too much of the aerodynamic heating to reach the cryogenic tanks, and an active heat removal scheme is required. Pegg et al. employed fuel as the heat transfer agent (Pegg et al. 1993). Others include water, water-saturated capillary blankets, and other phase-change materials between the backside of the shingle and the integral tank structure outside surface. All of these are appropriate for most of the structure for blended-body or all-body configurations. The leading edges are based on sodium heat pipes that move the thermal energy to a lower temperature area or a heat exchanger. Control surfaces are a case-by-case basis, and each is designed based on configuration and local flow conditions. In terms of the total vehicle and an advanced concept initial sizing, these have minimal impact on the final size and weight. But if the reader wishes to refine the estimate, the values in Table 4.7 can be improved by the following first-order correction. This correction assumes that the leading edges are 10% of the total surface area, and the control surfaces are 15% of the total surface area. Note that the corrections are based on values from (Pirrello and Czysz 1970) for an operational vehicle.

$$I_{str} = 5.87 + 0.75 \cdot (I_{str})_{\text{Table 4.7}} \tag{4.31}$$

Then, the VDK *current* structural index would become 21.6 kg/m^2.

(2) Given the thermal protection system and structural concept, the next most important determinant of the empty weight is the total volume of the vehicle, see Fig. 4.38. In some cases, the total volume is a response to the change in oxidizer-to-fuel ratio; in other cases, it is the inherent volume of the propulsion concept (ACES and PDE systems) as shown in Fig. 4.39.

(3) The gross weight is a direct result of the weight ratio to orbit (Fig. 4.36), which is determined by the propulsion system oxidizer-to-fuel ratio (Fig. 4.34).

(4) The threshold values for the oxidizer-to-fuel ratio and weight ratio, that clearly separate airbreathing systems from rocket-derived vehicles, are 3.9 and 6.5, respectively (Figs. 4.37 and 4.36). At these values, the W_{OWE} for a launcher with a 7 t payload is 71.48 t, the gross

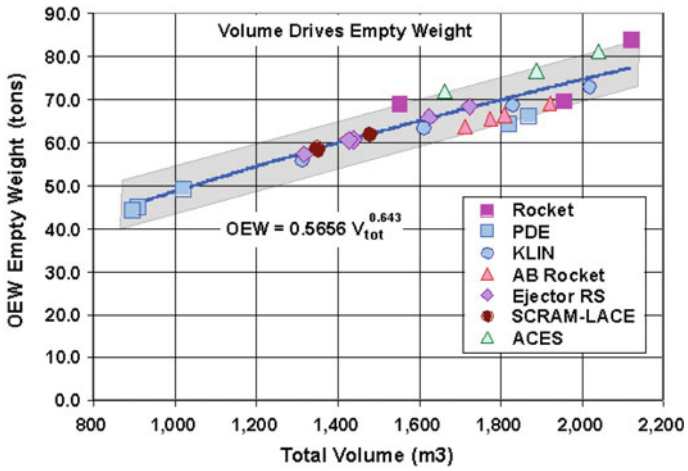

Fig. 4.38 Total volume decreases as the weight ratio decreases, except for ACES propulsion system

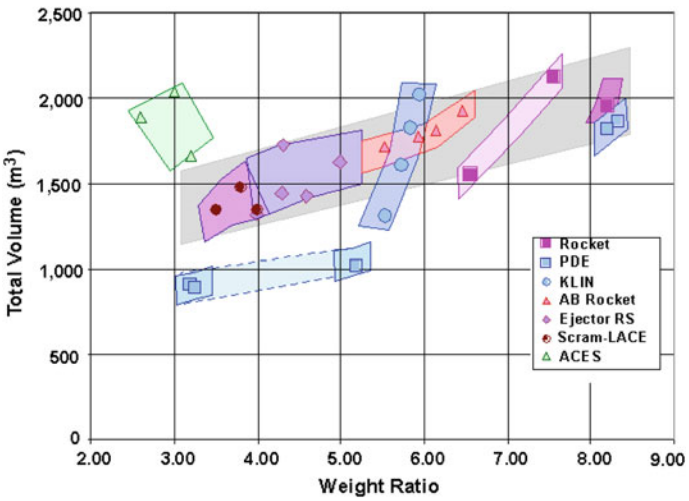

Fig. 4.39 Empty weight is less if total volume is less. ACES is heavier because volume is greater

weight is 510 t, overall less than the 690 t for the all-rocket case.

(5) The ACES system for a SSTO will have a greater volume than a corresponding ejector ram–scramjet propulsion system. Even though the weight ratio and oxidizer-to-fuel ratio are less, some of the weight ratio and oxidizer-to-fuel advantages may be offset (Figs. 4.37 and 4.39).

(6) Because of the reduced pumping system weights and the lesser installed volumes, the pulse detonation propulsion systems will have a smaller volume and less weight than a corresponding sustained operation propulsion system.

(7) Propulsion system weight has been assumed to be a constant, equal to that for the all-rocket with a gross weight of 690 t, liftoff thrust of 932 t, and a propulsion system weight of 16.9 t. The exceptions are the air-augmented rocket in which an ejector structure has been added to the airframe, the ACES system in which the air separation system has been added to the LACE or deeply cooled airbreathing rockets, and the PDEs where the conventional turbopumps have been replaced by lower-pressure-ratio turbocompressors (Fig. 4.35).

4.22 Operational Configuration Concepts: SSTO and TSTO

For the *rocket-derived vehicles*, the configuration is the hypersonic glider derived from the Air Force Flight Dynamics Laboratory FDL-7 C/D (Draper and Sieron 1991). This configuration is depicted accelerating to orbit in Fig. 4.40. As depicted, it is powered by either a LACE or a deeply cooled airbreathing rocket. Although sized as a SSTO vehicle, it could also represent the second stage of a TSTO accelerating to orbital speed. At the altitude shown, the Mach number is greater than 6, so the inward-turning inlet is retracted. As *Model 176*, see Fig. 3.9, the McDonnell Douglas version for MOL (Anon 2015), it was designed in 1964 for a fleet of 10 vehicles to fly between 75 and 90

flights per year with an individual aircraft flight rate between overhaul of 200 and an operational life of 25 years.

For the *airbreather-derived vehicles*, the configuration is derived from the McDonnell Blended Body, as shown in Fig. 4.41. The configuration is depicted in an accelerating climb with a combination of rocket and ramjet power as the vehicle accelerates through the transonic flight regime. It is depicted climbing from a C-5A Galaxy air launch, but it could just as easily have separated from an An-225 *Mriya*. If this were a TSTO vehicle, a smaller version of the vehicle in Fig. 4.40 would be on top, and separation would be in the Mach 8 to 14 range. As one of the reference operational vehicles for the 1970 HyFAC study (Pirrello and Czysz 1970), this airbreathing launcher was the first stage of the TSTO vehicle that staged at Mach 10 to 12. Later, as the CFD (Computational Fluid Dynamics) verification model for Copper Canyon and the subsequent NASP program (Schweikart 1998), it was a SSTO configuration which has been as well publicized as the *Orient Express* (Conway 2008; Davies 1998). Again, the design goals were for frequent flight, spanning a long operational life with significant flights between overhaul, as for the Model 176. Unfortunately, no actual goal numbers have survived.

In the authors' opinion, for a versatile and payload-flexible launcher, a TSTO vehicle offers the best options. And there have been some elegant and practical TSTO launchers designed, but unfortunately never built. Figure 4.42 shows two of those launchers, the MBB *Sänger* (upper) and the Dassault Aviation *Star-H* (lower). The MBB *Sänger* program also conceived the first stage being constructed as a hypersonic transport carrying over 200 passengers (Kuczera and Sacher 2011; Koelle et al. 2007). This highly refined blended wing-body was developed through extensive wind tunnel testing, including the detailed testing of the second-stage separation at Mach 7 in the Ludwig-Tube facility at the Göttingen DLR Institute in Germany (Jacob et al. 2005).

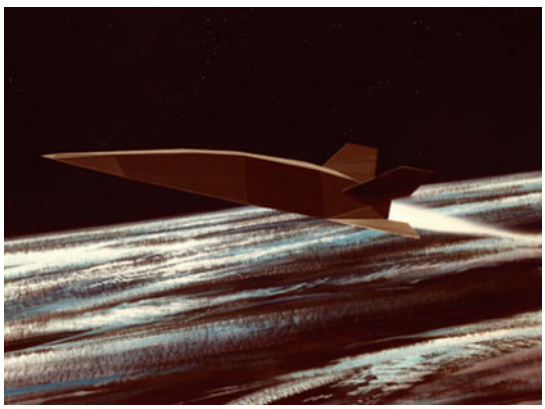

Fig. 4.40 LACE rocket-powered VTHL SSTO with a gross weight of 450 t, a weight ratio of 5.5 and an oxidizer/fuel ratio of 3.5

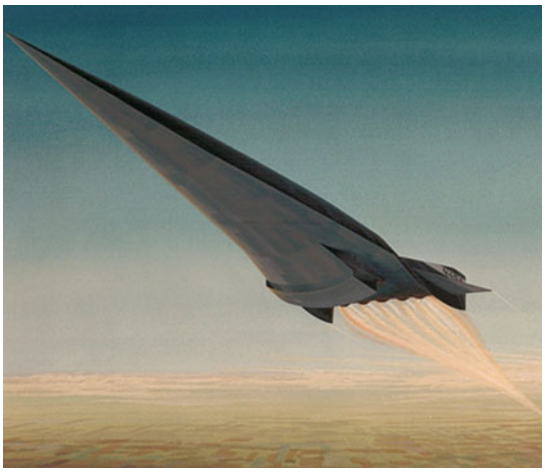

Fig. 4.41 Ejector ram–scramjet-powered HTHL SSTO with a gross weight of 300 t, a weight ratio of 4.3 and an oxidizer/fuel ratio of 2.2

The second stage of the MBB *Sänger* was a flat-bottom hypersonic glider that carried the ascent propellant and payload to orbit. It was designed as an automatically piloted vehicle. Considering that the net density of a passenger cabin is about 80 kg/m^3 and that of subcooled hydrogen is 76 kg/m^3, a hydrogen tank makes a perfect cabin for a weight of passengers equal to the weight of the hydrogen, with much less thermal insulation requirements. Switching the fuel to subcooled methane means that there is volume for both the passengers and methane, replacing the hydrogen and oxygen for the launcher.

Dassault Aviation *Star-H* used a different approach for the second stage (Kuczera and Sacher 2011; Kingsbury 1991). Since the thermally protected second-stage glider is the most costly, the Dassault Aviation *Star-H* approach has been to minimize its size and have it carry payload only; the propellant and thrust has been provided by a separate expendable rocket. This reduces the size of the hypersonic glider, in this case depicted as the Hermes (Hannigan 1994). This was also the philosophy of Gleb Lozino-Lozinskiy in the Mikoyan *Spiral 50-50* concept that dates back to 1968 (Harford 1997).

Both the MBB *Sänger* and the Dassault Aviation *Star-H* are elegant designs that could have been successful, in principle, had they been built. However, both suffered from a propulsion community mistaken assumption that the turbojet was the best accelerator for lower speed operation between Mach 2.5 to Mach 3.0. The resultant massive over-and-under turbojet/ramjet propulsion system of the MBB *Sänger* and the turboramjet propulsion system of the Dassault Aviation *Star-H* appear to have been their downfall. A rocket ejector ramjet or airbreathing rocket would have provided excellent acceleration capability instead.

In Chap. 3, we compare a TSTO powered by a rocket ejector ramjet with a TSTO powered by a turboramjet (Czysz

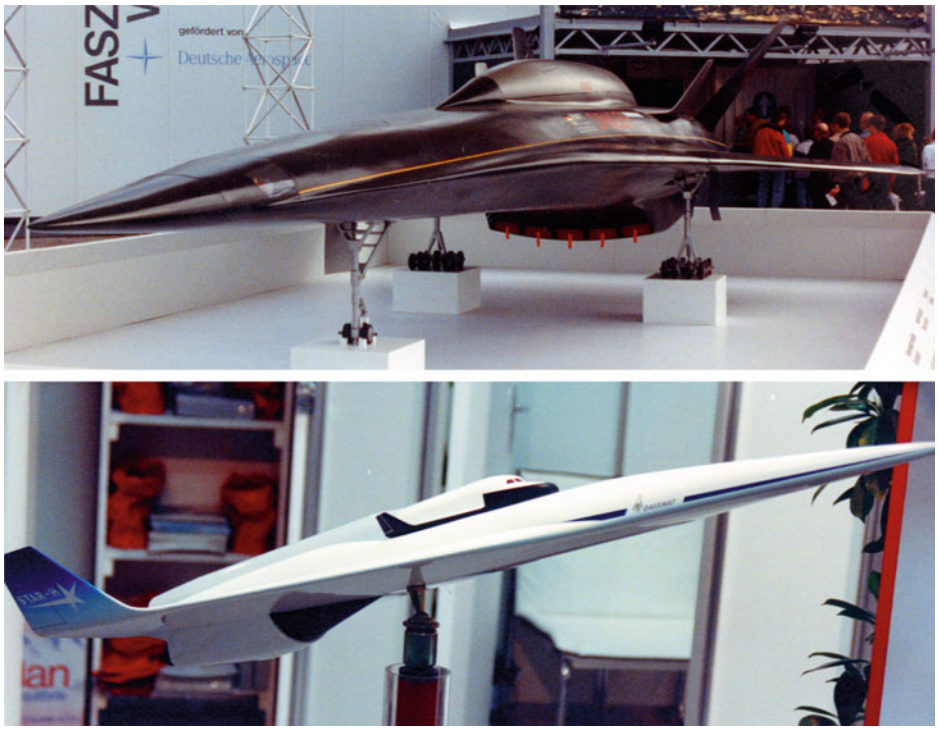

Fig. 4.42 Two elegant TSTO designs. The MBB Sänger (*top*) and Dassault Aviation Star-H (*bottom*)

and Vandenkerckhove 2000). Both TSTO launchers have been sized to deliver a 7 t payload to 463 km in a 28.5° inclination orbit. The staging Mach number selected is 7, which is the same as for the MBB *Sänger* system. In comparison, the turboramjet launcher consists of a second stage weighing 108.9 t, carried by a 282.7 t first stage for a total liftoff weight of 393.0 t. The rocket ejector ramjet launcher consists of a second stage weighing 118.4 t, carried by a 141.6 t first stage for a total liftoff weight of 261.0 t. We observe a significant weight difference; the ejector ramjet thrust is nearly constant from transonic to staging speeds, while the turboramjet at staging speed is only providing 25% of the transonic thrust. The turboramjet has significantly more thrust at takeoff, but that is not as important as maintaining a constant supersonic acceleration. The result is that the turboramjet launcher suffers a 50% gross weight penalty at takeoff when compared with the ejector ramjet launcher case.

If a commercial hypersonic transport version of the first stage was contemplated, then the propulsion system would have to be changed to a cruise-focused system, replacing the acceleration-focused system of the launcher. The *acceleration-focused system* must maximize thrust minus drag, $T - D$, and minimize zero-lift drag, C_{D0}. The *cruise-focused system* must maximize aerodynamic efficiency, L/D, and propulsion efficiency, θ. This change in focus almost precludes a single system from doing both missions. The exception might be Rudakov's combined cycle with the performance shown in Fig. 4.20. The attempt to get one gas turbine-based propulsion system to do both is the weakness of most of these legacy TSTO programs. Yet TSTO launchers are an excellent option, and with a suitably powered TSTO, a substantial saving in gross weight can be realized together with significant payload flexibility. Note that the more recent NASA-DARPA *Horizontal Launch Study* from 2011 (Bartolotta et al. 2011) does indeed employ gas turbine propulsion with the transonic carrier vehicle, as does the British Aerospace Interim HOTOL study from 1991 (Parkinson 1991), the NPO Molniya MAKS study from 1976 to 1981 (Lozino-Lozinskiy and Bratukhin 1997; Lozino-Lozinskiy et al. 1993), the recent 4-turbojet WhiteKnightTwo carrier aircraft being built by Virgin Galactic (Anon 2016), and Paul Allen's 6-turbojet carrier aircraft Stratolaunch (Anon 2014).

In the 1990s, Paul A. Czysz and the late Jean Vandenkerckhove extensively examined the SSTO compared to the TSTO based on rocket ejector ram–scramjet propulsion (Czysz and Vandenkerckhove 2000; Vandenkerckhove 1991, 1992a, b, 1993a, b). Figure 4.43 compares the takeoff gross weight (W_{TOGW}) results, and Fig. 4.44 compares the dry weight (W_{OEW}) results. Note that any crew for space operations, or crew rotation on an orbital station, are considered payload and not crew, that is, pilots. Nine comparisons are made as described below:

(1) SSTO with VDK *current* structural concept (reference: 21.0 kg/m^2) with 15% dry margin and crewed (piloted) by two crewmembers with provisions for orbital stay, powered by ejector ram–scramjet of VDK design, *Hyperjet* Mk 3 (Vandenkerckhove 1993a).

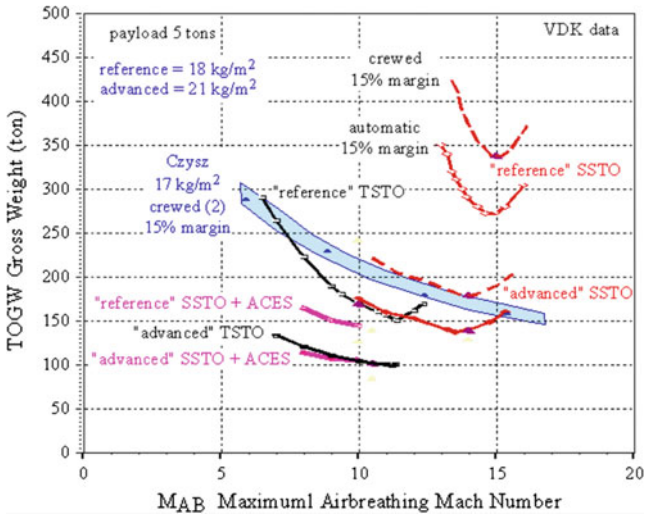

Fig. 4.43 Comparison of SSTO and TSTO results for W_{TOGW}

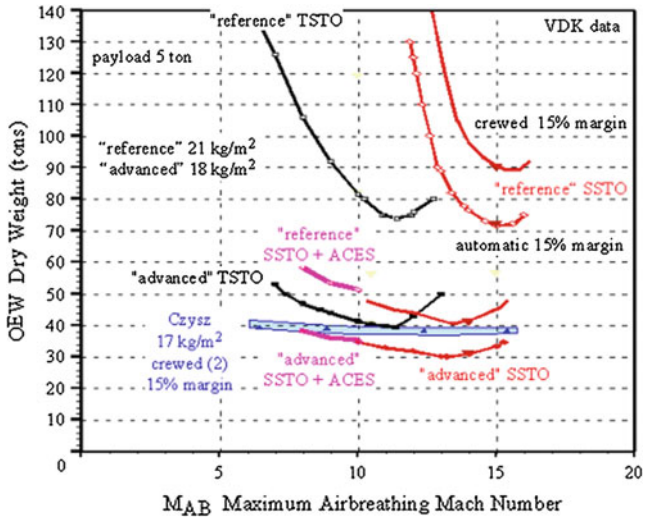

Fig. 4.44 Comparison of SSTO and TSTO results for W_{OEW}

(2) SSTO with VDK *current* structural concept (reference: 21.0 kg/m^2) with 15% dry margin and piloted by automatic flight control system, powered by ejector ram–scramjet of VDK design, *Hyperjet* Mk 3 (Vandenkerckhove 1993a).
(3) SSTO with VDK *future* structural concept (advanced: 18.0 kg/m^2) with 15% dry margin and crewed (piloted) by two crewmembers with provisions for orbital stay, powered by ejector ram–scramjet of VDK design, *Hyperjet* Mk 3 (Vandenkerckhove 1993a).
(4) SSTO with VDK *future* structural concept (advanced: 18.0 kg/m^2) with 15% dry margin and piloted by automatic flight control system, powered by ejector ram–scramjet of VDK design, *Hyperjet* Mk 3 (Vandenkerckhove 1993a).
(5) SSTO with Czysz structural concept from McDonnell HyFAC Study (17.0 kg/m^2) with 15% dry margin and piloted by automatic flight control system, powered by engines with maximum airbreathing Mach numbers from 6.0 to 12.0 from the engine sequence in Fig. 3.4 (Pirrello and Czysz 1970).
(6) TSTO with VDK *current* structural concept (reference: 21.0 kg/m^2) with 15% dry margin and piloted by automatic flight control system, powered by ejector ram–scramjet of VDK design, *Hyperjet* Mk 3 (Vandenkerckhove 1993a).
(7) TSTO with VDK *future* structural concept (advanced: 18.0 kg/m^2) with 15% dry margin and crewed (piloted) by two crewmembers with provisions for orbital stay, powered by ejector ram–scramjet of VDK design, *Hyperjet* Mk 3 (Vandenkerckhove 1993a).
(8) SSTO with VDK *current* structural concept (reference: 21.0 kg/m^2) with 15% dry margin and piloted by automatic flight control system, powered by ejector ram–scramjet of VDK design with ACES (air collection, enrichment, and collection).
(9) SSTO with VDK *future* structural concept (advanced: 18.0 kg/m^2) with 15% dry margin and piloted by automatic flight control system, powered by ejector ram–scramjet of VDK design with ACES (air collection, enrichment, and collection).

Because a specific engine design has been considered, the results have much sharper minima compared to the generic engine concepts. In Fig. 4.43, we can see the impact of piloted (crewed) systems for both "reference" SSTO and "advanced" SSTO launchers. For the reference case, the gross weight increment is almost 70 t. The minimum gross weight occurs at Mach 15 maximum airbreathing speed for the "reference" SSTO structural concept and Mach 14 for the "advanced" SSTO structural concept. The gross weight is driven by the difference in empty weight shown in Fig. 4.44. In this figure, the 20 t difference in W_{OEW} is clearly seen for the "reference" structural concept. The results from *Hypersonic Convergence* (Czysz 1987) are close to the results obtained by VDK's "advanced" solutions. The difference is that the family of combined-cycle propulsion systems yields a design point at each Mach number, whereas the VDK results are for a particular ejector ramjet engine configuration.

Examining the TSTO results, there are two interesting observations. (1) The first is that the minimum empty weight of both TSTO stages is about the same compared to the single SSTO system for both the "reference" and "advanced" structural concepts. This means that other than design and

engineering costs, the airframe cost based on weight should be quite comparable. Note that the design, engineering, and production costs are not the driving costs in launcher operations, see Fig. 3.2. (2) The second is that the gross weight for the "reference" TSTO is only slightly greater than the "advanced" SSTO, and that the "advanced" TSTO presents one of the lowest gross weights. This is due to the fact that much less mass (second stage only) must be delivered to orbit for the TSTO, compared to the entire (non-staging) SSTO vehicle. Clearly, the TSTO can have an acquisition and cost advantage over the SSTO implementation. If both vehicles are automatic, then crew costs are not a distinguishing factor.

The last comparison is the addition of ACES (air collection, enrichment, and separation) to the SSTO propulsion system. This permits the SSTO to have an offset capability analogous to the TSTO as it collects the enriched air oxidizer for ascent into orbit. Jean Vandenkerckhove and Patrick Hendrick wrote the complete ACES performance code themselves rather than depend on 1960s programs. The performance of the hardware came primarily from two sources, John Leingang in the USA (Leingang et al. 1992) and M. Maita and his colleagues with the National Aerospace Laboratories (now JAXA) in Japan (Maita et al. 1990). The results show that the addition of ACES to SSTO results in the SSTO vehicle weight now being equivalent to the TSTO vehicle. The results are different than those from Figs. 4.36 and 4.37; this is due to the fact that the Vandenkerckhove results are based on a detailed system analysis of individual hardware items, while the results presented with Figs. 4.36 and 4.37 are based on correlated results. However, the results are not that dissimilar in that both suggest that a SSTO with ACES is as light as an advanced TSTO.

Examining Figs. 4.36 and 4.37, there are a number of options that yield very similar results. Considering the "advanced" SSTO with automatic flight controls for a maximum airbreathing Mach number of 14, and the "reference" TSTO with automatic flight controls for a maximum airbreathing Mach number of 12, and the "reference" SSTO plus ACES with automatic flight controls for a maximum airbreathing Mach number of 10, we have three different systems, two of which use current materials and fabrication capability, with essentially the same gross weight and different empty weights. Considering the "advanced" TSTO with automatic flight controls for a maximum airbreathing Mach number of 12, and the "advanced" SSTO plus ACES with automatic flight controls for a maximum airbreathing Mach number of 10, we have two different systems with essentially the same gross weight and similar empty weights.

Clearly, there are two approaches to reach minimum weight launchers. One approach is to focus on TSTO with inherent payload size and weight flexibility, or alternatively focus on SSTO with ACES and a more focused payload capability, such as discussed for the Model 176 resupply and crew rescue vehicle for the MOL.

4.23 Emerging Propulsion System Concepts in Development

This section will discuss two propulsion systems that operate in a manner different from conventional airbreathing chemical combustion systems.

(1) The first propulsion system originated in the former Soviet Union, probably in the 1970s, as a total energy concept that coupled aerodynamic forces with electromagnetic forces, thereby requiring a local plasma flow to exist for the system to work. The name given by its inventor, the Russian V. Freishtadt, to the system is *Ayaks* (АЯКС), or Ajax, and is described as a magnetohydrodynamic (MHD) energy bypass system. If the flow inside (or even around) the aircraft is sufficiently ionized, i.e., in the plasma state, then the MHD system is equivalent to an induction generator that can remove energy (reduce velocity) from the flow in the form of an electrical current, with minimal aerodynamic diffusion (Tretyakov 1995). This reduces the energy lost through shock waves in conventional inlet aerodynamic deceleration, at the price of increasing drag. If that electrical power is transmitted to the equivalent of an induction motor (a Lorentz force accelerator), then electromagnetic interaction with the plasma can add energy (increase velocity) back to the flow.
The motivation for the MHD system is the realization that the electromagnetic energy transfer suffers less of an entropy rise (irreversible energy loss) than aerodynamic diffusion and expansion, therefore the net thrust is greater. If the flow field around the aircraft is a plasma, flow energy (Gorelov et al. 1995) can be removed at the nose by an MHD generator that alters the shock wave structure around the vehicle, overall reducing the total drag (Batenin et al. 1997). Again, because the flow is ionized, the flow in the propulsion inlet system can be turned by MHD Lorentz forces instead of physical inlet ramps, a form of morphing. That may dramatically reduce the weight and mechanical complexity of the inlet/nozzle system. In this chapter, the focus is on the energy bypass system, and it must be noted that a

rigorous evaluation of all concept elements has not been made, so that this concept is still controversial.

(2) The second propulsion system is creating heated air to produce thrust not by combustion, but by the interaction between matter (air) and intense electromagnetic radiation (either by a *laser* or by a *microwave beam*). The advantage is that only some working fluid (usually water) is needed to produce thrust; water is dense when stored liquid while producing a low molecular-weight gas when heated. Matter does not need to be combustible. Since the energy source is remote from the vehicle, a directed energy beam (from Earth, or the Moon, or a space station or wherever) must provide the power to the vehicle to produce thrust. This vehicle is named *Lightcraft* by its inventor, the late Professor Leik Myrabo, formerly at Rensselaer Polytechnic Institute.

4.23.1 MagnetoHydroDynamic (MHD) Energy Bypass System

The initial Ajax system information came from two sources (Novichkov 1990a, b). One was from a Russian document and the other an article in *Space Wings of Russia and the Ukraine* in the September 1990 magazine Echoes of the Planet/Aerospace. The article states that the project has originated in the State Hypersonic Systems Scientific Research Enterprise (GNIPGS) in St Petersburg, which was headed by Vladimir Freishtadt. The article elaborates on the cooperation of industrial enterprises, the Technical Institutes, the VPK (Military Industrial Commission), and the RAS (Russian Academy of Sciences). All the discussions with individuals about Ajax stress both the global range capability at hypersonic speeds and the directed energy device for peaceful purposes. Interestingly, the use as a space launcher is not mentioned.

Beginning in 1990, in Russian and Ukrainian literature articles started to appear about a new long-range hypersonic aircraft named Ajax, whose development had begun at least 10 years earlier. Its propulsion system employed a coupled magnetohydrodynamic (MHD) element that (reportedly) significantly increased the performance of and decreased the size of the hypersonic vehicle. With the available literature and after discussions by the authors with Russian and Ukrainian citizens, there was sufficient information to use first principles to analyze the system and determine whether the concept provided a real advantage.

In September 1996, as part of the Capstone Design Course, AE P 450-1, and the Hypersonic Aero-Propulsion Integration Course, AE P 452-50, at Parks College, Saint Louis University, a student design team took on the task of analyzing Ajax. The resulting performance increase reduced

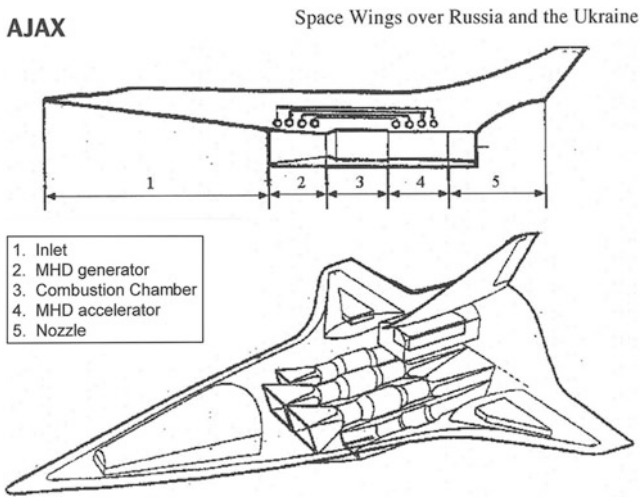

Fig. 4.45 Ajax from article by *Space wings over Russia and the Ukraine*

the size and weight of the performance-sized aircraft (Esteve et al. 1977). The student team members were Yago Sanchez, Maria Dolores Esteve, Alfonso Gonzalez, Ignacio Guerrero, Antonio Vicent, and Jose Luis Vadillo. Professor Mark A. Prelas, Department of Nuclear Engineering, University of Missouri-Columbia, was an advisor to the student team. After touring a number of Russian nuclear facilities, he provided first-hand knowledge of the ionization devices that are reported to be key components of the Ajax system.

From Novichkov (1990a) comes a sketch of the propulsion system with the coupled MHD generator-accelerator showing the energy bypass concept, see Fig. 4.45. The simple sketch gives a cross section similar to any airframe-integrated propulsion system, in which the bottom of the vehicle hosts the propulsion system, and the forebody is indeed the front part of the inlet. Also from Novichkov (1990b) are the features of the Ajax system and reasons the Ajax system was developed. They are as follows:

(1) *Energy bypass* via a coupled MHD generator-accelerator system (Gurianov and Harsha 1996; Carlson et al. 1996; Lin and Lineberry 1995): a portion of the free stream kinetic energy bypasses the combustion chamber, to reduce the entropy rise associated with aerodynamic diffusion and to augment the combustion process.

(2) *Reforming* of hydrocarbon fuel via a thermal decomposition process, followed by an electrical arc process into a high hydrogen fraction fuel, with about 20,200 Btu/lbm heat of combustion. It is assumed that the products are gaseous hydrogen, ethylene, and other combustible species, and possibly carbon monoxide. The quantity of water used or the disposal of the excess

carbon for this process is unclear (experimental data and analyses from various sources, including Russian, support qualitatively the relevance of this feature).

(3) *Ionization* of the airflow at the nose of the aircraft and of the airflow entering the engine, probably generated by the Russian-developed Plasmatron or, as reported by other Russian researchers, by streamers. One of these Plasmatron devices is operating in the plasma wind tunnel test facility at the von Kármán Institute (VKI) near Brussels. The former may alter the shock system surrounding the aircraft to reduce drag and to permit the MHD nose generator to extract enthalpy kinetic energy from the flow. The latter permits the MHD generator-accelerator to function with the magnetic field strengths possible with superconducting magnets and the flow velocities present within the engine module to produce a flow energy bypass system (Tretyakov 1995; Gorelov et al. 1996), (Russian information supported by analysis and available databases.)

(4) *Powering of the fuel-reforming process* by an MHD generator in the nose of the vehicle (Batenin et al. 1997), that with a particle beam generator in the nose, produces a plasma bubble at the vehicle nose and results in a reduction of the vehicle total drag (Gurijanov and Harsha 1996; Tretyakov 1995; Gorelov et al. 1996; Smereczniak 1996). Reportedly, a nose plasma bubble capable of absorbing radar waves is present in the Russian "Topol" ICBM (Russian information with experimental data obtained by one of the authors (C. Bruno) under an Italian research collaboration effort with the Russian Academy of Sciences (RAS-Novosibirsk)).

(5) *Increase in the combustion efficiency* within the engine by means related to injection of plasma or hydrogen ahead of the fuel injector struts (Tretyakov et al. 1995) (Russian information with experimental data obtained under Italian collaboration research effort with RAS-Novosibirsk.).

(6) *Diversion* of the bypassed energy to a directed energy device on an intermittent basis for peaceful purposes. Purposes listed are as follows: reduction of the ice crystal formation over Antarctica to reduce the size of the ozone hole, space debris burning (e.g., see Campbell and Taylor 1998), ionosphere and upper atmosphere research, ozone generation, communication with artificial satellites, water surface and atmosphere ecological conditions diagnostics, ore deposits prospecting, Earth vegetation research and monitoring, seismic conditions and tunnel monitoring, ice conditions and snow cover monitoring, and long-range communication and navigation.

In January 2001, Alexander Szames of *Air et Cosmos* interviewed Nikolai Novitchkov and Vladimir L. Freishtadt (Szames 2001). The article states that the project originated in the State Hypersonic Systems Research Institute (GNIPGS) in St Petersburg. Vladimir Freishtadt was the OKB Director, with members Viktor N. Isakov, Alexei V. Korabelnikov, Evgenii G. Sheikin, and Viktor V. Kuchinskii. It is clear from the literature that Ajax is primarily a global range hypersonic cruise vehicle. All the discussions with individuals about Ajax again stressed both the global range capability at hypersonic speeds and the directed energy device for peaceful purposes.

When the illustration shown in Fig. 4.46 was published in Paris in December 1999, it showed a vehicle concept that corresponded to correct hypersonic design criteria and a flow field significantly modified by MHD interaction. A paper presented in the 1997 IAF Congress held in Turin, Italy, provided details of an axisymmetric MHD nose generator; it describes in particular the nose MHD device that reportedly powers a fuel-reforming process of unknown description (Batenin et al. 1997). Its intent is to drive the device that creates plasma ahead of the nose. Researchers from Novosibirsk have stated such tests have been conducted in their hypersonic, high-temperature wind tunnels and presented very similar pictures. An AIAA paper by Dr. J. Shang of the Air Force Research Labs has similar data.

One of the difficulties with the MHD propulsion system analysis is that the only realistic analysis possible is for an

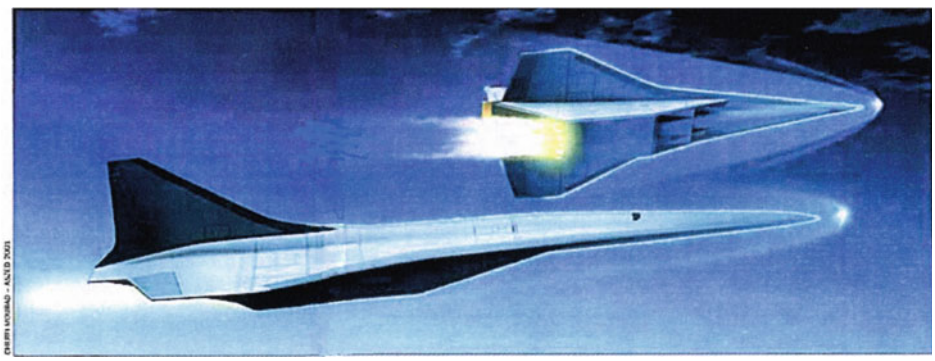

Fig. 4.46 Ayaks illustration in *Air et Cosmos* by Alexandre Szames from information obtained from Vladimir Freishtadt, the Program Director of AYAKS

aircraft in a free stream flow field without any ionization. The Szames illustration was also confirmed by Russian researchers who have stated that the propulsion system and aircraft operate as if they were in a modified Mach number gas flow field. In fact, the flow around the aircraft and entering the engine is a plasma flow. None of the aircraft or propulsion analyses these authors have done have actually considered this plasma flow field since the understanding of coupling and then solving the equations of electromagnetism (Maxwell) simultaneously with the Navier–Stokes equations of aerodynamics are still incomplete. Thus, the work by the authors investigated over the years the feasibility of single elements of only Ajax, see Bruno et al. (1997, 1998), Bruno and Czysz (1998), Czysz and Bruno (2001), Lee et al. (2002a, b, 2003a, b), Bottini et al. (2004) and concluded each element per se was feasible as claimed, but rigorous simulation of an integrated engine flowpath is still missing. Note that the plasma effect is not the same as a simple thermal modification of the gas properties. In contrast, since the atmosphere ahead of the flying aircraft has very low density, ionization followed by MHD interaction with the external upstream flow field appears definitely feasible and may be intense, covering to some extent the flowfield downstream.

The reported performance of an Ajax vehicle mission includes a 13,812 km (7458 nmi) range at Mach 8 and 33 km altitude for a mission duration of 129 min. Cruise speed is then 8005 ft/s. From historical aircraft performance correlations, the climb and descent time and distance are 46 min and 1250 nmi, respectively. With ground operation, the approach in Chap. 3 yields a cruise distance of 6208 nmi (11,497 km) and a mission time of 130 min. For a fuel fraction of 50%, we obtain a range factor predicting 16,590 km (8958 nmi). The sketch of Ajax, see Fig. 4.45, indicates a Küchemann τ of about 0.10. That yields a hypersonic, purely aerodynamic, lift-to-drag ratio $L/D_{\text{hypersonic}} = 4.1$. The integrated propulsion system and gravity relief result in a final $L/D_{\text{hypersonic}} = 4.7$. The reported heat of combustion for Russian reformed kerosene is about 30,000 Btu/lbm. With a 50% propulsion energy conversion efficiency, the $V{\cdot}I_{\text{sp}}$ is 1921 nmi (3557 km) and the I_{sp} is 1457 s. The resulting range factor is 9024 nmi (16,712 km). If low-level ionization were to be employed to reduce the cruise drag, then the mission range would be 25,309 km (13,666 nmi) in 204 min. Clearly, the reported Ajax performance is an Earth-circling range (more than antipodal) in three and one-half hours (Earth circumference is about 40,075 km or 21,639 nmi around) (Bruno et al. 1998).

For a cruise flight system, the total heat load can be an order of magnitude greater than for an atmosphere-exit trajectory. Then, some form of continuous energy management is required to prevent the airframe thermal capacitance from being saturated by excess energy (Pirrello and Czysz 1970). The heat capacity of some of the reformed hydrocarbon fuels can be greater than hydrogen. From the Szames article, the heat of formation is given as 62,900 kJ/kg or 59,620 Btu/lb for the case of reformed methane. In the case of Ajax, the thermal energy is not discarded but used to create thrust. As indicated in the Szames article, the Ajax system is an energy management system that minimizes the shock losses (entropy rise of the total aircraft system in hypersonic flight) and makes converted kinetic energy available for applications. The fraction of the thrust energy provided by the recovered aerodynamic heating reported in the Russian references, 30%, is in agreement with prior analyses (Czysz 1992; Ahern 1992).

MHD flows are governed by the interaction of aerodynamic and electromagnetic forces. As a result, the key MHD parameters have to contain elements of both. The seven most important considerations and parameters are (1) cyclotron frequency, (2) collision frequency, (3) the MHD interaction parameter, (4) the load parameter, (5) the Hall parameter, (6) the Hartmann number, and finally (7) the gas radiation losses. These parameters characterize and also constrain the performance of a MHD system. Parameters 1–2–3–7 are the four discussed in this chapter. One of the authors (C. Bruno) provided information related to the impact of each of these parameters. Four of them are critical to the operation of the MHD generator and accelerator in determining the existence and intensity of the Lorentz force (Bottini et al. 2003), that is the force that accelerates or decelerates the airflow via electromagnetic energy interaction with the ions in the plasma-containing flow. If the Lorentz force is not present, there is no electromagnetic acceleration or deceleration of the gas.

4.23.1.1 Cyclotron Frequency and Collision Frequency

Consider the motion of a single charged particle in a magnetic field $\vec{B}$. A single charged particle spirals around the $\vec{B}$ field lines with the electron cyclotron frequency. The charged particle of an ionized gas is thus guided ("confined," in plasma parlance) by the magnetic field (and thus can be separated by ions and create an $\vec{E}$ field and a voltage), but only on the condition that its mean free path (the distance a particle travels between collisions) is greater than the cyclotron radius. If this were not the case, after a collision with another particle, the particle would be scattered away from its spiral trajectory and "diffuse" across the field lines. This condition is the same as saying that the collision frequency must be less than the cyclotron frequency. The condition for guidance, accounting for collision frequency and cyclotron frequency, scales with B, pressure and temperature according to the following equation:

$$10^{-3} \cdot \left[\frac{B \cdot T^{1.5}}{p \cdot (1-\alpha)}\right] \gg 1 \tag{4.32}$$

where B = magnetic field strength (in tesla), T = gas static temperature (K), p = static pressure (atm), and α = ionization fraction. The left-hand side of Eq. (4.32) is the Hall parameter. Since the numerical factor in front of Eq. (4.32) is on the order of 10^{-3}, it is clear that this condition requires very high magnetic field strength, B, or very low pressure, p, or very high ionization fraction, α. Very high (non-equilibrium) electron temperature T_e can satisfy this last condition, provided B is on the order of 1 T or greater and pressure is on the order of 0.1 atm. This places a stringent condition on the operation of a MHD device. It is clear that this rules out equilibrium ionization for all practical purposes (the equilibrium temperature would have to be unrealistically high, of order of many thousand K), and that extraction can work efficiently after a certain amount of dynamic compression, but not inside the combustion chamber, where the pressure is of the order of 1 atm for a supersonic through-flow combustor and between 10 and 20 atm for the subsonic through-flow combustor. This condition favors hypersonic cruise vehicles, as their typical dynamic pressure (hence internal pressures) are at least 1/3 that of an accelerating launcher.

4.23.1.2 MHD Interaction Parameter (S)

The interaction parameter, S, defines the strength of the interaction, or coupling, between the magnetohydrodynamic energy and the airflow. S appears naturally by writing the fluid-dynamic Navier–Stokes equations and adding the electromagnetic Lorentz force to the momentum balance, therefore much simplifying the actual physics. The MHD interaction parameter is defined as

$$S = \frac{\sigma \cdot B^2 \cdot L}{\rho \cdot u} \tag{4.33}$$

with σ = fluid electrical conductivity (Ω m), ρ = gas density (kg/m^3), u = gas velocity along MHD device (m/s), and $\rho \cdot u$ = mass flow per unit area (kg/m^2/s). S is proportional to σ, so the plasma ion density must be sufficiently high for the field $\vec{B}$ to modify the airflow; a rule of thumb is at least 10^{14}–10^{16} charged particles/cm^3, but this depends also on $\vec{B}$ intensity.

The mass flow per unit area along a vehicle increases by 25 or more from the nose to the engine area as the flow is compressed. This means that the Russian installation of a nose MHD device and plasma generator, to drive the hydrocarbon fuel arc reforming process and alter the surrounding flow field to reduce drag, is using basic physics to advantage. Again, the nose mass flow per unit area is about an order of magnitude less for a hypersonic cruise vehicle compared to an accelerating space launcher, favoring the application of MHD to cruise vehicles. For the cruise vehicle, the pressure is less and the ionization potential to create a plasma much greater than for an accelerator, see Fig. 4.9. Note that the magnetic field strength, B, is squared, so a doubling of the $\vec{B}$ field increases the interaction by a factor of 4. The mass flow per unit area inside the combustor is too large to have a significant interaction at moderate magnetic field strengths. That is why the MHD generator and accelerator are placed where the local Mach number is higher and the mass flow per unit area and pressure are less. The $\vec{B}$ field for the MHD generator and accelerator is usually greater than that required for the nose device, because of the larger mass flow per unit area.

Work on application of $\vec{B}$ fields to propulsion, heat transfer, flow control, and drag reduction continues, although implementation in practical devices is not yet known. A recent survey of the status of the art in this field is in Poggie et al. (2016).

4.23.1.3 Radiative Losses

The plasma transport equations include energy transport. In terms of temperature, T, the radiative energy transport (loss) is the left side of Eq. (4.34):

$$\frac{\partial k \cdot T}{\partial t} + \frac{2}{3} \cdot k \cdot T \cdot \vec{V} \cdot v_i = \left(\frac{D_{recom}}{\sqrt{T}} + D_{Brems}\sqrt{T}\right) \cdot \alpha \cdot N_i \tag{4.34}$$

where the two terms on the right-hand side are the radiation heat transfer due to recombination of electrons and ions, D_{recom}, and the Bremsstrahlung radiation contribution, D_{Brems}. The number of ions per unit volume, N_i, and the degree of ionization, α, multiply the radiation heat transfer terms. Again, α needs to be a compromise, since it raises S but drives also radiation losses, and a similar compromise exists for the temperature T. Note that Eq. (4.34) is an approximation of the physical photonic distribution: depending on T, and for sufficiently large α, the photon mean free path may become so short that radiation can be confined inside the plasma and emerge as loss only at its boundary.

4.23.1.4 MHD Summary

The four MHD parameters briefly discussed: the (1) cyclotron frequency, (2) collision frequency, the (3) MHD interaction parameter, and the (4) gas radiation losses. Those four parameters do provide the minimum criteria for a MHD system to operate successfully. It is critical that any system seeking to operate as an MHD system must meet the criteria for the Lorentz force to exist in the first place. Although

appearing to be applicable to space launchers, the MHD energy bypass system is thus limited by the internal pressure in the propulsion system. The result is that an MHD system that has significant potential for a global range cruise aircraft actually will have only minimal potential for a space launcher (Bottini et al. 2003). In contrast to the propulsion case, the MHD interaction with the external flow, for reducing drag and permit electromagnetic deflection of the airflow (instead of a physical ramp system), is instead applicable to both, cruise aircraft and space launcher, because the external flow pressure is low in both cases.

4.23.2 Electromagnetic Radiation Propulsion

One of the limitations of the space launcher is the quantity of propellant that must be carried to achieve orbital speed. Even the most optimistic airbreathing system has a mass ratio of 4, the propellant is three times the operational weight empty. During the 1987 International Astronautical Congress held at Brighton, England, Viktor Pavlovitch Legostaev, General Designer of RSC Energia, approached the author to discuss space developments in the Soviet Union (Legostaev 1984). Part of the material presented was an experiment where a vertical launch rocket used water as a propellant and the energy to vaporize the water and produce thrust was provided by a focused microwave generator. An altitude of about a kilometer was achieved. Material was also presented from the Nikola Tesla museum in Belgrade, Serbia (Tasić 2006). In the translated Tesla manuscripts (Tesla 2007), there was a discussion of projected electromagnetic energy with minimum transmission losses. Tesla's claim was that a base on the Moon or Mars could be powered by a suitably located generator on Earth. Legostaev presented some data to the effect that experiments projecting energy from Siberia to an orbiting satellite and retransmitting the energy to Moscow achieved the transmission efficiencies Tesla had predicted. The picture of the power generating tube Legostaev showed was identical to the tube the author (P.A. Czysz) saw at the small museum at Tesla's birthplace in Smiljan, Croatia. In both cases, the evidence presented supported that a remote-powered vehicle was possible.

Note that direct propulsion by "pushing" a spacecraft to space by photon momenta had been proposed by Sänger (1956), and A. Kantrowitz extended the concept to laser-driven ablation propulsion (Kantrowitz 1978).

Professor Leik Myrabo, of Rensselaer Polytechnic Institute, Troy, New York, was developing a spacecraft based on focused electromagnetic energy (laser or microwave) for at least 20 years (Myrabo 1982, 1983, 2001; Myrabo et al. 1988, 1998). In this case, the vehicles are toroidal, the toroid forming a mirror to focus the received electromagnetic energy to vaporize and ionize water and air. Thus, the propulsion system becomes an MHD-driven space launcher. Myrabo demonstrated with USAF support a scale model propelled by a laser at Lawrence Livermore Laboratory (Myrabo and Lewis 2009). The importance of the Myrabo concept is that it is truly a combined-cycle concept. Through a series of propulsion configuration variants, the single spacecraft becomes four different MHD propulsion systems that can, in principle, reach low Earth orbital (LEO) speed and altitude, all powered by projected power, see Fig. 4.47. The power emitting system can be on Earth or in orbit. If there is an orbital power generator, spacecraft can be powered to the Moon (see Chap. 6), or a satellite can be powered to geosynchronous orbit with a minimum of Earthbound resources. If the power generator is placed on the Moon, then the system can provide propulsion to the nearby planets and moon systems. This concept is very interesting because it has the least onboard propellants of any system and hence provides the smallest weight.

The *Lightcraft* vehicle is an axisymmetric vehicle that begins its liftoff under beamed power, in this case from an orbiting laser, as shown in Fig. 4.48. Selective illumination of the laser windows provides lateral thrust, so sideways translation movement is possible in addition to vertical movement. In the liftoff phase, the propulsion system is configured for vertical takeoff or landing. Although forward acceleration to high subsonic speed is possible, the propulsion system soon transitions to the airbreathing rotary pulsejet mode. In this case, the rotating outer ring provides linear acceleration by ejecting an air plasma from an MHD engine segment. As speed increases, the entire vehicle acts as an MHD airbreathing fanjet to cover the supersonic and hypersonic speed regimes. In its final configuration, the pulsejet configuration now operates as a rocket, for instance with water as a working fluid (see Myrabo references for details and Chap. 5).

Since its inception, this concept has evolved, but the basic axisymmetric shape with toroidal mirrors to focus the

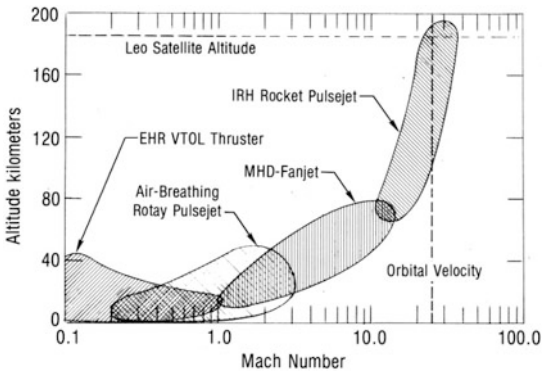

Fig. 4.47 Laser/microwave heated MHD spacecraft operating envelope enabled by a series of propulsion configuration adaptations

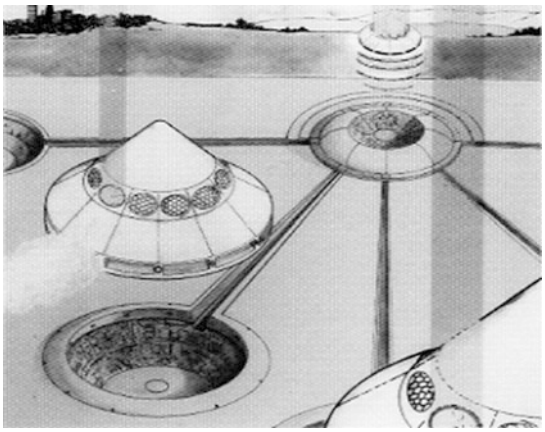

Fig. 4.48 Laser/microwave heated MHD spacecraft by Leik Myrabo of Rensselaer Polytechnic Institute, Troy, New York

radiated energy for producing a plasma remains. After Myrabo's death, R&D in this area was continued in Germany and the USA, where high power lasers are also investigated as weapons (a laser "gun" is currently being tested by the US Navy). Experimental data and the status of this technology can be found in Schall et al. (2007), Eckel and Schall (2008) and scaling laws in Yabe and Uchida (2007). For the theoretical foundations of the key interaction between laser and matter for propulsion applications, see (Phipps and Luke 2007).

4.23.3 Variable Cycle Turboramjet

Repeating part of the conclusion from Builder's 1964 report, there is an observation about a (then) hypothetical engine, the air turboramjet. To quote,

> … In a sense, a fan-ramjet might be a suitable name for such a cycle; the duct-burning turbofan and the air-turborocket could be considered close cousins to this hypothetical engine. At the higher speed end, around Mach 10, we can postulate a very efficient engine called the transonic combustion ramjet. There is still another important class of possibilities offered just outside the confines of the Brayton Cycle family: engines with non-adiabatic compression and expansion processes as a result of heat exchanges between the air and fuel. We might find a complete new spectrum of such engines awaiting our discovery. … (Builder 1964)

Such engines have been discovered, but have unfortunately never been pursued. In Fig. 4.49, there is a thumbnail insert of an original sketch of a variable cycle turboramjet based on the Rocketdyne SSME, sketched sometime in the early 1980s. Unfortunately, the identity of the sketch's source has long been lost. But it shows the ingenuity that was routinely discarded in favor of the rocket status quo. Although the details of the engine's operation are also lost, the originality in adapting an existing fixed cycle rocket engine with a fixed specific impulse to a variable cycle, airbreathing turboramjet/rocket is evident. As shown in the enlarged drawing based on the sketch, a rotating gas generator provides the power for the low-pressure ratio compressor. The engine operated as rocket-based turboramjet at lower Mach numbers and then transitions to the conventional rocket for the higher Mach numbers. With the flow-through LOX injector, if the airbreather thrust cannot provide sufficient low-speed acceleration, then the rocket could be ignited to provide an additional boost.

Who knows what the launchers of today would be like if innovations like this, based on current operational hardware, had been allowed to proceed. Dr. Nikolai Tolyarenko, formerly at TsIAM and more recently at the International Space University (Strasbourg), showed in 2010 to one author (C.

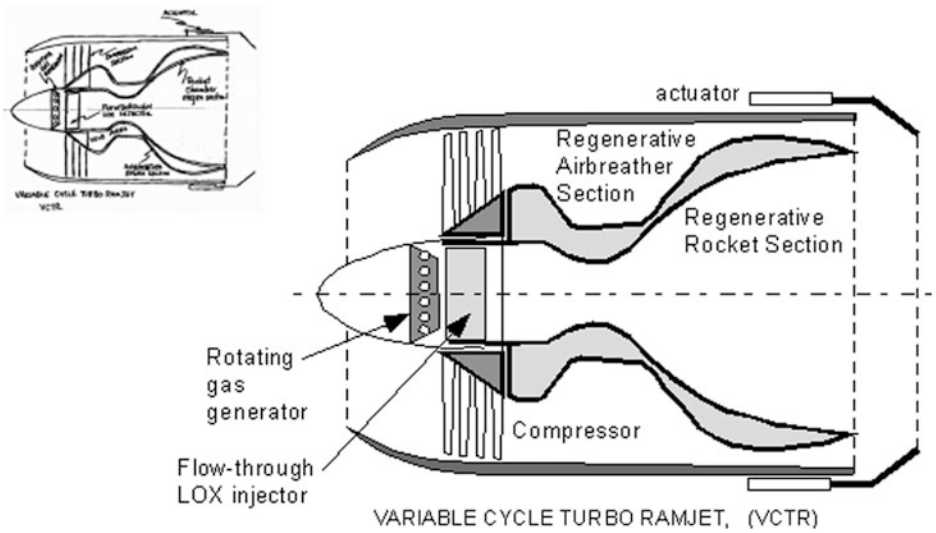

Fig. 4.49 Sketch of variable cycle ramjet based on Rocketdyne SSME, circa 1983

Bruno) a 1960s movie of the launch of the ramjet-powered *Buran* RSS-40 cruise missile he helped design, and said "... *were we let free to develop it, we would be on Mars now* ...."

It is not a lack of ideas or hardware concepts, or the lack of technology that confines us to low-performing rockets today, but a lack of imaginative designs based on correct decision-making, thus leadership to implement those ideas.

4.23.4 Aero-Spike Nozzle

The performance of the propulsion systems in this section is based on the conventional convergent-divergent nozzle, see Fig. 4.50 (Sutton and Biblarz 2010). At low altitudes, external atmospheric pressure causes the nozzle flow to separate from the nozzle wall (overexpanded in Fig. 4.50).

Because the nozzle exit area is now larger than the overexpanded flow, the transonic base drag can be very large. The 2-D and 3-D aero-spike nozzle, on the other hand, can accommodate higher external pressure while reducing base drag. The difference is that the convergent–divergent nozzle has one combustion chamber and throat, whereas the aero-spike nozzle has a number of smaller rocket chambers around the 2-D or 3-D periphery of the central 2-D or 3-D spike. To the author's knowledge, one of the first tests of an aero-spike nozzle was in the Cornell Aero Labs transonic wind tunnel in the late 1950s and early 1960s.

The Saint Louis Science Center sponsored the Russian Space Exhibition in 1992, when one of the authors (P.A. Czysz) was able to participate in some technical sessions with the Russian engineers. One engineer the author met was Konstantin Petrovich Feoktistov, who was the designer of Voskhod, Soyuz, Salyut, and Mir, and formerly a member of the Sergei Pavlovich Korolev team. Even though it is now over 50 years since the Russian Moon landing program (Johnson et al. 2014), the action of Glushko's OKB to block hardware from being delivered to Korolev is still resented. During the technical meetings, there would be angry exchanges in Russian between Valentin Glushko's OKB members and Feoktistov. When the author was able to visit Moscow and Saint Petersburg on an educational exchange in 1993, he was able to visit Feoktistov at his apartment. Feoktistov had a bookcase on one wall that was filled with his design studies. One was for a multi-launch space launcher designed around an aero-spike nozzle that he had tested full-scale.

The Lockheed Martin X-33 subscale VTHL SSTO employed the 2-D or linear aerospike engine (Stine 1996; Butrica 2003; Miller 2001). Among the numerous suggested applications of the 3-D aerospike engine is the TSTO *Orion-III* aerospaceplane in the epic science-fiction film *2001: A Space Odyssey* that employed a combined-cycle propulsion system with two aft fuselage-embedded 3-D aerospike nozzles (Bizony 2014; Frayling 2015), see Fig. 4.51.

4.23.5 ORBITEC Vortex Rocket Engine

In a conventional rocket engine, there is an ejector plate at the base of the combustion chamber that injects fuel and oxidizer into the combustion chamber at a specified fuel-to-oxidizer ratio. The key challenge is to control the combustion process such that heat transfer to the walls is minimized. The group that best controlled wall heating was probably the former Soviet Union rocket engine designers, see (Kalmykov et al. 2008), and in the 1990s one of the authors (C. Bruno) was offered information on a vortex combustion-powered rocket engine developed in the Soviet Union (Golovitchev 1990).

Eric Rice, President of ORBITEC until 30 September 2008, had a different approach with his founding team some years ago. This approach involved controlling combustion

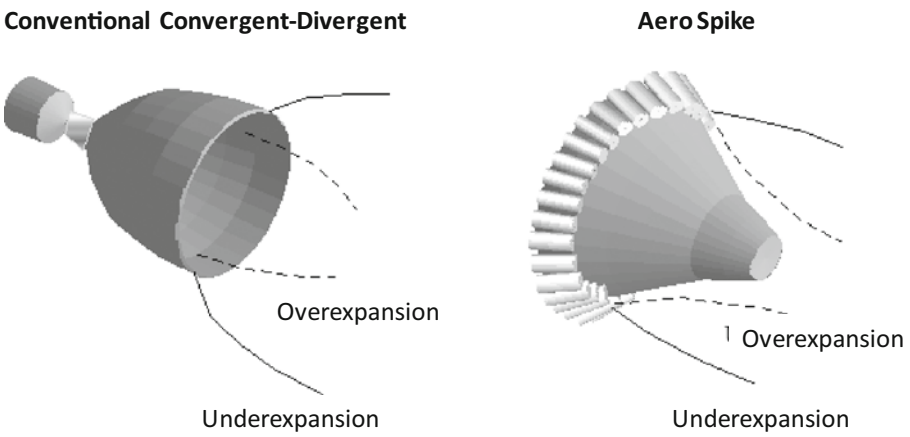

Fig. 4.50 Two 3-D expansion-nozzle configurations alternatives

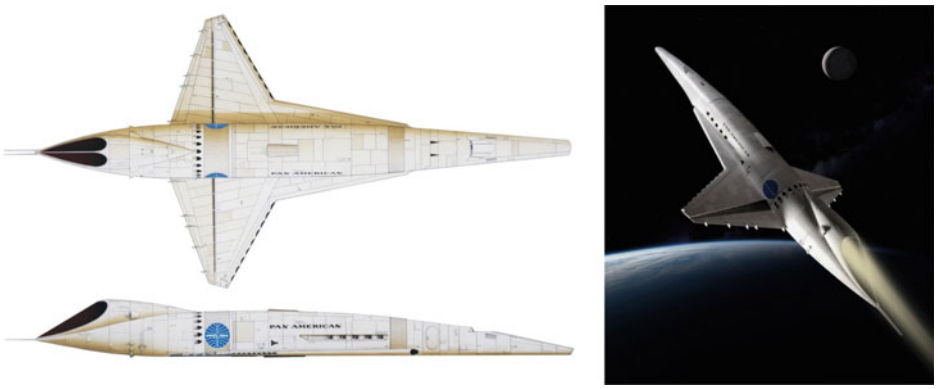

Fig. 4.51 Orion III 2-view artwork by Simon Atkinson (www.satkinsoncreativearts.com) and large display model by B. P. Taylor

and wall heating using the intense mixing and combustion driven by interaction between vortical flows.

ORBITEC's patented Vortex Combustion Cold-Wall (VCCW) thrust chamber employs a unique propellant swirl injection method that generates a pair of coaxial, co-swirling counter-flowing vortices in the combustion chamber. Combustion of the propellants is confined to the inner vortex. The outer vortex cools and protects the chamber wall from excessive heat loads that ordinarily result from the hot combustion products. Successful testing has demonstrated operation flexibility, burning various propellant combinations including gaseous oxygen/gaseous methane, gaseous oxygen/RP-1, liquid oxygen/RP-1, gaseous oxygen/gaseous hydrogen, liquid oxygen/gaseous hydrogen, gaseous oxygen/gaseous carbon monoxide, and liquid oxygen/liquid propane. "*... ORBITEC is also applying the coaxial vortex flow field to hybrid rocket engine systems that produce fuel regression rates significantly higher than conventional hybrid configurations. This increase in fuel regression rate enables the use of a simple circular grain port and leads to significant gains in performance, reliability, and durability of hybrid systems ...*" [ORBITEC].

A vortex cylindrical combustion chamber burning gaseous oxygen and gaseous hydrogen at a mixture ratio of 6 was equipped with an acrylic chamber (measured wall temperature ~60 °C) for optical visualization of the combustion zone (~3000 °C). The acrylic chamber clearly showed the central core combustion vortex away from the acrylic wall. Specific impulse efficiencies of about 98% have been obtained in non-optimized lab-scale chambers.

Current efforts apply VCCW thrust chamber assemblies at chamber pressures of 1000 psi and thrust levels of 7500–30,000 lbf (this thrust was reached in 2015) using liquid oxygen/gaseous propane, liquid oxygen/gaseous methane, liquid oxygen/liquid methane, and liquid oxygen/RP-1. RP-1 is a kerosene blend specially formulated for application as rocket propellant. These efforts were initially supported by lab-scale, large prototype and flight-weight engine testing, computational fluid dynamic simulations, and numerical analysis of the vortex flow field. Orbitec is now a subsidiary of Sierra Nevada Corporation (SNC), the commercial space company approved in 2016 for NASA funding of its proprietary *Dream Chaser* hypersonic glider competing with SpaceX and Orbital ATK for lifting cargo to the ISS. Although no decision has been made, the Orbitec engine may eventually power the SNC *Dream Chaser* shuttle.

The advantage of vortex combustion is that it opens up the opportunity of considering different propellant approaches. One such approach consists of novel versions of the hybrid rocket engine.

4.23.5.1 Vortex Hybrid Rocket Engine (VHRE)

With the goal of achieving practical and functional hybrid rocket propulsion systems, ORBITEC has patented a unique hybrid propulsion technology called the vortex hybrid rocket engine. Rather than injecting oxidizer parallel to the fuel port at the head-end, as in a classic hybrid, oxidizer is injected tangentially through a swirl ring at the aft-end of the fuel grain. This injection method generates a bidirectional, co-axial vortex flow field in the combustor. The swirling, high-velocity gas enhances heat transfer to the fuel surface which, in turn, drives high solid-fuel regression rates. Testing has already demonstrated regression rates up to 650% faster than a classical hybrid for a given mass flux. The rapid regression rate allows the use of a single cylindrical grain port which offers significant benefits including (1) increased volumetric grain loading, (2) simplified grain manufacture and grain mechanical strength, and (3) reduced grain sliver at engine burnout. Additionally, the unique flow field enhances mixing and increases combustion efficiency.

ORBITEC has applied vortex hybrid technology to paraffin and other fuel blends. With paraffin, extremely high regression rates, compared with classic hybrids with rubber-based fuels, have been obtained. Blending paraffin

and other fuels adds another degree of freedom for tailoring the regression rate to precise specifications and may provide fuel strength advantages over pure paraffin.

The vortex hybrid rocket engine features:

- Application flexibility,
- Very high regression rates,
- Simplified grain geometry,
- Reduced grain sliver at burnout,
- Increased volumetric fuel loading,
- Enhanced combustion performance,
- Excellent safety and low risk,
- Low cost and reusability,
- Significantly large design, experimental, and analytical database.

To appreciate these features, one must understand conventional hybrid engines. In the classical hybrid engine, the fuel and oxidizer are physically separate and stored in different phases. Classic hybrid rocket engines have several important operational and safety advantages over both liquid-propellant and solid-propellant rocket engines. Unlike solid-propellant grains, solid-fuel grains are inert, insensitive to cracks and imperfections, and safe to manufacture, transport, store, and handle. Like liquid-propellant engines, hybrid engines can be throttled, but require only half the feed system hardware. Due to their relatively simple design and inherent safety, classic hybrid engines should display lower manufacture and launch costs than current propulsion systems.

However, current classical hybrid engines suffer from low solid-fuel regression rates, low volumetric loading, and relatively low combustion efficiency. Common solid fuels, such as hydroxyl-terminated polybutadiene (HTPB), usually regress quite slowly compared with solid propellants. Complex cross-sectional geometries with large burning surface areas must be employed to obtain the necessary fuel flow rate consistent with the desired thrust level. Such grains require large cases and display poor volumetric loading and high manufacturing costs. The fuel may occupy as little as 50% of the total grain case volume. As the grain webs thin down near the end of burn, they are prone to release fuel chunks which results in sharp thrust pulses.

The combustion of fuel and oxidizer in a classic hybrid occurs in a boundary layer flame zone, distributed along the length of the combustion chamber above the fuel surface. Portions of the propellants may pass through the chamber without reacting. Secondary combustion chambers at the end of the fuel grain are often employed to complete propellant mixing and increase combustion efficiency. These chambers add length and mass to any conventional design and may serve as a potential source of combustion instability. These drawbacks are avoided in the vortex hybrid rocket engine (VHRE).

The vortex hybrid propulsion system has the potential to mature into a significant size range of propulsion systems. The systems would be suited for applications ranging from zero-stage strap-on boosters to pump-fed, large, reusable first-stage boosters and second-stage sustainer engines for highly reusable launch vehicles. The vortex hybrid is also efficient in smaller sizes and should find applications as propulsion for orbit transfer stages, orbital maneuvering systems for space vehicle propulsion, the *Orion* crew exploration vehicle escape capsule propulsion, and for orbit insertion kick stages. Additionally, the vortex hybrid has the potential to serve as an in-space refuel-able propulsion system. Such a system would be refueled in space by fuel grain cartridges and pre-packaged liquid-oxidizer tanks launched for the purpose and continue to serve for extended periods from a parking orbit in space. ORBITEC has been evaluating the use of vortex hybrid upper-stage propulsion for satellite and booster applications. Another family of applications concerns a vortex hybrid that would make use of in situ resources from a lunar or Martian base. In more advanced future systems, propellant supplies could be delivered from lunar resources at lower energy due to the weaker gravity well of the Moon. For example, it may be feasible to produce metallic fuel grains of aluminum to burn with oxygen extracted from oxides present in lunar regoliths.

4.23.5.2 Stoichiometric Combustion Rocket Engine (SCORE)

SCORE is a high-performing, low-thrust, gaseous hydrogen/oxygen rocket engine designed by ORBITEC to operate at a stoichiometric mixture ratio as part of the water rocket program being sponsored by DARPA for Earth orbit spacecraft.

SCORE is a small (20 lbf) on-orbit spacecraft rocket engine intended to serve as the primary thruster for the water rocket system. The water rocket calls for the use of liquid water as a propellant supply. The liquid water is electrolyzed on orbit into hydrogen and oxygen gas, which is then stored and used as needed for orbital maneuvers. Because the propellants are made from water, they are available in stoichiometric proportion, and the overall performance of the propulsion system is optimized by using all of the available propellant. This approach also eliminates complicated, heavy, and costly cryogenic storage systems while providing high performance.

Other applications include reboost/repositioning for orbiting facilities such as the ISS space platforms or spacecraft. The water rocket has several major advantages over conventional stored liquid propellants such as MMH/NTO.

It offers dramatically improved I_{sp}, it is environmentally friendly, and its lack of toxicity simplifies launch operations. In addition to these advantages related to the propulsion system, the water rocket also doubles as a battery; stored hydrogen and oxygen gas may be converted back to water to generate electricity in a fuel cell during periods of darkness.

The water rocket requires a long-life engine that can deliver high performance at relatively low thrust in the harsh conditions of high-temperature stoichiometric combustion. SCORE uses ORBITEC's patented cold-wall vortex flow field to accomplish just that. The vortex protects most of the chamber wall from combusting propellants whilst minimizing the heat load. Development work has progressed toward a flight-type engine which is regeneratively cooled and will exhaust to simulated altitude conditions.

4.23.5.3 Cryogenic Hybrid Rocket Engine Technology

This technology originated in both Europe, at the Aerospace Institute in Berlin, see (Lo et al. 2005), and in the USA, where ORBITEC has developed technology in cryogenic hybrid rocket engines. This patented family of engines uses a cryogenic solid as the fuel (or oxidizer) grain. The cryogenic hybrid offers the safety and relative simplicity of hybrid engines coupled with the performance of cryogenic bipropellant engines. The latest addition to this family, the ACHRE-I, uses a solid-oxygen (SOX) grain with liquid-hydrogen fuel. Fully loaded, the ACHRE holds a 5 kg SOX grain and produces 120 lbf thrust. Liquid hydrogen is used both as the fuel for firing and the coolant for the SOX grain formation process. The ACHRE is intended for use as a high-performance launch vehicle kick stage or orbital transfer vehicle. Future work with the ACHRE will explore the use of solid-ozone (SOZ) mixed in with the SOX grain. Addition of 50% SOZ will result in a significant performance gain: the specific impulse is increased by nearly 20 s.

Numerous successful hot-firing tests have been performed with various propellant combinations with ORBITEC's "workhorse" Mark II cryogenic hybrid rocket engine, exploring solid oxygen/gaseous hydrogen, solid hydrogen/gaseous oxygen, solid carbon monoxide/gaseous oxygen, solid methane/gaseous oxygen, and other solid hydrocarbon fuels.

Bibliography

Ahern, J.E. (1983) Briefing for Robert Williams on Second Law Thermodynamics, DARPA Copper Canyon manager, Washington, DC, 1983.

Ahern, J.E. (1992) "Thermal Management of Air-Breathing Propulsion Systems", AIAA Paper 92-0514, *30th Aerospace Sciences Meeting*, Reno, Nevada, January 1992.

Anfimov, N.A. (1997) "In Searching for an Optimal Concept of Future Russian Reusable Space Transportation System", in: Proceedings of the *International Workshop on Spaceplane/RLV Technology Demonstrators,* Tokyo, Japan, 10–12 March 1997, pp. 67–96.

Anon. (1963) "Marquardt Needs Advanced Propulsion Engineers", Full-Page Advertisement, Aviation Week & Space Technology, 20 May 1963.

Anon. (1967) "A Study of Advanced Airbreathing Launch Vehicles with Cruise Capability", Lockheed Report IR 21042, The Lockheed Aircraft Corporation, 1967.

Anon. (1985) "Single-Stage-to-Orbit Concept Comparison', Aerospace Corporation, 86-2602-301-ADA, October 1985.

Anon. (2014) "Stratolaunch Eagles', Stratolaunch Systems, Orbital ATK, 2014.

Anon. (2015a) "Space Launch System at a Glance", NP-2015-09-83-MSFC, Marshall Space Flight Center, NASA, September 2015.

Anon. (2015b) "Declassified Manned Orbiting Laboratory (MOL) Records", National Reconnaissance Office, October 2015.

Anon. (2016) Virgin Galactic – Human Spaceflight Vehicles Fact Sheet", Virgin Galactic, February 2016.

Aoki, T. and Ogawara, A. (1988) "Study of LACE Cycle for SSTO Space Plane", Paper IAF-88-252, presented at the *39th International Astronautical Federation Congress*, Bangalore, India, 08–15 October 1988.

Balepin, V.V. (1996) "Air Collection Systems", *Developments in High-Speed-Vehicle Propulsion Systems*, edited by S.N.B. Murthy and E.T. Curran, Progress in Astronautics and Aeronautics Series, Vol. 165, AIAA, Reston VA, 1996, pp. 385–419.

Balepin, V.V. and Tjurikov E.V. (1992) "Integrated Air Separation and Propulsion System for Aerospace Plane with Atmospheric Oxygen Collection", SAE Technical Paper SAE-92-0974, *Society of Automotive Engineers, Aerospace Atlantic Conference*, Dayton, OH, 07–10 April 1992.

Balepin, V.V. and Hendrick, P. (1998) "Application of the KLIN Cycle to Vertical Take-Off Lifting Body Launcher", AIAA Paper 98-1503, *8th AIAA International Space Planes and Hypersonic Systems and Technologies Conference,* Norfolk, VA, 27–30 April 1998.

Balepin, V.V., Dulepov, N., Folomeev, E., Harchevnikova, G., *et al.* (1993) "Flight Liquid Oxygen Plants for Aerospace Plane: Thermodynamic and Integration Aspects", SAE Technical Paper 931452, Society of Automotive Engineers, April 1993.

Balepin, V.V., Czysz, P.A., Maita, M. and Vandenkerckhove, J. (1995) "Assessment of SSTO Performance with In-Flight LOX Collection", AIAA Paper AIAA-95-6047, presented at the *AIAA 6th International Aerospace Planes Conference*, Chattanooga, TN, 1995.

Balepin, V.V., Maita, M., Tanatsugu, N., and Murthy, S.N.B. (1996) "Deep-Cooled Turbojet Augmentation with Oxygen (Cryojet) for a SSTO Launch Vehicle", AIAA Paper 96-3036, presented at the *32nd Joint AIAA, ASME, SAE and ASEE Propulsion Conference and Exhibit*, Lake Buena Vista, FL, 1–3 July 1996.

Baranovsky, S.I., Davidenko, D.M. and Levin, V.M. (1992a) "Combustion Chamber of Ramjet for Aerospace Plane", Vol. 3, presented at the *9th World Hydrogen Conference*, Paris, June 1992, pp. 1583–1591.

Baranovsky, S.I., Davidenko, D.M. and Konovalov, I.V. and Levin, V. M. (1992b) "Experimental Study of the Hydrogen Supersonic Combustor", Vol. 3, presented at the *9th World Hydrogen Conference,* Paris, June 1992, pp. 699–1708.

Barrère, M. and Vandenkerckhove, J. (1993) ''Energy Management'', Paper ISABE 93-7016, presented at the XI International Symposium on Air Breathing Engines, Tokyo, Japan, September 1993.

Bartolotta, P.A., Buchen, E., Engelund, W.C., Huebner, L.D., Moses, P.L., Schaffer, M., Voland, R.T., Voracek, D.F. and Wilhite, A.W.

(2011) "Horizontal Launch: A Versatile Concept for Assured Space Access," NASA SP 2011-215994, Report of the NASA-DARPA Horizontal Launch Study, December 2011.

Batenin, V.M., Bityurin, V.A., Ivanov, G.S., Inozemzev, N.N. and Gorozhankin, P.A. (1997) "Electromagnetic Complex Concept for the Horizontal Start and Landing of a Reusable Air-Space Aircraft", paper presented at the *48th International Astronautical Congress*, Turin, Italy, 06–10 October 1997.

Billig, F.S. (1989) "Hypersonic Vehicles II", *Proceedings of the Short Course of Engine Airframe Integration,* School of Mechanical Engineering, Purdue University, July 1989.

Billig, F. S. (1993) "The Integration of the Rocket with a Ram-Scramjet as a Viable Transatmospheric Accelerator", AIAA Paper 93-7017, Vol. 1, Proceedings of the 11th ISABE, International Symposium on Air Breathing Engines, Tokyo, Japan, 20–24 September 1993, pp. 173–187.

Bizony, P. (2014) "The Making of Stanley Kubrick's 2001: A Space Odyssey", 1st Edition, Taschen, August 2014.

Bond, W.H. and Y, A.C. (1993) "Prospects for Utilization of Air Liquefaction and Enrichment System (ALES) Propulsion in Fully Reusable Launch Vehicles", AIAA Paper AIAA-93-2025, presented at the *29th AIAA/SAE/ASME/ASEE Joint Propulsion Conference,* Monterey, 28–30 June 1993.

Bottini, H., Bruno, C. and Czysz, P.A. (2003) "Is The MHD Scramjet Really An Advantage?" AIAA 2003-5046, presented at the *39th AIAA/ASME/SAE/ASEE Joint Propulsion Conference and Exhibit*, Huntsville, Alabama, 20–23 July 2003.

Bottini, H., Bruno, C. and Czysz, P.A. (2004) "Analysis of Kerosene-Fueled MHD SCRJ Cruiser Performance", paper AIAA 2004-4127, presented at the *40th AIAA/ASME/SAE/ASEE Joint Propulsion Conference,* Fort Lauderdale FL, 12–14 July 2004.

Bruno,C. Czysz, P.A. and Murthy, S.N.B. (1997) "Electro-Magnetic Interactions in Hypersonic Propulsion Systems", paper AIAA 97-3389, presented at the *33rd AIAA/ASME/SAE/ASEE Joint Propulsion Conference*, Seattle WA, 6–9 July 1997.

Bruno, C. and Czysz, P.A. (1998) "*An Electro-Magnetic-Chemical Hypersonic Propulsion System*," AIAA Paper 98-1582, presented at the AIAA 8th International Spaceplanes and Hypersonic Systems and Technologies Conference, Norfolk, Virginia, 27–30 April 1998.

Bruno, C., Golovitchev, V.I. and Tretyakov, P.K. (1998) "New Trends in Improving Hypersonic Vehicles Aerodynamics and Propulsion Flow Control by External Energy Supply", Paper 98-0-1-08V, *21st International Symposium on Space and Technology (ISTS)*, Omiya, Japan, May 1998.

Buhlman, M. and Siebenhaar, A. (1995a) "The Strutjet: The Overlooked Option for Space Launch", Paper AIAA-95-3124, presented at the *31st AIAA/ASME/SAE/ASEE Joint Propulsion Conference,* San Diego, CA, 10–12 July 1995.

Buhlman, M. and Siebenhaar, A. (1995b) "The Strutjet Engine: Exploding the Myths Surrounding High Speed Airbreathing Propulsion", Paper AIAA-95-2475, presented at the 31st AIAA/ASME/SAE/ASEE Joint Propulsion Conference, San Diego, CA, 10–12 July 1995.

Builder, C.H. (1964) "On the Thermodynamic Spectrum of Airbreathing Propulsion", AIAA-64-243, *1st AIAA Annual Meeting*, Washington, DC, June–July 1964.

Bunin, B.L. (1991) "Update on Douglas' High-Speed Civil Transport Studies", N94-33450, NASA-CP-10087, 1st High-Speed Research Workshop, Williamsburg, Virginia, 14–16 May 1991.

Burnett, D.R. and Czysz, P.A. (1963) "Supersonic Hydrogen Combustion Studies", AEDC ASD-TDR-63-196, Project Nr. 3012, Task Nr. 301201, Aerodynamic Division, Directorate of Engineering Test, Air Force Systems Command, Wright-Patterson AFB, Ohio, April 1963.

Butrica, A.J. (2003) *Single Stage to Orbit – Politics, Space Technology, and the Quest for Reusable Rocketry*, The John Hopkins University Press, October 2003.

Campbell, J.W. and Taylor, C.R. (1998) "Ground-Based Laser Propulsion for Orbital Debris Removal", in: *Space Technology and Applications International Forum (STAIF)-1998*, ed. by M.S. El-Genk, American Institute of Physics CP420.

Carlson, C.P.P., Kessler, R. and Schmitt, E.W. (1996) "Magnetohydrodynamic Generator Design for a Combined-Cycle Demonstration Powerplant", *Journal of Propulsion and Power*, Vol.12. No. 2, March–April 1996.

Chertok, B. (2011) "Rockets and People: The Moon Race (Volume IV)", 1st Edition, NASA SP-2011-4110, NASA History Series, NASA History Program Office, 2011.

Cocks, P.A.T., Holley, A.T., Greene, C.B. and Haas, M. (2015) "Development of a High Fidelity Simulation Capability", AIAA paper 2015-1823, presented at the *53rd AIAA Aerospace Sciences Meeting,* Kissimmee, FL, Jan. 5–9, 2015.

Cocks, P.A.T., Holley, A.T. and Rankin, B. (2016) "High Fidelity Simulations of a Non-Premixed Rotating Detonation Engine", AIAA paper 2016-0125, presented at the *54th AIAA Aerospace Sciences Meeting*, San Diego CA, Jan. 4–8, 2016.

Conway, E.M. (2008) "High-Speed Dreams: NASA and the Technopolitics of Supersonic Transportation, 1945–1999", 1st Edition, New Series in NASA History, John Hopkins University Press, October 2008.

Curran, E.T. (1993) "The Potential and Practicality of High Speed Combined Cycle Engines", in: *Hypersonic Combined Cycle Propulsion,* AGARD Conference Proceeding No. 479, AGARD, Neuilly-Sur-Seine, France, 1993, pp. Kl-9.

Czysz, P.A. (1987) "*Hypersonic Convergence – Technology Interdependance Inhibits Technology Independence*," © McDonnell Douglas, April 1987, Purdue University Engine-Airframe Integration Short Course, July 1987.

Czysz, P.A. (1988) "Air Breather vs. Rocket: Is the Rocket the Only Reliable, Demonstrable Space Propulsion System?", presented at the *SAE Aerospace Atlantic Conference & Exposition*, Dayton, OH, April 1993.

Czysz, P.A. (1988a) "Thermodynamic Spectrum of Airbreathing Propulsion", SAE Technical Paper 881203, presented at the *Future Transportation Technology Conference and Exposition*, San Francisco, CA, 08–11 August 1988.

Czysz, P.A. (1992) "Space Transportation Systems Requirements Derived from the Propulsion Performance", Paper IAF-92-0858, presented at the 43rd IAF (International Astronautical Federation) Congress, Washington, DC, September 1992.

Czysz, P.A. (1993a) "Rocket Based Combined Cycle (RBCC) Propulsion Systems Offer Additional Options", in: *11th ISABE Proceedings*, Vol 1, Tokyo, Japan, 20–24 September 1993, pp. 119–137.

Czysz, P.A. (1993b) "Hydrogen Combustion Studies – Revisited", presented at the *1993 JANNAF Propulsion Meeting Conference,* Monterey, CA, 15–19 November 1993.

Czysz, P.A. (1995) "Interaction of Propulsion Performance with the Available Design Space", in: *Proceedings of the XII International Symposium on Airbreathing Engines* (ISABE), Melbourne, Australia, September 1995.

Czysz, P.A. (1999) "Combined-cycle Propulsion - is it the Key to Achieving Low Payload to Orbit Costs?", ISABE Paper 99-7183, presented at the XIV International Symposium on Air Breathing Engines (ISABE), Florence, Italy, 11 September 1999.

Czysz, P.A., and Bruno, C. (2001) "MagnetoHydroDynamic Coupled Ramjet Propulsion System: A Perspective", Paper ISABE 2001-1230, presented at the *XV ISABE Symposium*, Bangalore, India, September 2–7, 2001.

Czysz, P.A. and Murthy, S.N.B. (1991) "Energy Analysis of High-Speed Flight Systems", in: *High-Speed Flight Propulsion Systems*, edited by S.N.B. Murthy and E.T. Curran, Progress in Astronautics and Aeronautics Series, Vol. 137, AIAA, Reston VA, pp. 183–186.

Czysz, P.A. and Richards, M.J. (1998) "Benefits from Incorporation of Combined Cycle Propulsion", AIAA Paper 98-S.5.10, presented at the *48th International Astronautical Congress*, Melbourne, Australia, October 1998.

Czysz, P.A. and Vandenkerckhove, J. (2000) "Transatmospheric Launcher Sizing" in Curran, E.T. and Murthy, S.N.B. *Scramjet Propulsion*, Progress in Astronautics and Aeronautics Series, Vol. 189, Reston VA., Chapter 16, 2000.

Daniau, E. (2002) "Pulse Detonation Engine: Concept, Performance and Applications", ISU/AAAF Short Course, Versailles, France, May 2002.

Davies, R.E.G. (1998) "Supersonic (Airliner) Non-Sense: A Case Study in Applied Market Research", Paladwr Press/Airlife Publishing Ltd, 1998.

Davies, P., Hempsell, M. and Varvill, R (2015) "Progress on Skylon and SABRE", Paper IAF-15-D2.1.8, presented at the *66th International Astronautical Federation (IAF) Congress*, Jerusalem, Israel, 12–16 October 2015.

Doublier, M., Pouliquen, M. and Scherrer, D. (1988) "Combined Engines for Advanced European Launchers", Paper IAF-88-251, presented at the *39th International Astronautical Federation (IAF) Congress*, Bangalore, India, 08–15 October 1988.

Draper, A.C. and Sieron, T.R. (1991) "Evolution and Development of Hypersonic Configurations 1958–1990", WL-TR-91-3067, Flight Dynamics Directorate, Wright-Patterson Air Force Base, Ohio, September 1991.

DuPont, A.A. (1999) "Further Studies of Optimized Inlets for Hypersonic Turbine Engines", ISABE 99-7039, *presented at the XIV International Symposium of Air Breathing Engines (ISABE),* Florence, Italy, September 1999.

Eckel, H.A. and Schall, W. (2008) "Laser Propulsion Systems", in *Advanced Propulsion Systems and Technologies: Today to 2000*, edited by C. Bruno and A.G. Accettura, AIAA Progress in Astronautics and Aeronautics Series, Vol. 223, AIAA, Reston, VA., Chapter 14, March 2008.

Escher, W.J.D. (1966) "A Study of Composite Propulsion Systems for Advanced Launch Vehicle Applications – Volume 1: Summary Report", Report 25,194, Ref.: 5402/855/5580, NASA Contract NAS7-377, Marquardt Corporation, Rockedyne Lockheed California Company, Van Nuys, CA, September 1966.

Escher, W.J.D., Flornes, B.J. et al., (1967) "A Study of Composite Propulsion Systems for Advanced Launch Vehicle Applications", Marquardt Corporation Final Report, NASA Contract NAS7-377, Van Nuys CA, April 1967.

Escher, W.J.D. (1994) "Motive Power for Next Generation Space Transports: Combined Airbreathing + Rocket Propulsion", private communication with P.A. Czysz, 1994.

Escher, W.J.D. (1995) "Rocket-Based Combined Cycle (RBCC) Powered Spaceliner Class Vehicles Can Advantageously Employ Vertical Takeoff and Landing (VTOL)", AIAA Paper 95-6145, presented at the 1995 AIAA Aerospace Sciences Meeting, January 1995.

Escher, W.J.D. (1996) "A Winning Combination for Tomorrow's Spaceliners", *Aerospace America,* Vol. 34, No. 2, February 1996, pp. 38–43.

Escher, W.J.D. (1998) "A History of RBCC Propulsion in the U.S. - A Personal Recounting", White Paper, Kaiser Marquardt, Van Nuys, CA, 1998.

Escher, W.J.D. (2001) "The Seven Operating Modes of the Supercharged Ejector Scramjet (SESJ) Combined-Cycle Engine", Paper AIAA-2001-34041, presented at the *37th AIAA/ASME/SAE/ASEE Joint Propulsion Conference,* Salt Lake City, Utah, 08–11 July 2001.

Escher, W.J.D. and Czysz, P.A. (1993) "Rocket-Based Combined-Cycle Powered Spaceliner Concept", Paper IAF-93-S.4.478, presented at the *45th International Astronautical Federation Congress,* October 1993.

Escher, W.J.D., Roddy, J.E. and Hyde, E.H. (2000) "Marquardt's Mach 4.5 Supercharged Ejector Ramjet (SERJ) high-Performance Aircraft Engine Project: Unfulfilled Aspirations Ca. 1970", Paper AIAA-2000-3109, presented at the *36th AIAA/ASME/SAE/ASEE Joint Propulsion Conference and Exhibit, Huntsville*, Alabama, 16-19 July 2000.

Esteve, M.D. et al. (1977) "ODYSSEUS, Technology Integration for a Single Stage to Orbit Space Transport Using MHD Driven Propulsion", Senior Design Study, Parks College of Aerospace and Aviation, Saint Louis University, St. Louis, MO, 1977.

Fermi, E. (1956) *Thermodynamics,* 1st Edition, Chapter 5, Dover Publications, New York, June 1956.

Flack, R.D. (2005) *Fundamentals of Jet Propulsion with Applications*, 1st Edition, Cambridge University Press, January 2005.

Frayling, C. (2015) "The 2001 File: Harry Lange and the Design of the Landmark Science Fiction Film", 1st Edition, Reel Art Press, December 2015.

Gallagher, B. and Webster-Smith, R. (2015) "BAE Systems and Reaction Engines to Develop a Ground Breaking New Aerospace Engine", Press Release, Reaction Engines and BAE Systems, 02 November 2015.

Glassman, I. and Sawyer, R.F. (1970) The Performance of Chemical Propellants, NATO AGARDograph 129, Technivision Services, Slogh (UK). Chapter II.C, January 1970.

Golovitchev, V.I. (1990), personal communication.

Goodall, J. and Miller, J. (2003) *Lockheed's SR-71 'Blackbird' Family*, 1st Edition, AeroFax, Midland Publishing, March 2003.

Gopalaswami, R., Gollakota, S., Venugolapan, P., Nagarathinam, M. and Sivathanu, P.A. (1988) "Concept Definition and Design of a Single-Stage-To-Orbit Launch Vehicle HYPERPLANE", Paper IAF-88-194, presented at the *39th International Astronautical Federation (IAF) Congress,* Bangalore, India, 08–15 October 1988.

Gorelov, V.A., Gladyshev, M.K. et al. (1995) "Ionization Near Hypersonic Vehicles: The Experience of Numerical, Laboratory and Flight Investigations", paper AIAA 95-1940, presented at the *26th AIAA Plasmadynamics and Lasers Conference*, San Diego, CA, 19–22 June, 1995.

Gorelov, V.A., Gladyshev, M.K., Kireev, A.Y., Korolev, A.S., Yegorov, I.V. and Byzov, V.N. (1996) "Computational and Experimental Investigations of Ionization near Hypersonic Vehicles", *Journal of Spacecraft and Rockets*, Vol. 33, No. 6, November–December 1996.

Gounko, Y.P., Kharitonov, A.M., Latypov, A.F., Mazhul, I.I. and Yaroslavtsev, M.I. (2000) "Technique for Determination of Heat Fluxes and Force Characteristics of Ramjet/Scramjet Models in a Hot-Shot Wind-Tunnel", Institute for Theoretical and Applied Mechanics SB RAS, Novosibirsk, 2000.

Graf, D.A. and Welge, H.R. (1991) "1989 High-Speed Civil Transport Studies - Summary", NASA CR-187545, Contract NAS1-18378, HSCT Concept Development Group, Advanced Commercial Programs, McDonnell Douglas Corporation, September 1991.

Gurijanov, E.P. and Harsha, P.T. (1996) "AJAX - New Directions in Hypersonic Technology", AIAA Paper 96-4609, presented at the *7th Aerospace Planes and Hypersonic Technologies Conference,* Norfolk VA, April 1996.

Hannigan, R.J. (1994) *Spaceflight in the Era of Aero-Space Planes*, 1st Edition, Krieger Publishing Company, 1994.

Harford, J. (1997) *Korolev: How One Man Masterminded the Soviet Drive to Beat America to the Moon*, 1st Edition, John Wiley & Sons, April 1997.

Harney, D.J. (1967) "Similarity of Nonequilibrium Air Expansion in Hypersonic Nozzles", USAF FDL-TM-67-1 (AD664084), Air Force Flight Dynamics Laboratory, Wright-Patterson AFB, Ohio, May 1967.

Harper, R.E. and Zimmerman, J.H. (1942) "An Investigation of Rocket Engine Thrust Augmentation with a Nozzle-Ejector System", Arnold Engineering Development Center Report TRD-62-42, March 1942.

Heiser, W.H. and Pratt, D.T. (2002) "Thermodynamic Cycle Analysis of Pulse Detonation Engines", *AIAA Journal of Propulsion and Power*, Vol. 18, No. 1, pp. 68–76.

Hellmold, W. (1999) *Die V1 – Eine Dokumentation*, 1st Edition, Bechtermünz Verlag, 1999.

Hendrick, I.P. (1996) "SSTO and TSTO LOX Collection System Performances: Influence of LOX Plant Architecture", Paper ICAS-96-3.8.3, presented at the *1996 International Council of the Aeronautical Sciences,* Sorrento, Italy, 08–13 September 1996.

Holley, A.T., Wong, W.Y., Rowland, R.A., Meyers E.T., and Freese, R.A. (2012) "Combined Experimental and Modeling Pulsed Detonation Engine Combustor Performance Evaluation Technique", JANNAF paper presented at the CS/APS/EPSS/PSHS Joint Subcommittee Meeting, Monterey CA 3–7 December 2012.

Jacob, D., Sachs, G. and Wagner, S. (Editors) (2005) "Basic Research and Technologies for Two-Stage-to-Orbit Vehicles", Final Report of the Collaborative Research Centres 253, 255 and 259, Deutsche Forschungsgemeinschaft, Wiley-VCH Verlag, December 2005.

Jenkins, D.R. (2001) *Space Shuttle: The History of the National Space Transportation System, The First 100 Missions*, 3rd Edition, Midland Publishing, March 2001.

Jenkins, D.R. (2007) "X-15: Extending the Frontiers of Flight", NASA SP-2007-562, NASA, 2007.

Johnson, M., Stevens, N. et al. (2014) *For the Moon and Mars: N-1 – A Reference Guide to the Soviet Superbooster*, 1st Edition, ARA Press, March 2014.

Kailasanath, K. (2002) "Recent Developments in the Research on Pulse Detonation Engines" (Invited), Paper AIAA-2002-0470, presented at the *40th AIAA Aerospace Sciences Meeting & Exhibit*, Reno, NV, 14–17 January 2002.

Kalmykov, G.P. *et al.* (2008) "LOX-Hydrocarbon Engines in Russia", in *Advanced Propulsion Systems and Technologies: Today to 2000*, edited by C. Bruno and A.G. Accettura, AIAA Progress in Astronautics and Aeronautics Series, Vol. 223, AIAA, Reston, VA., Chapter 14, March 2008.

Kantrowitz, A. (1978) "Laser-Assisted Propulsion Research", in: *Radiation Energy Conversion in Space*, ed. by K.W. Billman, AIAA Progress in Aeronautics and Astronautics Series, Vol. 61, p. 271.

Kingsbury, N.R. (1991) "Aerospace Plane Technology: Research and Development Efforts in Europe", GAO/NSIAD-91-194, *Report to the Chairman, Committee on Science, Space, and Technology, House of Representatives*, United States General Accounting Office, July 1991.

Koelle, D.E. (1989) "On the Optimum Cruise Speed of a Hypersonic Aircraft", IEEE Aerospace and Electronic Systems Magazine, Vol. 4, No. 5, May 1989, pp. 13–16.

Koelle, D.E., Sacher, P.W., and Grallert, H. (2007) "Deutsche Raketenflugzeuge und Raumtransporter-Projekte", 1st Edition, Band 34, Die Deutsche Luftfahrt, Buchreihe über die Entwicklungsgeschichte der Deutschen Luftfahrttechnik, 2007.

Kroon, R.P. (1952) "Turbojet Performance Manual", Engineering Department, Dept. A-1200, Westinghouse Electric Corporation, Aviation Gas Turbine Division, 1952

Kuczera, H. and Sacher, P.W. (2011) *Reusable Space Transportation Systems*, 1st Edition, Springer/Praxis Publisher, London, January 2011.

Lashin, A.I., Kovalevski, M.M., Romankov, O.N. and Tjurikov, E.V. (1993) "Combined Propulsion System for Advanced Multipurpose Aerospace Plane (ASP)", Paper IAF-93-S.4.479, presented at the *44th International Astronautical Federation Congress*, Graz, Austria, October 1993.

Lee, Y.-M., Czysz, P.A. and Bruno, C. (2002a) "Magnetohydrodynamic Energy Bypass Performance Analysis for Hypersonic Vehicles", paper AIAA 2002-3571, presented at the *38th AIAA/ASME/SAE/ASEE Joint Propulsion Meeting*, Indianapolis, IN, 7–10 July 2002.

Lee, Y.-M., Czysz, P.A., Bruno, C. and Petley, D. (2002b) "Implementation of Magnetohydrodynamic Energy Bypass Process for Hypersonic Vehicle" Paper IECEC-20174, presented at the *37th AIAA/IEE/ASME/SAE/ANS/AIChE Intersociety Energy Conversion Engineering Conference*, Washington DC, 28 July–01 August 2002.

Lee, Y.M., Nikolic-Tirkas, B., Tarrant, G.S., Balepin, V., Petley, D. and Czysz, P.A. (2003) "Vortex Tube Air Separation Applications for Air Collection Cycle Hypersonic Vehicles", Paper AIAA-2003-374, presented at the *41st AIAA Aerospace Sciences Meeting and Exhibit,* Reno, NV, 06–09 January 2003.

Lee, Y.-M., Czysz, P.A., and Bruno, C. (2003) "Implementation of Magnetohydrodynamic Energy Bypass for Hypersonic Vehicles", Paper IAC-03-S.5.07, presented at the *54th International Astronautical Congress,* Bremen, 28 September–03 October 2003.

Legostaev, V.P. (1984) Private communication with P.A. Czysz, 38th International Astronautical Congress (IAF), Brighton, UK, 10–17 October 1984.

Leingang, J.L. (1991) Personal communication with P.A. Czysz, Dayton, OH, 1991.

Leingang, J.L., Maurice, L.Q. and Carreiro, L.R. (1992) "Space Launch Systems Using Collection and Storage", Paper IAF 92-0664, presented at the *43rd Congress of the International Astronautical Federation*, Washington, DC, 28 August–05 September 1992.

Lin, B.C. and Lineberry, J.T. (1995) "An Assessment of T-Layer MHD", Paper AIAA 95-1933, presented at the *26th AIAA Plasmadynamics and Lasers Conference*, San Diego, CA, 19–22 June 1995.

Lindley, C.A. (1965) "Performance of Air Breathing and Rocket Engines for Hypervelocity Aircraft", in: Proceedings of the *4th International Council of the Aeronautical Sciences (ICAS) Congress*, Paris, 1964, Spartan Books, Washington, DC, 1965, pp. 941–976.

Lo, R.E., Adirim, H., Pilz, N., Schildknecht, A. *et al.* (2005) "Acquisition and Evaluation of Cryo-Solid Propulsion (CSP); Final Report: Summary of Most Important Results", Technical Report TR Nr.36/03-2005, Aerospace Institute (AI), Berlin, Final Report to the European Space Agency ESA ESTEC, Contract 16830/02/NL/CP, Noordwijk, The Netherlands, March 2005.

Lozino-Lozinskiy, G.E. and Bratukhin, A.G. (Editors) (1997) *Aerospace Systems: Book of Technical Papers*, 1st Edition, Publishing House of Moscow Aviation Institute, Moscow, 1997.

Lozino-Lozinskiy, G.E., Skorodelov, V.A. and Plokhikh, V. P. (1993) "International Reusable Aerospace System MAKS - Present State of the Art and Perspectives", presented at the *5th AIAA/DGLR International Aerospace Planes and Hypersonics Technologies Conference*, Munich, Germany, 30 November–03 December 1993.

Maita, M., Ohkami Y., Yamanaka, T. and Mori T. (1990) "Conceptual Study of Space Plane Powered by Hypersonic Airbreathing

Propulsion System", Paper AIAA-90-5225, presented at the *2nd International Aerospace Planes Conference*, Orlando, FL, 29–31 October 1990.

Maurice, L.Q., Leingang, J.L. and Carreiro, L.R. (1992) "The Benefits of In-Flight LOX Collection for Air Breathing Space Boosters", AIAA paper, presented at the *4th International Aerospace Planes Conference*, Orlando, FL, 01–04 December 1992.

Merlin, P.W. (2002) "Mach 3+ NASA/USAF YF-12 Flight Research, 1969-1979", Monographs in Aerospace History #25, NASA SP-2001-4525, 2002.

Miki, Y., Taguchi, H. and Aoki, H. (1993) "Status and Future Planning of LACE Development", Paper AIAA-93-5124, presented at the 5th International Aerospace Planes & Hypersonics Technology Conference, Munich, Germany, 30 November–03 December 1993.

Miller, J. (2001) *The X-Planes - X-1 to X-45*, 3rd Edition, Midland Publishing, Hinkley, UK, 2001.

Morring, F. (2016) "Dream Chaser Wins Spot in 2nd Round ISS Cargo Contract", Aviation Week & Space Technology, 14 January 2016.

Mulready, D. (2001) *Advanced Engine Development at Pratt & Whitney (The Inside Story of Eight Special Projects 1946-1971)*, SAE International, Warrendale, PA., 2001, ISBN: 0-76800664-3.

Myrabo, L.N. (1982) "A Concept for Light-Powered Flight", Paper AIAA-78-698, presented at the *18th AIAA Joint Propulsion Conference*, Cleveland, OH, 21–23 June 1982.

Myrabo, L.N. (1983) "Advanced Beamed-Energy and Field Propulsion Concepts", NASA-CR-176108, BDM Corporation publication BDM/W-83-225-TR, Final Report for the California Institute of Technology and Jet Propulsion Laboratory under NASA contract NAS7-1000, Task Order RE-156, May 1983.

Myrabo, L.N. (2001) "World Record Flights of Beam-Riding Rocket Lightcraft: Demonstration of 'Disruptive' Propulsion Technology", Paper AIAA-2001-3798, presented at the 37th AIAA Joint Propulsion Conference and Exhibit, Salt Lake City, UT, 08–11 July 2001.

Myrabo, L.N. *et al.* (1988) "Apollo Lightcraft Project", NASA-CR-184749, Final Report, prepared for NASA/USRA Advanced Design Program, 4th Annual Summer Conference, Washington, DC, 13–17 June 1988.

Myrabo, L.N. and Lewis, J.S. (2009) *Lightcraft Flight Handbook: LTI-20*, 1st Edition, Apogee Books, May 2009.

Myrabo, L.N., Messit, D.G. and Mead, F.B. (1998) "Flight and Ground Tests of a Laser-Boosted Vehicle", Paper AIAA-98-3735, presented at the *34th AIAA/ASME/SAE/ASEE Joint Propulsion Conference and Exhibit,* Cleveland, OH, 13–15 July 1998.

Neufeld, M.J. (1995) *The Rocket and the Reich – Peenemünde and the Coming of the Ballistic Missile Era*, 1st Edition, The Free Press, 1995.

Nicholas, T.M.T., Narayanan, A.K. and Muthunayagam, A.E. (1996) "Mixing Pressure-Rise Parameter for Effect of Nozzle Geometry in Diffuser-Ejectors", *Journal of Propulsion and Power,* Vol. 12, No. 2, 1996, pp. 431–433.

Norris, G. (2003) "Pulse Power", Flight International, Vol. 163, No. 4887, 1–23 June 2003, pp. 50–52.

Norris, G. (2015) "Air-breathing Sabre Concept Gains Credibility", Aviation week & Space Technology, 30 July 2015.

Nouse, H., Minoda, M., *et al.* (1988) "Conceptual Study of Turbo-Engines for Horizontal Take-Off and Landing Space Plane", Paper IAF-88-253, presented at the *39th International Astronautical Federation Congress,* October 1988.

Novichkov, N. (1990a) "Space Wings of Russia and the Ukraine", Article in Magazine *Echoes of the Planet/Aerospace*, Moscow, September 1990.

Novichkov, N. (1990b) Private communication, 41st International Astronautical Federation Congress (IAF), Dresden, Germany, 06–12 October 1990.

Ogawara, A. and Nishiwaki, T. (1989) "The Cycle Evaluation of the Advanced LACE Performance", Paper IAF-89-313, presented at the *40th International Astronautical Federation Congress,* Malaga, Spain, October 1989.

Osborn, K. (2015) "AF Chief Scientist: Air Force Working on New Hypersonic Air Vehicle", Defense Tech, 01 June 2015.

Parkinson, R.C. (1991) "The An-225/Interim HOTOL Launch Vehicle", AIAA Paper AIAA-91-5006, presented at the *3rd AIAA International Aerospace Planes Conference*, Orlando, Florida, December 1991.

Pegg, J., Hunt, L. and Petley, D.H. (1993) "Design of a Hypersonic Waverider-Derived Airplane", Paper AIAA-93-0401, presented at the *31st AIAA Aerospace Sciences Meeting and Exhibit,* Reno, NV, 11–14 January 1993.

Phipps, C.R. and Luke, J.R. (2007) "Laser Space Propulsion", in: *Laser Ablation and Its Applications*, Springer, New York. Chapter 16, 2007.

Pirrello, C.J. and Czysz, P.A. (1970) "Hypersonic Research Facilities Study", Volumes I–VI, National Aeronautics and Space Administration Contract NAS2-5458 by McDonnell Aircraft Company (MCAIR), NASA CR 114322-114331, October 1970.

Poggie, J., McLaughlin, T. and Leonov, S. (2016) "Plasma Aerodynamics: Current Status and Future Directions", Journal AerospaceLab, AL 10-01, December 2015.

Rife, J.P. and Cantelon, P.L. (2010) "Speeds Up to Orbital': A History of the William H. Avery Advanced Technology Development Laboratory", John Hopkins APL Technical Digest, Vol. 28, Number 4, 2010, pp. 306–323.

Riggins, D.W. (1996) "Brayton Cycle Engine/Component Performance Assessment Using Energy and Thrust-based Methods", Paper AIAA-1996-2922, presented at the *32nd AIAA Joint Propulsion Conference and Exhibit,* Lake Buena Vista, FL, 01–03 July 1996.

Roed, A. (1972) "Development of the Saab-Scania Viggen", Canadian Aeronautics and Space Journal, Vol. 18, June 1972, pp. 167–175.

Rudakov, A.S. and Balepin, V.V. (1991a) "Propulsion Systems with Air Precooling for Aerospaceplane", SAE Technical Paper 911182, Society of Automotive Engineers, April 1991.

Rudakov, A.S., Gatin, R.Y., Dulepov, N.P., Koralnik, B.N., Harchevnikova, G.D. and Yugov, O.K. (1991b) "Analysis of Efficiency of Systems with Oxidizer Liquefaction and Accumulation for Improvement of Spaceplane Performance," Paper IAF-91-270, presented at the *42nd International Astronautical Federation Congress,* Montreal, Canada, October 1991.

Sänger, E. (1956) "Flight Mechanics of Photon Rockets", *Aero Digest*, 1956, p. 68–73.

Schall, W.O., Eckel, H.A., and Bohn, W.L. (2007) "Laser Propulsion Thrusters for Space Transportation", in: *Laser Ablation and Its Applications*, ed. by C.R. Phipps, Springer, New York, Chapter 17, 2007.

Scherrer, D. (1988) "Evaluation du Concept de Fusée-Statoréacteur Pour la Propulsion Hypersonique", ONERA Activities 1988, ONERA, Paris, April 1988.

Schweikart, L. (1998) "The Hypersonic Revolution: Case Studies in the History of Hypersonic Technology; Volume III: The Quest for the Orbital Jet: The National Aero-Space Program (1983–1995)", 2nd Printing, Volume III, Air Force History and Museum Program, 1998.

Scott, T. and Riggins, D.W. (2000) "Work Interaction in Quasi-One Dimensional Flows", Journal of Propulsion & Power, Vol. 16, No. 6, pp. 1053–1059.

Smereczniak, P. (1996) "Electromagnetic Drag Reduction (EMDR) Program", Contract F33657-96-D-2004-0002, Developed for Aeronautical Systems Center Planning Directorate (ASC/XR), 1996.

Stine, G.H. (1996) *Halfwhere to Anywhere – Achieving America's Destiny in Space*, 1st Edition, M. Evans and Company, Inc., October 1996.

Stroup, K.E. and Pontez, R.W. (1968) "Advanced Ramjet Concepts – Volume 1: Ejector Ramjet Systems Demonstration", Report AFAPLTR-67-118, US AF Contract AF33(615)-3734, The Marquardt Corporation Final Report, May 1968.

Sutton, G.P. and Biblarz, O. (2010) *Rocket Propulsion Elements*, 8th Edition, Wiley Publisher, New York, February 2010.

Swithenbank, J. (1967) "Hypersonic Airbreathing Propulsion", Progress in Aerospace Sciences, Vol. 8, Pergamon Press, New York, 1967, pp. 229–294.

Swithenbank, J. (1984) Oral presentation on scramjet research at Sheffield University, May 1984.

Swithenbank, J. and Chigier, N.A. (1969) "Vortex Mixing for Supersonic Combustion", XXI (International) Symposium on Combustion, The Combustion Institute, Pittsburgh, PA, 1969, pp. 1154–1162.

Szames, A. (2001) "Enquête sur une énigme: l'avion hypersonique Ajax", Air et Cosmos, No. 1777, January 2001, pp. 22–24.

Tanatsugu, N., Inatani, Y, Makino, T. and Hiroki, T. (1987) "Analytical Study of Space Plane Powered by Air-Turbo Ramjet with Intake Air Cooler", Paper IAF-87-264, presented at the *International Astronautical Federation (IAF) Congress*, Brighton, UK, October 1987.

Tasić, J. (2006) "The Name of Nikola Tesla in Belgrade: Following the Trail of Light", BelGuest, Summer 2006.

Tesla, N. (2007) *Nikola Tesla: Colorado Spring Notes, 1899–1900*, 1st Edition, BN Publishing, June 2006.

Togawa, M., Aoki, T. et al. (1991) "A Concept of LACE for SSTO Space Plane", AIAA Paper 91-5011, presented at the *3rd International Aerospace Planes and Hypersonics Technologies Conference*, December 1991.

Townend, L. (1986) Oral presentation to NASP technical team on scramjet test in 1966, Hampshire, UK, April 1986.

Townend, L. and Vandenkerckhove, J. (1994) "External Afterburning and Shock-Confined Combustion in Supersonic Flow", APECS-VDK 001/94, ESA contract 120285, European Space Agency, 1994.

Tretyakov, P. (1995) "Supersonic Flow Around Axisymmetric Bodies with External Supply of Mass and Energy", Institute of Theoretical and Applied Mechanics SB RAS, Novosibirsk, Russia, 1995.

Tretyakov, P.K., Golovitchev, V.I. and Bruno, C. (1995) "Experimental and Numerical Study of Counterflow Jet Flame Stabilization in a Supersonic Air Stream", paper presented at the *XII International Society of Air Breathing Engines (ISABE)*, Melbourne, Australia, 10–15 September 1995.

Vandenkerckhove, J.A. (1986) Personal communication with P.A. Czysz about Von Kármán at CalTech, March 1986.

Vandenkerckhove, J.A. (1991) "A First Assessment of Scramjet-Propelled Single-Stage-to-Orbit (SSTO) Vehicles", WLC Phase 5, WP 260, Chapter 1, VDK System S.A., Brussels, Belgium, February 1991.

Vandenkerckhove, J.A. (1992a) "A Peep Beyond SSTO Mass Marginality", Paper IAF-92-0656, presented at the *43rd International Astronautical Federation Congress*, 28 August–05 September 1992.

Vandenkerckhove, J.A. (1992b) "SSTO Configuration Assessment", Chapter 2, Revision 1, VDK System S.A., WLC Phase 5, WP 260, Brussels, Belgium, August 1992.

Vandenkerckhove, J.A. (1993a) "HYPERJET Mk #3, A Rocket-Derived Combined Engine", VDK System Report, April 1993.

Vandenkerckhove, J.A. (1993b) "Comparison Between Ejector-Ramjets & Turbo-Ramjets for T.S.T.O. Propulsion", Paper AIAA-93-5095, presented at the *5th International Aerospace Planes and Hypersonics Technologies Conference*, Munich, Germany, 30 November–03 December 1993.

Weeden, B. (2010) "X-37B Orbital Test Vehicle Fact Sheet", Secure World Foundation, 23 November 2010.

Werrell, K.P. (1985) *The Evolution of the Cruise Missile*, 1st Edition, Air University Press, September 1985.

Wu, Y., Ma, F. and Yang, V. (2003) "System Performance and Thermodynamic Cycle Analysis of Air-Breathing Pulse Detonation Engines", Journal of Propulsion and Power, Vol. 19, No. 4, July–August 2003.

Yabe, T. and Uchida, S. (2007) "Laser Propulsion", in: *Laser Ablation and Its Applications*, ed. by C.R. Phipps and Luke, J.R., Springer, New York, Chapter 18, 2007.

Yamanaka, T. (2000) "Innovative Breakthroughs to a Reusable STS", private communication with P.A. Czysz, 2000.

Yamanaka, T. (2004) "Fundamentals of Airbreathing Rocket Combined Cycle (ARCC) Engine and Design of an ARCC Engine Powered Single-Stage-To-Orbit (SSTO) Vehicle", Beyond the Atmosphere CDROM, July 2004.

Yugov, O. K., et al. (1989) "Optimal Control Programs for Airbreathing Propulsion System or Single-Stage-to-Orbit Vehicles", Paper IAF-89-308, presented at the *40th IAF Congress, International Astronautical Federation*, Malaga, Spain, October 1989.

Yugov, O.K., Dulepov, N.P. and Harchenvnikova, G.D. (1990) "The Analysis of Hypersonic and Combined Cycle Engines in the Propulsion System of the SSTO Vehicles", presented at the *41st IAF (International Astronautical Federation) Congress*, Dresden, Germany, October 1990.

Zagainov, G.I. and Plokhikh, V.P. (1991) "USSR Aerospace Plane Program", Paper AIAA-91-5103, presented at the *3rd International Aerospace Planes and Hypersonics Technologies Conference*, Orlando, FL, 03–05 December 1991.